CHARACTERIZATION OF BIOMASS ASH /CHAR AND USE FOR TREATMENT OF SULPHUR AND SELENIUM OXY-ANIONS

by

© Bhagya Maheshi Kumari Range

A Thesis submitted to the

School of Graduate Studies

in partial fulfillment of the requirements for the degree of

Master of Engineering

Faculty of Engineering and Applied Science

Memorial University of Newfoundland

May 2014

St. John's Newfoundland

Abstract

This thesis presents the chararacteristics of eight biomass ash/char samples obtained from three pulp and paper mills in Canada. It also discusses the results from the adsorption studies conducted using these biomass ash/char to remove sulfur and selenium oxy-anions from mining effluent water streams such Acid Mine Drainage (AMD). Chemical, physical, thermal and structural characteristics investigated in this study confirmed the suitability of using these ash/char as adsorbents in waste water treatment applications. Batch equilibrium adsorption experiments were performed using individual solutions of thiosulphate, trithionate, tetrathionate, selenite and selenate by varying different parameters (ash type, initial pH, adsorbent dose, temperature). Maximum adsorption efficiency and adsorption capacity values obtained for sulphur oxy-anions were 35.6% and 14.24 mg/g of CBM-W biomass char. For selenium oxy-anions, the maximum adsorption efficiency and adsorption capacity values were at 15.2% and 0.211 mg/g of CLM2 biomass ash. Thermodynamic parameters were calculated and the data were fitted using Langmuir and Freundlich isotherm equations. The results confirmed that sulphur and selenium oxy-anions have considerable affinity towards biomass ash/char. However, further characterization of spent biomass ash/char needs to be carried out in order to identify the adsorption mechanism and also to modify biomass ash/char chemically or thermally to yield high removal efficiencies. Therefore, this study substantially contributes in assessing the feasibility of using one waste stream to treat another waste stream in the field of sustainable waste management.

Acknowledgements

Last two years as a master's student has been a truly remarkable period in my life and the support and guidance I received from many people has been amazing.

First and foremost, I'm greatly thankful to my supervisor, Dr. Kelly Hawboldt for all the guidance and encouragement she gave me and also for the financial support provided. Also, I greatly acknowledge the funding received by the Engage grants program of the Natural Sciences and Engineering Research Council, Canada and School of Graduate Studies, Memorial University. I would also like to thank Dr. Christina Bottaro and Michael Pappoe for their advice and support.

Furthermore, my deep appreciation goes to all the research and administration staff I worked with: Michael Shaffer; Lakmali Hewa; Julie Collins; Pam King; Dr. David Grant, Dr. Wanda Aylward; Alison Pye; Dr. Geert Van Biesen; Misuk Yun; Ferdinanda; Moya Crocker; Colleen Mahoney and everyone else who helped me in some way. I would also like to say a heartfelt thank you to all my dearest friends and colleagues for their support, Punyama Jayasinghe, Oscar De Silva, Nilanthi De Silva, Jingjing Cai, Adeoti Ibrahim, Clemente Miranda, Kelly LeShane, Migara Liyanage and Samith Rathnayake.

Lastly, I would like to thank my parents for all their love and encouragement, and most of all, my loving, supportive, encouraging, and patient husband, Pradeep Dalpatadu for simply being the wonderful person that he is. Thank you!

Table of Contents

List of Tables

List of Figures

List of Appendices

List of Symbols, Nomenclature or Abbreviations

^{o}C	Degree Celsius
ΔG	Gibbs free energy change of adsorption
ΔH	Enthalpy change
ΔS	Entropy change
Ag	Silver
Al	Aluminum
AMD	Acid Mine Drainage
As	Arsenic
ASAP	Accelerated Surface Area and Porosimetry
ASTM	American Society for Testing and Materials
ATR	Attenuate Total Reflectance
B	Boron
Ba	Barium
BC	British Columbia
Be	Beryllium
BET	Brunauer–Emmett–Teller
Bi	Bismuth
BSE	Backscattered Electron Emission
C	Carbon
Ca	Calcium
$CaCO_3$	Calcium carbonate

CANMET	Canada Centre for Mineral and Energy Technology
CBPPL	Corner Brook Pulp and Paper Limited
CBM	Corner Brook Mill (first sample)
CBM-D	Second sample collected from CBM (dry)
CBM-W	Third sample collected from CBM (wet)
CBM-D2	Corner Brook Mill dry sample (size: 500 µm < d < 1.18 mm)
CBM-D1	Corner Brook Mill dry sample (size: d < 500 µm)
CBM-W	Corner Brook Mill wet sample (size: 1.18 mm < d < 4 mm)
C-CART	Centre for Chemical Analysis, Research and Training
Cd	Cadmium
Ce	Cerium
CEC	Cation Exchange Capacity
CLM	Zelstoff Celgar Mill
CLM2	Zelstoff Celgar Mill sample (size: 500 µm < d < 1.18 mm)
CLM1	Zelstoff Celgar Mill sample (size: d < 500 µm)
Co	Cobalt
CO_2	Carbon dioxide
Cr	Chromium
CREAIT	Core Research Equipment and Instrument Training Network
Cs	Cesium
Cu	Copper
DAB	3,3-diaminobenzidine

DFT	Density Functional Theory
E	Mean free energy of adsorption
EA	Elemental Analyzer
EDS	Energy Dispersive X-ray-Spectra
FA	Fly ash
Fe	Iron
FEG	Field Emission Gun
FHAp	Fish scale hydroxyapatite
FTIR	Fourier Transform Infrared Spectroscopy
GC	Gas Chromatography
GFAAS	Graphite furnace atomic absorption spectrometry technique
H_2O_2	Hydrogen peroxide
H_2CO_3	Carbonic acid
H_2SO_4	Sulphuric acid
HCl	Hydrochloric acid
He	Helium
HF	Hydrofluoric acid
Hg	Mercury
HNO_3	Nitric acid
HG-AAS	Hydride generation atomic absorption spectrometry
ICP-OES	Inductively coupled plasma optical emission spectrometry
ICP-MS	Inductively coupled plasma mass spectrometry

ICSD	Inorganic Crystal Structure Database
K	Kelvin
K	Potassium
KBM	Kruger Brompton Mill (sample)
KBM2	Kruger Brompton Mill sample (size: 1.18 mm < d < 4 mm)
KBM1	Kruger Brompton Mill sample (size: d < 1.18 mm)
kV	kilovolts
La	Lanthanum
Li	Lithium
LFD	Large Field Detector
mA	milli-amperes
MCL	Maximum Contaminant Level
Mg	Magnesium
MLA	Mineral Liberation Analysis
Mn	Manganese
Mo	Molybdenum
MW	Megawatt
MDI	Materials Data Inc.
N	Normality
N	Nitrogen
N_2	Nitrogen gas
nA	nano-amperes

NA	Not applicable
Na	Sodium
Ni	Nickel
NL	Newfoundland and Labrador
O	Oxygen
OPUS	Optical User Software
P	Phosphorus
Pb	Lead
pH_{IEP}	Isoelectric point
pH_{PZC}	Point of zero charge pH
P/P0	Relative pressure
ppm	Parts per million
PRB	Permeable Reactive Barrier
PVP	poly 4-vinyl pyridine
QTFAAS	Quartz tube furnace atomic absorption spectrometry
R^2	Regression coefficient
Rb	Rubidium
rpm	Revolutions per minute
RT	Room temperature (21^oC)
$S_2O_3^{2-}$	Thiosulphate
$S_3O_6^{2-}$	Trithionate
$S_4O_6^{2-}$	Tetrathionate

SANS	South African National Standard
S	Sulphur
Sb	Antimony
Se	Selenium
Se(0)	Elemental selenium
SeO_3^{2-}	Selenite
SeO_4^{2-}	Selenate
SEM	Scanning Electron Microscope
Si	Silicon
SiO_2	Silica
Sn	Tin
SO_2	Sulphur dioxide
Sr	Strontium
TBAH	Tetrabutylammonium hydroxide
TCD	Thermal Conductivity Meter
TERRA	The Earth Resources Research and Analysis Facility
TGA	Thermal Gravimetric Analysis
Ti	Titanium
Tl	Thallium
TiO_2	Anatase
U	Uranium
US EPA	US Environmental Protection Agency

V	Vanadium
WHO	World Health Organization
w/v	Weight/Volume
XPS	X-ray Photoelectron Spectroscopy
XRD	X-ray Diffraction
ZCLP	Zellstoff Celgar Limited Partnership
Zn	Zinc
ZnSe	Zinc selenide

Chapter 1 : Introduction and Overview

1.1 Introduction

Biomass ash is generated as a byproduct of combustion of forestry residue and/or fossil fuels that are used for energy generation in cogeneration plants. It has been estimated that approximately 476 million tons of biomass ash is generated worldwide annually based on combustion of 7 billion tons of biomass with 6.8% mean ash yield on dry basis (Vassilev et al., 2013a). Ash is generally disposed of in landfills which involve significant costs in ash handling and disposal such as fuel, manpower, obtaining permits for the landfill and also, heat of ash can cause landfill fires which is a serious environmental and safety concern. Due to the limited availability of landfills as well as the strict environmental regulations, it has become necessary to find alternative uses for these biomass ashes.

On the other hand, discharge of untreated mining effluent waste streams such as AMD can lead to pH reduction, depletion of dissolved oxygen, and dissolution of metals from the sediment in the receiving natural water bodies which is extremely harmful to aquatic species (Dinardo and Sally, 1998). Sulphur oxy-anions present in mining effluent water, also known as thiosalts have relatively low toxicity, however, sulphuric acid formed by thiosalt oxidation can cause severe effect to aquatic life along with other adverse effects stated above. Selenium, on the other hand, is an essential nutrient for plants, animals and humans, however, it is toxic at higher concentrations (Bleiman and Mishael, 2010).

1.2 Scope and Objectives

There are extensive studies done on using coal fly ash for different applications such as cement and concrete products, structural fill and cover material, roadway, addition to construction materials, infiltration barrier and mine back filling, and soil, water and environmental remediation (Ahmaruzzaman, 2010). However, there are no published studies to be found on treatment of selenium and sulphur oxy-anions from waste water using biomass ash/char obtained from pulp and paper mill boilers. Utilization of biomass ash for treatment of sulphur and selenium oxy anions in mining effluent water is a beneficial and sustainable approach to waste treatment as one waste stream is used to treat another waste stream. Therefore, possibility of using biomass ash as an adsorbent to treat sulphur and selenium oxy-anions present in mining effluent water was investigated in this study.

The main objectives are;

- Investigation of past data on adsorption of sulfur and selenium oxy-anions using various adsorbents through a comprehensive literature review
- Chemical, physical, thermal, structural characterization of biomass ash/char collected from three pulp and paper mill boilers and determining the suitability of using these ash/char to treat sulfur and selenium oxy-anions from effluent water streams

- Designing and conducting batch equilibrium adsorption tests using individual solutions of thiosulphate, trithionate, tetrathionate, selenite and selenate by varying different parameters (ash type, initial pH, adsorbent dose, temperature)
- Determining adsorption efficiencies, adsorption capacities and thermodynamic parameters to understand the nature and extent of adsorption
- Adsorption isotherm modeling to investigate the surface properties and affinity of the adsorbent

1.3 Thesis Structure

This thesis is written in the manuscript format and is divided into seven chapters including the Introduction and Overview (Chapter 1) and Summary (Chapter 7) chapters. Figure 1-1 illustrates the interdependency of these chapters and each chapter is briefly outlined in the following paragraphs.

Chapter 2 provides a comprehensive review on removal of thiosalts and sulphates from mining effluent water mainly with reference to adsorption and ion exchange applications. Importance of thiosalts, behavior of thiosalts at different temperature and pH as well as current thiosalt treatment methods are discussed in this chapter. This paper is being considered to be published as a critical review in the Environmental Chemistry journal.

Chapter 3 provides a comprehensive literature review on removal of selenite and selenate from aqueous media by adsorption. The areas discussed in this chapter includes chemistry

of selenium, batch adsorption studies, list of various adsorbents used and their adsorption capacities. Adsorption isotherms, kinetics and thermodynamics are further discussed in this chapter. This paper is being submitted as a critical review in the Environmental Science and Technology journal.

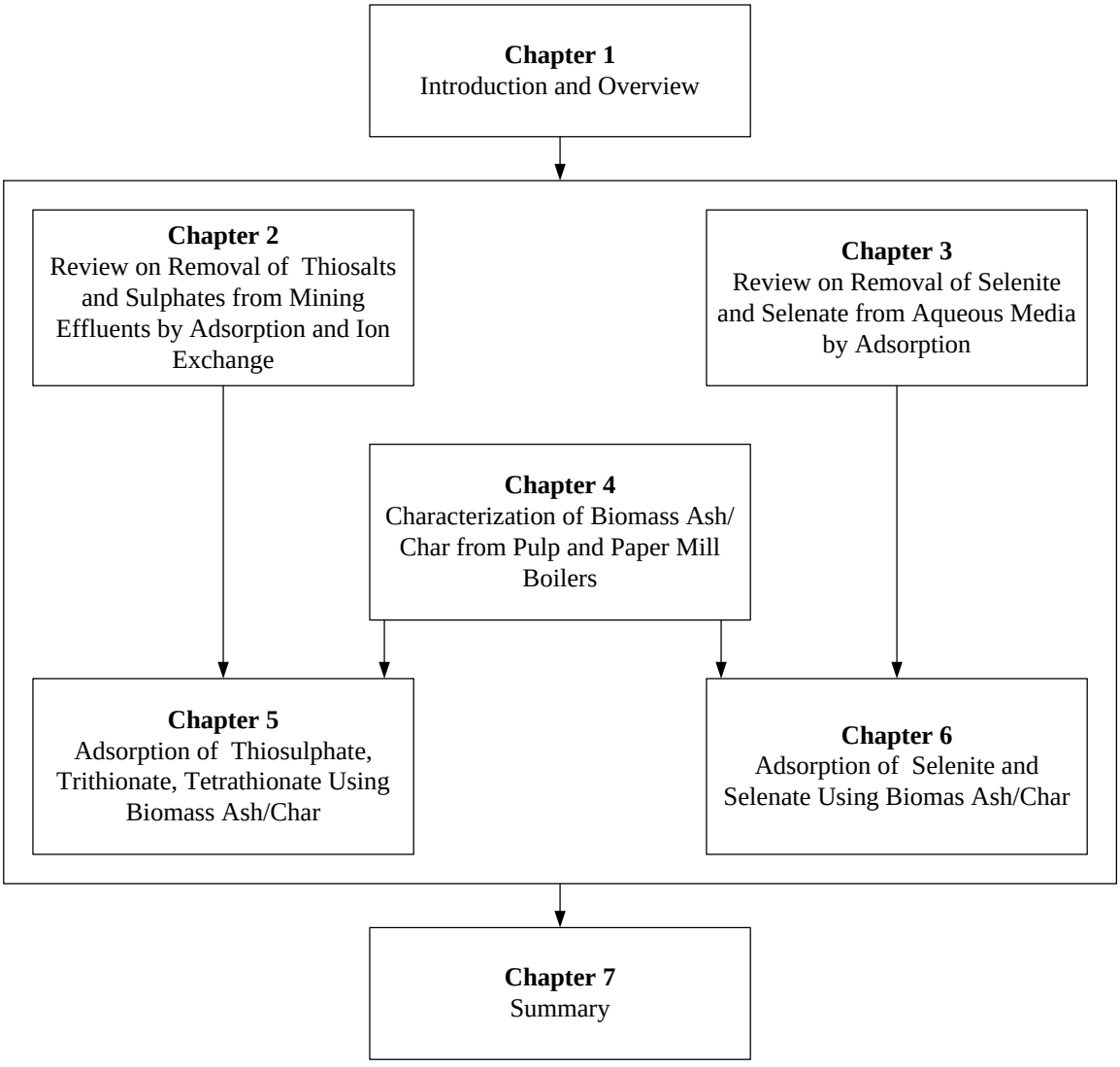

Figure 1-1: Structure of the Thesis

Chapter 4 is on characterization of biomass ash/char obtained from three pulp and paper mill boilers. Eight ash/char samples were characterized chemically, physically, thermally, and structurally by inductively coupled plasma mass spectrometry and optical emission spectrometry (ICP-MS, ICP-OES), CNS (carbon, nitrogen, sulfur) elemental analysis, mineral liberation analysis (MLA), X-ray diffraction (XRD), Fourier transform infrared spectroscopy (ATR-FTIR), scanning electron microscopy (SEM), specific surface area, pore volume, bulk density, pH, total alkalinity, thermo-gravimetric analysis (TGA) and results are discussed in detail. This paper is being submitted to the Journal of Environmental Chemical Engineering.

Chapter 5 is on treatment of sulphur oxy-anions (thiosulphate, trithionate, tetrathionate) using biomass ash/char. Batch mixing experiments were conducted with different types of ash/char and at different parameters (pH 2, 4, 7, 9; biomass ash/char dose 20, 50, 80 g/L; Temperature 5, 21, 35 ^{o}C). The data were fitted using Langmuir and Freundlich adsorption isotherm models. Also, some suggestions for future work are provided. This paper will be submitted to the Journal of Hazardous Materials.

Chapter 6 is on treatment of selenium oxy-anions (selenite, selenate) using biomass ash (CLM2 sample). Batch mixing experiments were conducted by varying the experimental parameters (pH 2, 4, 7, 9; biomass ash dose 20, 50, 80 g/L; Temperature 5, 21, 35 ^{o}C). The thermodynamic parameters were calculated (Gibbs free energy, entropy, enthalpy

change) to understand the nature of adsorption. Also, some suggestions for future work are provided. This paper will be submitted to the Journal of Hazardous Materials.

Co-authorship Statement

In all the papers presented in the following chapters, myself, Bhagya Maheshi Kumari Range, is the principal author and my supervisor Dr. Kelly Hawboldt provided technical guidance, support with analysis and editing of this thesis. I was responsible for developing the test plan, execution and data analysis and also for preparing the manuscript.

Chapter 2 : Review on Removal of Thiosalts and Sulphates from Mining Effluents by Adsorption and Ion Exchange

Bhagya M.K. Range, Kelly A. Hawboldt

Faculty of Engineering and Applied Science, Memorial University of Newfoundland,

St John's, NL, Canada. A1B3X5

Abstract

Thiosalts are generated as intermediate products in the oxidation of sulphide ores in the presence of oxygen and water. Although, thiosalts have relatively low toxicity, sulphuric acid formed as the final product in the oxidation of these sulphide ores, leads to pH depression in the receiving water bodies creating toxic conditions for aquatic plant and animal life. Further, these effluents may even contaminate the groundwater. Therefore, proper management and treatment of mining effluent water containing these sulphur species is of great importance. This paper discusses the generation and importance of Acid Mine Drainage (AMD), different sulphur species present in AMD, mainly, sulphate and thiosalts (thiosulphate, trithionate, tetrathionate), behavior of thiosalts at different pH (2, 4, 7, 9) and temperature (4, 15, 30 ^{o}C) and various thiosalt treatment methods such as natural degradation, chemical oxidation, biological oxidation. Furthermore, use of various carbonaceous adsorbents, ion exchange resins, fly ash and fly ash zeolites used for sulphate and thiosalt removal by adsorption and ion exchange are discussed in detail.

2.1 Introduction

Acid Mine Drainage (AMD) is an unintended, yet unavoidable by-product of mining and mineral industry. AMD is formed due to oxidation of reactive mine tailings (Hendricks, 2005). According to estimates by the Government of Canada, the Canadian mining industry generates 1 million tonnes of waste rock and 950,000 tonnes of tailings per day totaling 650 million tonnes of mine waste per year that have the potential to create AMD (MiningWatch Canada, 2003). AMD is generated when sulphide minerals such as pyrite (FeS_2) found in mines undergo an oxidation process in the presence of water, oxygen and bacteria, which results in the generation of weak sulphuric acid (H_2SO_4) that mobilizes heavy metals and other rock compounds (Vadapalli et al., 2012). Pyrite is one of the most extensively studied minerals with respect to AMD. Mineralogy and other factors affecting AMD production vary from site to site. Iron sulphides are the underlying cause of most AMD production (Akcil and Koldas, 2006). Under anoxic and dry conditions sulphide minerals are relatively stable, however, exposure to oxygen and water accelerates the oxidation of pyrite (FeS_2) and other sulphidic minerals. This process is accelerated by a factor up to 10^6 in the presence of chemolithotrophic microorganisms (Johnson, 2003). The generation of AMD from metal sulphides (mainly pyrite, pyrrhotite, and marcasite) is well established and the overall reaction for pyrite oxidation is outlined below.

$$FeS_2 + 7/2\ O_2 + H_2O \rightarrow Fe^{2+} + 2SO_4^{2-} + 2H^+ \qquad (2\text{-}1)$$

It should be noted this is a global reaction equation and the actual mechanism is made up of several steps (Miranda-Trevino et al., 2012).

AMD is characterized by high acidity (pH 2–4), high sulphate concentrations (1–20 g/L) as well as high concentrations of elements such as Fe, Mn, Al, Cu, Zn, Pb and Cd. Further complexation of ferrous and ferric oxidation products dissolved in water gives the red/orange colour in AMD streams (Hendricks, 2005; Surender, 2009). The extreme pH and high content of dissolved heavy metals make the wastewater highly toxic which leads to persistent environmental problems. AMD has a detrimental effect on aquatic plant and animal life in receiving water streams if discharged without proper treatment. Further, groundwater contamination due to AMD is another very serious concern (Gitari, 2006).

This paper gives an overview on AMD generation and importance with regards to various sulphur species present in AMD, mainly sulphates and thiosalts (sulphur oxyanions). Thiosalt behaviour at different pH and temperatures and conventional thiosalt treatment methods are reviewed. Furthermore, thiosalts and sulphate removal from mining effluent water using carbonaceous adsorbents, ion exchange resins, coal fly ash and coal fly ash derived zeolites is discussed in detail.

2.2 Thiosalts and Sulphates in AMD

Inorganic sulphur compounds are present in nature as sulphides, polysulphides, elemental sulphur, sulphite, sulphate, thiosulphate, and polythionates (Mohapatra et al., 2008) and

also as metal thiosulphate complexes (O'Reilly et al., 2001). Most traditional forms of AMD treatment focuses on sulphate as the predominant sulphur species. However, several studies have shown that thiosalts, sulphur oxyanions of the form thiosulphate ($S_2O_3^{2-}$) and polythionates ($S_xO_6^{2-}$ where $3 \leq x \geq 10$), and polysulphides (S_n^{2-}), where n is greater than or equal to 2), play an important role in the chemical and biological reactivity of mining waters/tailings (Dinardo and Sally, 1998; Miranda-Trevino et al., 2012; Wasserlauf and Dutrizac, 1982).

2.2.1 Sulphates

As stated earlier, oxidation of sulphide minerals leads to formation of weak sulphuric acid, and therefore effluent from the mining processes has a high concentration of sulphate. Sulphate (SO_4^{2-}) is a harmful contaminant in aquatic environments due to the potential toxicity caused by high acidity as well as due to the resulting metal mobility.

Mining activities are considered to be the primary source of sulphate generation in British Columbia, Canada (Meays and Nordin, 2013). The Ministry of Environment of British Columbia has set Ambient Water Quality Guidelines for sulphate to protect drinking water and freshwater aquatic life. As per the guidelines, dissolved sulphate concentration in freshwater should not exceed 100 mg/L at any time to protect aquatic life and the sulphate guideline for drinking water is 500 mg/L. AMD data from a South African mine shows that, AMD can even contain sulphate concentrations in excess of 20,000 mg/L (Surender, 2009). South African National Standard (SANS 241:2006) specifies the

sulphate limit for potable water as less than 400 mg/L (Surender, 2009). This requires that more than 98% of sulphate to be removed from the typical mining process. Traditional systems require significant volumes of chemicals and other treatment agents to meet these standards. Ideally, if the amount of sulphate in the wastewater could be reduced through sulphur management of the wastewaters, the footprint of treatment systems and associated chemicals used would be reduced.

2.2.2 Thiosalts

Thiosalts occur as intermediates in the oxidation of sulphide ores, such as pyrite. Pyrite oxidation occurs via two major oxidants, Ferric ion (Fe^{3+}) and oxygen (O_2) (Miranda-Trevino et al., 2012). Pyrite oxidation is a complex process and products will depend on the conditions of the solution. Thiosalts are also known as polythionates with the following general formula, $S_nO_m^{2-}$. Thiosalt species present in mining effluent water are thiosulphate ($S_2O_3^{2-}$), trithionate ($S_3O_6^{2-}$), tetrathionate ($S_4O_6^{2-}$) and also very low concentrations of higher polythionates (Dinardo and Sally, 1998; Miranda-Trevino et al., 2012). Thiosulphate ($S_2O_3^{2-}$) is considered to be the first thiosalt product of pyrite oxidation. Other sulphur species resulting from pyrite oxidation are trithionate ($S_3O_6^{2-}$), tetrathionate ($S_4O_6^{2-}$) and sulphate (SO_4^{2-}) (Miranda-Trevino et al., 2012). Several studies have identified key factors in the generation of thiosalts in the mining process such as sulphur content in the ore, grinding and flotation pH, residence time in the mill, agitation rate, temperature, SO_2 addition, dissolved oxygen in the grinding solution, air flow in

flotation and chemicals used in the system (Miranda-Trevino et al., 2012; Negeri et al., 1999).

The reactivity of thiosalts is complex and depends on many factors such as temperature, pH, dissolved oxygen content, microorganisms and presence of heavy metals. At typical tailing pond conditions most sulphur compounds oxidize to sulphate, however, partially oxidized species, such as thiosalts are slow to oxidize and can also be present in the tailings pond (Miranda-Trevino et al., 2012; Wasserlauf and Dutrizac, 1982).

Although thiosalts have relatively low toxicity (Dinardo and Sally, 1998) and their concentrations are not been strictly regulated, sulphuric acid formed by thiosalt oxidation can cause severe effect to aquatic life along with other adverse effects like depletion of dissolved oxygen, reduction in buffering capacity and dissolution of metals from the sediment (Dinardo and Sally, 1998).

The Environmental Code of Practice for Metal Mines in Canada states that proper thiosalt management practices should be in place at sites where there is a risk of thiosalts occurring in wastewater from ore processing, which are summarized as follows: minimize the discharge of thiosalt-bearing wastes to the environment by recycling the water back to the ore processing facility; implementing measures to ensure thiosalt degradation on site; monitor concentrations of thiosalts in wastewater and also check for pH depression

downstream; minimize the concentration of thiosalts in mining effluent before it is discharged to the environment (Environment Canada, 2009).

2.2.3 Importance of Thiosalts

Most of the prevention and remediation techniques used in the treatment of AMD are not designed to treat intermediate sulphur species formed during the mining operations or in the tailing ponds and these intermediate species can cause serious impact if left untreated. For example, a solution with a thiosulphate concentration of 500 ppm could have a serious effect resulting in a pH depression of 5 units if oxidized completely (Miranda-Trevino et al., 2012).

2.2.4 Thiosalt Behaviour at Different pH and Temperature

Behaviour of thiosulphate, trithionate, tetrathionate at different pH (2, 4, 7, 9) and temperature (4, 15, 30 ^{o}C) is given in Table 2-1. It should be noted these are not mixtures, but rather solutions with single thiosalt species.

Table 2-1: Thiosalt behaviour at different pH and temperature

(Modified from Miranda-Trevino et al., 2012; Vongporm, 2008)

pH	Thiosalt species	4°C	15°C	30°C
2	Thiosulphate $S_2O_3^{2-}$	Decomposes to $S_3O_6^{2-}$, SO_4^{2-}, $S_4O_6^{2-}$		
	Trithionate $S_3O_6^{2-}$	Stable		Decomposes to $S_2O_3^{2-}$, SO_4^{2-}, $S_4O_6^{2-}$
	Tetrathionate $S_4O_6^{2-}$	Stable		
4	Thiosulphate $S_2O_3^{2-}$	Stable		
	Trithionate $S_3O_6^{2-}$	Stable	Decomposes to $S_2O_3^{2-}$, SO_4^{2-}, $S_4O_6^{2-}$	
	Tetrathionate $S_4O_6^{2-}$	Stable		
7	Thiosulphate $S_2O_3^{2-}$	Stable		
	Trithionate $S_3O_6^{2-}$	Stable	Decomposes to $S_2O_3^{2-}$, SO_4^{2-}, $S_4O_6^{2-}$	
	Tetrathionate $S_4O_6^{2-}$	Stable		
9	Thiosulphate $S_2O_3^{2-}$	Stable		Decomposes to $S_3O_6^{2-}$, SO_4^{2-}, $S_4O_6^{2-}$
	Trithionate $S_3O_6^{2-}$	Stable		Decomposes to $S_2O_3^{2-}$, SO_4^{2-}, $S_4O_6^{2-}$
	Tetrathionate $S_4O_6^{2-}$	Decomposes to $S_2O_3^{2-}$, SO_4^{2-}, $S_3O_6^{2-}$		

2.3 Thiosalt Treatment Methods

Typical methods to treat thiosalts focus on oxidizing the thiosalts using peroxide and/or ferric sulphate and then liming as per AMD treatment, natural degradation, and other biological and chemical methods (Miranda-Trevino et al., 2012). Natural degradation is limited in cold climates due to reduced bacterial and chemical reactivity in winter months due to reduced temperature and sunlight. The chemical/physical methods and biological oxidation could achieve a target concentration of <100 mg/L thiosalts. However, these methods are expensive both from a cost and environmental perspective (Dinardo and Sally, 1998).

In the following sections, the traditional thiosalt treatment technologies in the mining industry are summarized.

2.3.1 Chemical Oxidation

Chemical oxidation of thiosalts is the most common treatment approach. Hydrogen peroxide (H_2O_2), chlorine (Cl_2), ozone (O_3), Cu-catalyzed air, SO_2-air are typical oxidants. The advantages of using chemical oxidation as outlined by Dinardo and Sally (1998) include, fast reaction rates with short retention time, dosages can be varied to accommodate seasonal and operational caused variations in thiosalts concentration and flow rate, potential high treatment efficiencies (depending on the thiosalt species). Some disadvantages include, high initial capital investment and costs of chemical oxidants, and by-product formation (Dinardo and Sally, 1998).

2.3.2 Metal Catalyzed Air Oxidation

Air oxidation of thiosalts under normal pressures and temperatures is a very slow process and it is not practical for thiosalts oxidation from large volumes of effluent. Catalysts containing metals such as copper, manganese, nickel, cobalt, tungsten, zirconium, and titanium are considered as effective catalysts in oxidizing sulphur compounds contained in effluents. Advantages are; low cost method; process does not require reagents; do not produce toxic by-products; complete oxidation of thiosalts can be achieved; sulphur bonded catalysts (e.g. natural chalcopyrite) have good long term catalytic activity and is inexpensive. Disadvantages are; most catalysts require frequent regeneration resulting in high operational costs; catalysts are not effective at low temperatures; gypsum precipitation on the catalyst may reduce the active surface (Dinardo and Sally, 1998).

2.3.3 Biological Oxidation

In biological oxidation, bacteria may enhance oxidation of thiosalt to produce elemental sulphur, polythionates and sulphate. However, under suitable environmental conditions, sulphate is the final end-product. Studies indicate that indigenous Thiobacillus species can oxidize thiosalts at a pH of 2. Biological oxidation of thiosalts is site specific and the treatment process is mainly a function of temperature and pH. Advantages include the process is relatively safe with respect to handling and storage due to non toxic by-products, low energy requirements, and the process is simple in design (Abbassi and Hawboldt, 2011; Dinardo and Sally, 1998). The disadvantages are, reduced efficiency at

low temperatures, ability to treat all species of thiosalt, additional treatment may be required (Dinardo and Sally, 1998; Miranda-Trevino et al., 2012).

2.3.4 Reverse Osmosis and Other Membrane Processes

Reverse Osmosis (RO) is a technically feasible process which has proven to remove thiosalts from synthetic solutions. However, the operational and maintenance costs of a RO system is very high and extensive pre-treatment is required to prevent membrane fouling due to scale formation and growth of bacteria (Dinardo and Sally, 1998).

2.3.5 Electrochemical Oxidation

Electrochemical oxidation is a technically feasible process for treatment of thiosalts. Catalysts could be combined with electro oxidation to improve the efficiency of the cell to oxidize thiosalts and reduce power requirement. One disadvantage is that electrochemical treatment of effluent is generally limited to specific streams with low flows and high concentrations (Dinardo and Sally, 1998).

2.3.6 Natural Degradation

Natural degradation in the treatment ponds is a conventional method used to treat thiosalts in milling effluents. This involves a long retention period in the pond, usually up to one year allowing time for bacterial oxidation to happen. Low water temperature, low dissolved oxygen and short retention time limit natural oxidation in the ponds. However,

in the summer it is an effective and economic method as the rate of oxidation of thiosalts increases due to temperature and sunlight. It is not a feasible year-round method due to the reduced bacterial activity during autumn and winter seasons particularly in northern climates such as Canada (Dinardo and Sally, 1998).

2.4 Adsorption and Ion Exchange Applications

Adsorption is used in many industries such as chemical, food, petroleum, and pharmaceutical for pollution control and it is a well established technology in treating industrial wastewaters. In the adsorption process, contaminants are accumulated at a solid surface from a liquid or gaseous medium. There are two types of adsorption; physical adsorption and chemisorption. In physical adsorption, the bonds between the solid surface and the adsorbed molecules are weak van der waals forces which makes it relatively easy to reverse the process. In chemisorption, contaminant molecules are adsorbed on to the solid surface by forming strong chemical bonds and as such it is more energy intensive to reverse the process. In ion exchange, similarly charged ions are exchanged between a liquid and a solid phase until equilibrium conditions is achieved and it is a reversible process. Ion exchange is a stoichiometric reaction unlike the adsorption process (Gupta et al., 2009).

There have not been many studies using ion exchange and adsorption processes for thiosalts removal although there are some studies carried out on sulphate removal from AMD using adsorbents derived from coal fly ash and fly ash derived zeolites. The

following sections will review these literature to understand the application of adsorption and ion exchange principles in removing thiosalts and sulphates from laboratory synthesized solutions as well as from AMD.

2.4.1 Thiosalts Removal Using Carbonaceous Adsorbents

A limited number of studies have focused on thiosalt adsorption using different adsorbents namely, activated carbon, bone charcoal, activated charcoal, bituminous coal , peat, alumina, diatomaceous earth and clay. These studies indicate that only activated carbon was able to remove significant quantities of thiosalt. Details of these studies can be found in CANMET (Canada Centre for Mineral and Energy Technology) reports by Dinardo and Sally (1998), Rolia and Barbeau (1979), Wasserlauf and Dutrizac (1983), and Wasserlauf et al. (1985).

In the study conducted by Rolia and Barbeau, 1979 using activated charcoal, no thiosalt removal from synthetic solutions of thiosulphate, tetrathionate and trithionate was achieved despite varying the pH, temperature and residence time in the range of 6 to 12, 20^{o}C to 65^{o}C and 30 min to 230 min (Rolia and Barbeau, 1979).

Noranda Research Centre conducted laboratory scale studies using activated carbon as an adsorbent and had been successful in removing significant quantities of thiosalts. Batch tests were done with six commercial activated carbon brands where Calgon Filtrasorb 200 brand performed the best with a loading capacity of 10 kg thiosalts/100 kg of carbon

(Wasserlauf and Dutrizac, 1982). Depending on the extent of removal of thiosalts and metal contaminants, the effluent from the columns was either directly discharged or sent for further treatment. A number of regeneration options were studied. Alkaline regeneration of the carbon bed was found to be uneconomical and thermal regeneration was found to be even more expensive. Biological regeneration was suggested as an economic alternative. However, the high capital and operational cost involved in managing an activated carbon adsorption system was identified as a major limitation in implementation (Wasserlauf and Dutrizac, 1982; Wasserlauf et al., 1985).

Activated carbon adsorption can typically meet environmental standards (depending on contaminants) with no major health, safety, or environmental issues associated with operating the system. However, there is little data on the treatment efficiency using activated carbon adsorption for thiosalts, issues around disposal and regeneration of spent carbon, suspended solids, and oil and grease in the effluent, and bacterial growth on the bed could reduce the effectiveness of process and regeneration. Also, fine carbon particles may be difficult to remove from the treated effluent, and carbon requirements may be higher than calculated amounts due to adsorption of other contaminants such as metals and sulphate on to carbon which can reduce the available active sites for thiosalt removal (Dinardo and Sally, 1998; Wasserlauf et al., 1985).

2.4.2 Thiosalts Removal Using Ion Exchange Resins

There have been several studies on detection of thiosalts by using anion-exchange resins mostly on the chromatographic elution of sulphur anions (Aly et al., 1977; Chanda et al., 1984; Druschel et al., 2003; Iguchi, 1958; Jeffrey and Brunt, 2007; Wolkoff and R. H. Larose, 1975).

A detailed study on sorption isotherms and kinetics of ion exchange sorption of thiosalts was done by Chanda et al. (1984). In this study, high selectivity of the ion exchanger for thiosalts over sulphate was observed. Ion exchange sorption behaviour of thiosuphate ($S_2O_3^{2-}$) and tetrathionate ($S_4O_6^{2-}$) on two commercially available gel type weak-base resins; cross-linked PVP (poly 4-vinyl pyridine) and Amberlite IRA 68 was studied in batch equilibrium conditions as well as in a column. The resins were converted to the acid form by treatment with excess 0.5 M H_2SO_4 before use in the ion-exchange study. In the batch equilibrium studies, measured amounts of protonated resin were vigorously shaken with specific volumes of thiosalt solutions for 15 hours in a tightly sealed flask. The tests were carried out with different concentrations of thiosulphate and tetrathionate solutions (Chanda et al., 1984). The ion exchange characteristics of resins after treatment with the acid are outlined below in the Table 2-2.

Table 2-2: Sorbent details after treatment with excess H_2SO_4 (Chanda et al., 1984)

Characteristic	PVP - H_2SO_4	IRA-68 - H_2SO_4
Bulk density	0.65 gcm^{-3}	0.73 gcm^{-3}
Moisture content	45.6% (by wt.)	57% (by wt.)
Proton content	3.25 mmol g^{-1}	2.07 mmol g^{-1}

The sorption of $S_2O_3^{2-}$ by PVP-H_2SO_4 occurs due to exchange of counter ions, that is exchange of $S_2O_3^{2-}$ in place of SO_4^{2-}. The equilibrium data for the sorption of $S_2O_3^{2-}$ and $S_4O_6^{2-}$ on PVP-H_2SO_4 and IRA-68-H_2SO_4 are plotted against the equilibrium solution concentrations in Figure 2-1.

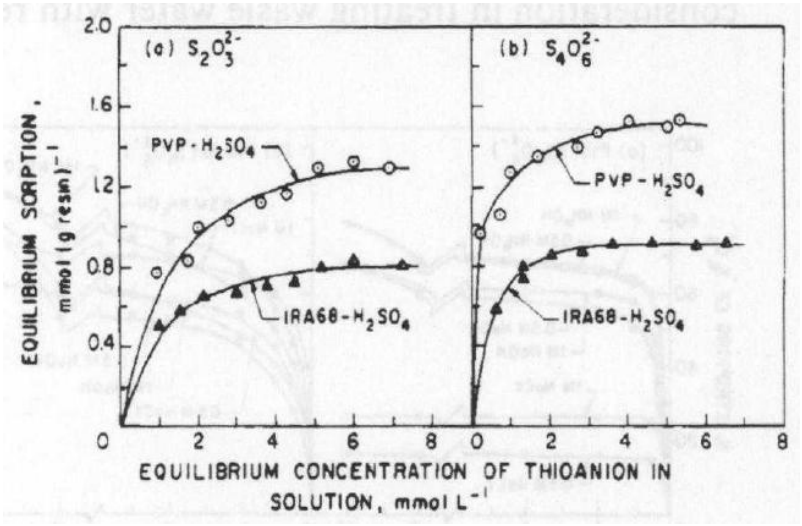

Figure 2-1: Sorption isotherms for $S_2O_3^{2-}$ and $S_4O_6^{2-}$ (Chanda et al., 1984)

Temperature 24 ^oC; pH =7.0-8.5 for $S_2O_3^{2-}$ and pH = 5.7-6.2 for $S_4O_6^{2-}$; Resin Loading; PVP-H_2SO_4 4 g/L and IRA-68-H_2SO_4 6 g/L.

The equilibrium sorption data of $S_2O_3^{2-}$ and $S_4O_6^{2-}$ were fitted to Langmuir and Freundlich isotherms. The Langmuir isotherm provided an excellent fit to the equilibrium sorption data for both resins and the calculated equation parameters indicated that $S_4O_6^{2-}$ is more strongly bound to both resins than $S_2O_3^{2-}$ (Chanda et al., 1984).

The effect of change in solution pH on the thiosalt equilibrium sorption capacity on to both resins is shown in Figure 2-2.

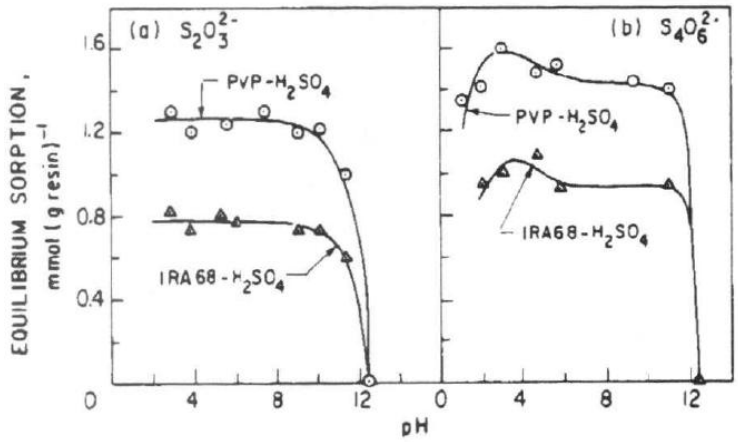

Figure 2-2: Effect of pH on equilibrium sorption of $S_2O_3^{2-}$ and $S_4O_6^{2-}$ by the resins (Chanda et al., 1984)

Temperature 24^{o}C; Thiosalt concentration 10 mmol/L; Resin Loading PVP-H_2SO_4 4 g/L and IRA-68-H_2SO_4 6 g/L.

The sorption capacity is not affected by pH in the range 5-9. There's a small increase in sorption of $S_4O_6^{2-}$ between pH 2-5, as some free basic sites in the resin may be protonated and become active due to acidic nature leading to sorption of more ions. This effect is not

observed in $S_2O_3^{2-}$ adsorption due to the instability of thiosulphate ion at acidic conditions. At pH>9, the sorption capacity with respect to both $S_2O_3^{2-}$ and $S_4O_6^{2-}$ falls rapidly (Chanda et al., 1984).

The sorption of $S_2O_3^{2-}$ and $S_4O_6^{2-}$ on both resins was measured with time under vigorous agitation at ambient temperature to determine kinetics and the results are shown in Figure 2-3.

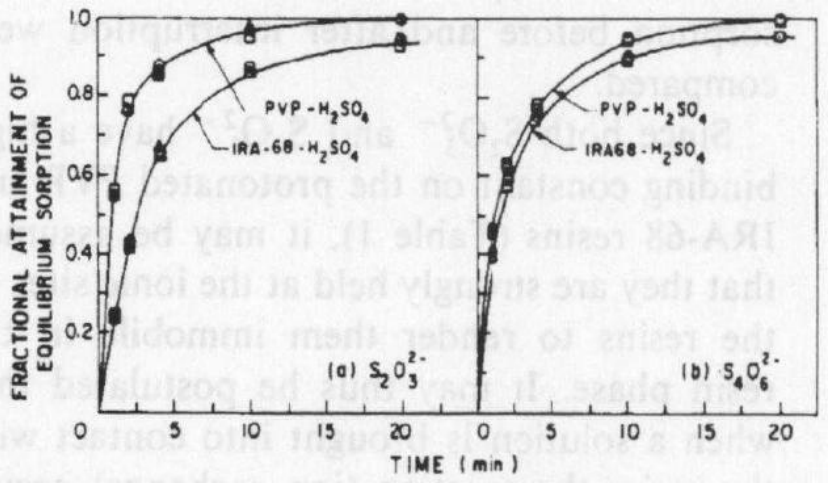

Figure 2-3: Sorption of $S_2O_3^{2-}$ and $S_4O_6^{2-}$ by both resins with time under vigorous agitation (Chanda et al., 1984)

Temperature 24 ^oC; pH 7.0 - 7.9 for $S_2O_3^{2-}$ and pH = 5.8 - 6.3 for $S_4O_6^{2-}$; Resin Loading: PVP-H_2SO_4 0.4% (w/v) slurry and IRA-68-H_2SO_4 0.6% (w/v) slurry; Initial concentration of thioanion 4 mmol/L (--O), 6 mmol/L (--Δ), 8 mmol/L (--□).

The time to equilibrium sorption for both $S_2O_3^{2-}$ and $S_4O_6^{2-}$ appears to be independent of the thiosalt concentrations in solution. The ion-exchange sorption processes under the

conditions given was concluded to be particle-diffusion controlled. Since the sorbent resins have cross-linked matrices, the resin particle size was assumed to remain unchanged with sorption (Chanda et al., 1984).

The performance of the ion exchangers in continuous operation in columns was studied with the two resins outlined above and a third gel-type strong base resin IRA-458 (in Cl^- form). Figure 2-4 shows the breakthrough curves obtained with the three types of resins. The PVP resin provided the sharpest breakthrough (Chanda et al., 1984).

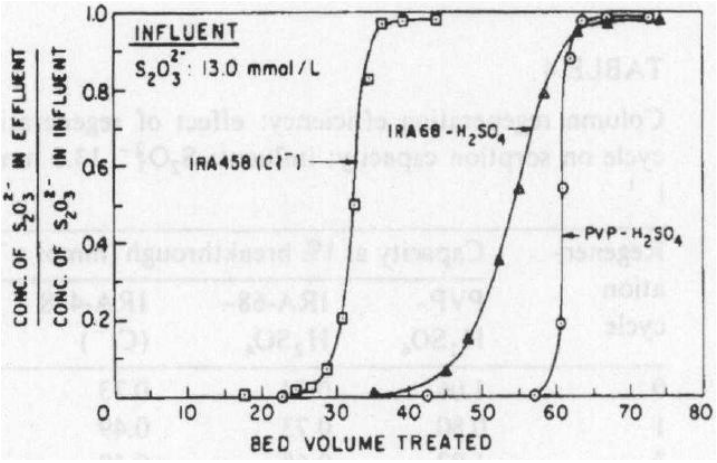

Figure 2-4: Breakthrough curves for $S_2O_3^{2-}$ obtained by ion exchange (Chanda et al., 1984)

Bed height 34 cm; PVP - H_2SO_4 resin details: 7 g, column diameter 0.64 cm, influent rate 1.77 mL/min; IRA-68 - H_2SO_4 resin details: 17 g, column diameter 0.91 cm, influent rate 5.6 ml/min; IRA- 458 resin details: 17 g, column diameter 0.91 cm, influent rate 5.6 mL/min.

It was concluded, that thiosulphate and tetrathionate anions in aqueous effluents can be removed efficiently by ion exchange on protonated PVP and IRA-68 resins within the operating pH range of 3-8. The protonated PVP has a faster rate of thianion sorption than the protonated IRA-68. Also, it is concluded that sorption kinetics on both the resins are particle-diffusion controlled (Chanda et al., 1984). Trithionate had not been studied, which is problematic as trithionate has been proposed as a key intermediate in various studies (for a review of these studies see Miranda-Trevino et al., 2012 (Miranda-Trevino et al., 2012)).

2.4.3 Sulphate Removal from Aqueous Effluents Using Coal Fly Ash/ Zeolites

Many of the studies on sulphate adsorption/ion exchange from synthesized solutions, mining effluent waters or any other sources focus on coal fly ash and fly ash derived zeolites.

The feasibility of treatment of AMD using coal fly ash (from a power plant in South Africa) and the creation of a zeolite from the AMD treated adsorbent were studied by Gitari et al., 2007; Vadapalli et al., 2012. The impact of pH was analyzed by varying the ratio of FA used for treatment with AMD. Initial concentration of sulphate in the AMD was approximately 11890 mg/L. After AMD treatment the sulphate concentration was reduced to 2414 - 5483 mg/L, depending on AMD:FA ratios. The maximum sulphate removal of 79% was achieved using a mixture of AMD: FA ratio 2.5: 1 (Gitari et al., 2007; Vadapalli et al., 2012).

The mechanism of SO_4^{2-} removal from AMD using FA treatment was proposed as CaO in the FA dissolving due to the AMD and reacting with the SO_4^{2-} to form gypsum precipitate $CaSO_4.2H_2O$, followed by Ba and Sr salts in the FA dissolving and forming barite ($BaSO_4$) and celestite ($SrSO_4$) or a mixed (Ba,Sr) SO_4 salt by interacting with SO_4^{2-}. At pH 3, Fe^{3+} precipitates as hydroxides and oxyhydroxides which has the potential to adsorb SO_4^{2-} ions and as the pH rises to about pH 9, a mineral phase known as ettringite [$Ca_6Al_2(SO_4)_3(OH)$] precipitates which causes further reduction in SO_4^{2-} concentration in the effluent (Vadapalli et al., 2008, 2012).

Another study conducted by Surender, 2009 found that the sulphate absorbance by fly ash was 98 % in beaker scale experiments with 1:1 fly ash: AMD ratio. This is comparable to membrane and ion exchange systems and exceeded the performance of limestone treatment (Surender, 2009).

There are large number of other similar studies conducted in the area of sulphate treatment using fly ash (Adeoti, 2011; Gitari, 2006; Gitari et al., 2005; Hendricks, 2005; Madzivire, 2009; Surender, 2009).

2.4.4 Sulphate Removal Using Ion Exchange Resins

The key issue in using ion exchange resins for AMD treatment is that scale formation and fouling of the resins by the calcium sulphate in the neutralized AMD. Several studies report regarding a highly efficient ion exchange process called GYP-CIX which can be used to treat AMD and is capable of overcoming the above mentioned limitation (Dill et al., 2012; Haghsheno et al., 2009; Schoeman and Steyn, 2001; Surender, 2009).

This particular GYP-CIX process utilizes a counter current fluidized bed ion exchange method and a single fluidized bed bath regenerator and uses low cost sulphuric acid (H_2SO_4) and lime ($Ca(OH)_2$) to regenerate the cations and anions separately producing gypsum as a waste by product. It was applied to treat underground mine water discharged at the Grootvlei mines in South Africa. The resultant product is neutralized water, low in calcium, sulphate, heavy metals as well as other ions. The GYP-CIX process is best suited to waters with sulphate concentrations below 1500 – 2000 mg/L. At higher sulphate concentrations, liming is a cheaper treatment option. Large volume of gypsum sludge produced during regeneration of the ion exchange resins is one major disadvantage of the GYP-CIX system (Surender, 2009).

2.4.5 Sulphate Removal Using Permeable Reactive Barriers (PRB)

Smyth and Bain (2004) in their study, illustrate (Figure 2-5) how a vertical permeable reactive barrier (PRB) can be installed to intercept and treat horizontal plumes of contaminated groundwater adjacent to a mining waste management area. Generally a

PRB should have a similar or higher hydraulic conductivity than the surrounding waste materials or aquifer system. AMD impacted groundwater may need to reside for more than several days within the PRB based on the extent and rates of reaction of contaminant removal (Smyth and Bain, 2004).

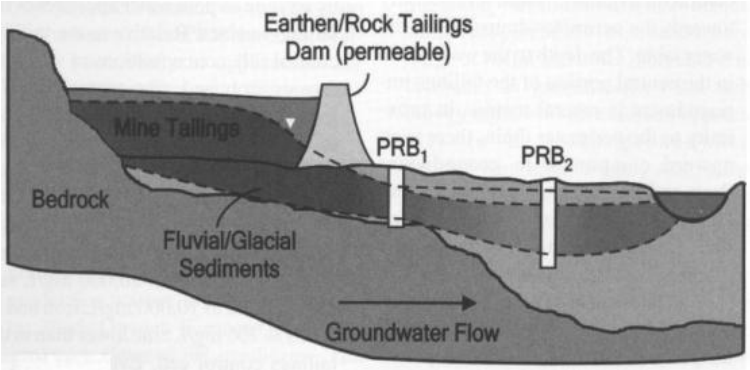

Figure 2-5: PRB application on site (Smyth and Bain, 2004)

In another study by Benner et al., 1999, a PRB was designed and installed into an aquifer containing effluent from mine tailings to remove metals and generate alkalinity by promoting sulphate reduction and metal sulphide precipitation. Flow of groundwater through the barrier resulted in excellent improvement in water quality. There were decreases in concentrations of SO_4^{2-} (by 2000-3000 mg/L), Fe (by 270-1300 mg/L), and increases in alkalinity (by 800-2700 mg/L). However, it was concluded that sulphate reduction by the reactive mixture is mainly bacterially mediated (Benner et al., 1999).

2.5 Conclusion

Management and treatment of AMD is a concern of growing importance. Although, thiosalt concentrations in these effluent streams are not strictly regulated, the ultimate result of oxidation of these intermediate sulphur oxyanions to acidic sulphuric acid has a detrimental impact on aquatic species. Thiosalt behaviour is complex at different pH and temperature which makes it difficult to implement cost effective and efficient treatment methods. Ion-exchange and adsorption systems may be a cheaper alternative for thiosalt treatment than chemical oxidation and a faster alternative than natural degradation/biological oxidation. Cost of operating such a thiosalt adsorption/ion exchange system could possibly be reduced, if industrial by-products such as biomass ash can be modified to be used in place of more expensive ion exchange resins or activated carbon. However, technical concerns regarding continuous operation, adsorbent regeneration and/or disposal of such a system must also be addressed.

Bibliography - Chapter 2

Abbassi, R. and Hawboldt, K.: Report on Biological Oxidation of Thiosalts, Memorial University of Newfoundland, St John's, Canada., 2011.

Adeoti, I. A.: Characterization and Alternative Use Study of Fly Ash, 160 pp., Memorial University of Newfoundland., 2011.

Akcil, A. and Koldas, S.: Acid Mine Drainage (AMD): causes, treatment and case studies, J. Clean. Prod., 14(12-13), 1139–1145, doi:10.1016/j.jclepro.2004.09.006, 2006.

Aly, H. F., Abdel-Hamid, M. M. and Abdel Rassoul, A. A.: Gradient chromatographic elution of sulphur anions, J. Radioanal. Chem., 40(1-2), 65–73, doi:10.1007/BF02517314, 1977.

Benner, S. G., Blowes, D. W., Gould, W. D., Herbert,, R. B. and Ptacek, C. J.: Geochemistry of a Permeable Reactive Barrier for Metals and Acid Mine Drainage, Environ. Sci. Technol., 33(16), 2793–2799, doi:10.1021/es981040u, 1999.

Chanda, M., O'Driscoll, K. F. and Rempel, G. L.: Ion-Exchange Sorption of Thiosulfate and Tetrathionate on Protonated Poly(4-Vinyl Pyridine), React. Polym., 2, 269–278, 1984.

Dill, S., Cowan, J., Wood, A. and Bowell, R. J.: A review of sulfate removal options from mine waters., 2012.

Dinardo, O. and Sally, J.: Treatment of Thiosalts in Milling Effluents: A Review of Treatment Processes., 1998.

Druschel, G. K., Schoonen, M. a. a., Nordstrom, D. K., Ball, J. W., Xu, Y. and Cohn, C. a.: Sulfur geochemistry of hydrothermal waters in Yellowstone National Park, Wyoming, USA. III. An anion-exchange resin technique for sampling and preservation of sulfoxyanions in natural waters, Geochem. Trans., 4(3), 12, doi:10.1039/b211951j, 2003.

Environment Canada: Environmental Code of Practice for Metal Mines., 2009.

Gitari, M. W., Petrik, L. F., Etchebers, O., Key, D. L. and Iwuoha, E.: Treatment of Acid Mine Drainage with Fly Ash : Removal of Major Contaminants and Trace Elements, J. Environ. Sci. Heal., (December 2012), 37–41, 2007.

Gitari, W. M.: Evaluation of the Leachate Chemistry and Contaminants Attenuation in Acid Mine Drainage by Fly Ash and its derivatives, University of Western Cape., 2006.

Gitari, W. M., Somerset, V. S., Petrik, L. F., Key, D., Iwuoha, E. and Okujeni, C.: Treatment of Acid Mine Drainage with Fly Ash : Removal of Major , Minor Elements , SO 4 And Utilization of the Solid Residues for Wastewater, in World of Coal Ash (WOCA), Lexington, Kentucky, USA., 2005.

Gupta, V. K., Carrott, P. J. M., Ribeiro Carrott, M. M. L. and Suhas: Low-Cost Adsorbents: Growing Approach to Wastewater Treatment—a Review, Crit. Rev. Environ. Sci. Technol., 39(10), 783–842, doi:10.1080/10643380801977610, 2009.

Haghsheno, R., Mohebbi, A., Hashemipour, H. and Sarrafi, A.: Study of kinetic and fixed bed operation of removal of sulfate anions from an industrial wastewater by an anion exchange resin., J. Hazard. Mater., 166(2-3), 961–6, doi:10.1016/j.jhazmat.2008.12.009, 2009.

Hendricks, N. R.: The application of high capacity ion exchange adsorbent material, synthesized from fly ash and acid mine drainage, for the removal of heavy and trace metals from secondary co-disposed process waters, 287 pp., University of Western Cape., 2005.

Iguchi, A.: The Separation of Sulfate , Sulfite , Thiosulfate and Sulfide Ions with Anion-Exchange Resins, Bull. Chem. Soc. Jpn, 31(5), 600–605, 1958.

Jeffrey, M. I. and Brunt, S. D.: The quantification of thiosulfate and polythionates in gold leach solutions and on anion exchange resins, Hydrometallurgy, 89(1-2), 52–60, doi:10.1016/j.hydromet.2007.05.004, 2007.

Johnson, D. B.: Chemical and Microbiological Characteristics of Mineral Spoils and Drainage Waters at Abandoned Coal and Metal Mines, ChemInform, 34(36), 47–66, doi:10.1002/chin.200336230, 2003.

Madzivire, G.: Removal of sulphates from South African mine water using coal fly ash, 151 pp., University of Western Cape., 2009.

Meays, C. and Nordin, R.: Ambient Water Quality Guidelines For Sulphate, British Columbia., 2013.

MiningWatch Canada: Mining in Canada: The Bigger Picture., 2003.

Miranda-Trevino, J. C., Pappoe, M., Hawboldt, K. and Bottaro, C.: The importance of thiosalts speciation: review of analytical methods, kinetics and treatment, Crit. Rev. Environ. Sci. Technol., doi:10.1080/10643389.2012.672047, 2012.

Mohapatra, B. R., Gould, W. D., Dinardo, O. and Koren, D. W.: An Overview of the Biochemical and Molecular Aspects of Microbial Oxidation of Inorganic Sulfur

Compounds, CLEAN - Soil, Air, Water, 36(10-11), 823–829, doi:10.1002/clen.200700213, 2008.

Negeri, T., Paktune, A. D., Boisclair, M. and Kingston, D. M.: Characterization of Thiosalts Generation During Milling of Sulphide Ores., 1999.

O'Reilly, J. W., Dicinoski, G. W., Shaw, M. J. and Haddad, P. R.: Chromatographic and electrophoretic separation of inorganic sulfur and sulfur–oxygen species, Anal. Chim. Acta, 432(2), 165–192, doi:10.1016/S0003-2670(00)01389-1, 2001.

Rolia, E. and Barbeau, F.: Oxidation of thiosalts by SO2 plus air, charcoal plus air, and chlorine., 1979.

Schoeman, J. J. and Steyn, A.: Investigation into alternative water treatment technologies for the treatment of underground mine water discharged by Grootvlei Proprietary Mines Ltd into the Blesbokspruit in South Africa, Desalination, 133(1), 13–30, doi:10.1016/S0011-9164(01)00079-0, 2001.

Smyth, D. and Bain, J.: Application of Permeable Reactive Barriers for Treating Mine Drainage and Dissolved Metals in Groundwater, Waste Geotech., (March), 39–44, 2004.

Surender, D.: Active Neutralisation and Ameliorisation of Acid Mine Drainage, 182 pp., University of Western Cape., 2009.

Vadapalli, V. R. K., Gitari, M. W., Petrik, L. F., Etchebers, O. and Ellendt, A.: Integrated acid mine drainage management using fly ash, J. Environ. Sci. Health. A. Tox. Hazard. Subst. Environ. Eng., 47(1), 60–9, doi:10.1080/10934529.2012.629582, 2012.

Vadapalli, V. R. K., Klink, M. J., Etchebers, O., Petrik, L. F., Gitari, W., White, R. A., Key, D. and Iwuoha, E.: Neutralization of acid mine drainage using fly ash , and strength development of the resulting solid residues, S. Afr. J. Sci., 104(August), 2008.

Vongporm, Y.: Thiosalt Behaviour in Aqueous Media, 171 pp., Memorial University of Newfoundland., 2008.

Wasserlauf, M., Condy, A. and Wheeland, K. G.: Techno - Economic Evaluation of Thiosalt Treatment Processes., 1985.

Wasserlauf, M. and Dutrizac, J. E.: The Chemistry, Generation and Treatment of Thiosalts in Milling Effluents - A Non-Critical Summary of CANMET Investigations 1976-1982, CANMET Report 82-4E., 1982.

Wasserlauf, M. and Dutrizac, J. E.: An overview of CANMET's project on the chemistry, generation and treatment of thiosalts in milling effluents., 1983.

Wolkoff, A. W. and R. H. Larose: Separation and Detection of Low Concentrations of Polythionates by High Speed Anion Exchange Liquid Chromatography, Anal. Chem., 47(7), 1003–1008, 1975.

Chapter 3 : Review on Removal of Selenite and Selenate from Aqueous Media by Adsorption

Bhagya M.K. Range, Kelly A. Hawboldt

Faculty of Engineering and Applied Science, Memorial University of Newfoundland,

St John's, NL, Canada. A1B3X5

Abstract

Adsorption of selenite, Se(IV) and selenate, Se(VI) using various adsorbents is reviewed in this paper. Although selenium is an essential nutrient for living organisms, it can be toxic at higher concentrations. Adsorption is an effective and economic method of selenium treatment among other high cost treatment processes such as chemical precipitation, catalytic reduction, membrane filtration. This paper summarizes recent work on adsorbent types used in selenium oxy-anions (selenite and selenate) treatment such as activated carbon, biomass, biomass ash, iron oxides, aluminium based adsorbents, silica, apatite, rutile etc. The effect of pH (1.5 - 11.5), temperature (18 - 50 ^{o}C), initial concentration of selenium in the solution (0.8 - 100 mg/L), adsorbent dosage(0.5 - 20 g/L) on the sorption capacity is reviewed. Monolayer sorption capacities for selenium ranging from 0.081 mg/g to 126.99 mg/g of adsorbent have been reported. Further details on isotherm models, kinetic models and thermodynamic parameters such as Gibbs free energy change, enthalpy change, entropy change as well as techniques used in adsorbent characterization (XRD, SEM, FT-IR, BET surface area, point of zero charge pH, and analytical determination of selenium are also discussed.

3.1 Introduction

Selenium is an essential nutrient for plants, animals and humans, but can be toxic at higher concentrations. Selenium can exist in inorganic or organic forms (Sheha and El-Shazly, 2010). Inorganic forms of selenium are selenate, selenite, insoluble elemental selenium, selenides (Li et al., 2013). Selenium exists in several oxidation states, (-2, 0, +2, +4, +6). The most common selenium species in aqueous systems are selenite (SeO_3^{2-}) and selenate (SeO_4^{2-}) (Figure 3-1) (Li et al., 2013). Selenium species in the +4 (SeO_3^{2-}) state are considered to be more toxic than the selenium species in their +6 (SeO_4^{2-}) (Jordan et al., 2013b; Tuzen and Sarı, 2010). Mildly oxidizing and neutral pH conditions favor the formation of selenites. Acidic and reducing conditions reduce inorganic selenites to insoluble elemental selenium. High pH and oxidizing conditions favor the formation of selenates (World Health Organization, 2003) .

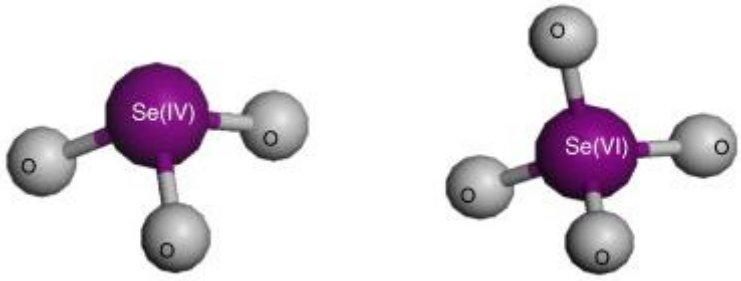

Figure 3-1: Molecular geometry of selenite (SeO_3^{2-}, Se(IV)) and selenate (SeO_4^{2-},Se(VI)) in aqueous medium (Aurelio et al., 2010)

Selenium is widely used in various industries such as electrolytic copper refining, insecticides manufacturing, production of glass, production of rectifiers and semiconductors, in xerography, solar cells and also as a catalyst in the synthesis of urea and urethane (Sheha and El-Shazly, 2010; Tuzen and Sarı, 2010). Selenium is also found in effluents from oil refineries and smelting plants, by products from fossil fuels combustion in thermal power stations (El-Shafey, 2007a). In the mining industry, the source of selenium is due to mine drainage.

Selenium is generally found in mining effluent waters in concentrations ranging from 3 µg/L to even above 12,000 µg/L (Envirogen Technologies, 2011). According to the guidelines set for selenium by the Ministry of Environment of British Columbia, Canada, the mean concentration of total selenium should not exceed 2 µg/L to protect freshwater and marine aquatic life (Environment protection Division Ministry of Environment Government of British Columbia, 2001). As per WHO Guidelines for Drinking Water Quality, maximum allowable concentration of selenium in drinking water is 10 µg/L (World Health Organization, 2003), while the US EPA sets a maximum contaminant level (MCL) of selenium in drinking water at 50 µg/L (US EPA, 1992).

3.2 Removal of Selenium from Aqueous Media

The selenium removal processes from water sources are coagulation, chemical precipitation, ion exchange, adsorption, reverse osmosis, catalytic reduction, bacterial treatment (El-Shafey, 2007a; Li et al., 2013; Nettem and Almusallam, 2013), evaporation,

membrane filtration (Tuzen and Sarı, 2010), phytoremediation (Gonzalez et al., 2010). The disadvantages of most popular treatment methods such as chemical precipitation, catalytic reduction, coagulation, membrane filtration and reverse osmosis, adsorption by activated alumina, are the high cost of reagents used, large volumes of sludge created, high membrane process energy consumption, interference of competing anions, low removal efficiency under alkaline conditions, need of highly selective materials that function across a wide range of pH, long time required for the removal process (El-Shafey, 2007a; Kongsri et al., 2013).

3.3 Studies on Selenium Removal by Adsorption

Adsorption by naturally available adsorbents can be a cost effective process in treatment of selenium in aqueous media. There have been a number of studies focused on adsorbents and selenium adsorption capacity to understand the sorption mechanisms, and to assess the ability of using these adsorbents to remove selenium oxyanions from industrial effluents. A summary of adsorbents used in the removal of Se(IV) and Se(VI) ions is given in the Table 3-1.

Table 3-1: List of different adsorbents used in Se(IV) and Se(VI) adsorption

Adsorbent	Details and Reference
Activated carbon derived adsorbents	Activated carbon (Bertolino et al., 2006; Kubota et al., 1995) Surface modified activated carbon (Tsoi and Leung, 2011)

	Granular and powdered activated carbon (Wasewar et al., 2009b) Metal loaded activated carbon (Afkhami and Madrakian, 2002; Dobrowolski and Otto, 2013; Latva et al., 2003a; Peraniemi and Ahlgrén, 1995) Iron oxide coated GAC adsorbents (Yan et al., 2011) Iron coated GAC adsorbents (Zhang et al., 2008, 2010)
Biomass and biomass ash	Aspergillus sp. J2 microorganism (Li et al., 2013) Ganoderma Lucidum Biomass (Nettem and Almusallam, 2013) Green algae (Cladophora hutchinsiae) (Tuzen and Sarı, 2010) Bagasse Fly Ash (Wasewar et al., 2009a) Rice husk ash (Gulipalli et al., 2011) Sulphuric acid treated peanut shells (El-Shafey, 2007a) Modified rice husk (El-Shafey, 2007b) Wheat bran (Hasan and Ranjan, 2010)
Cellulose coated with metal hydroxides	Cellulose fibre coated with Mg–$FeCO_3$ layered double hydroxides (LDHs) (Chen and An, 2012) Cellulose coated with lanthanum hydroxide (Chen et al., 2009)
Iron oxides	Maghemite (Jordan et al., 2013b) Magnetite (Jordan et al., 2009; Kim et al., 2012; Martínez et al., 2006; Missana et al., 2009) Iron oxyhydroxides (Parida et al., 1997)

	Iron oxides and hydroxides (Peak and Sparks, 2002) Iron oxide/hydroxide-based nanoparticles (Zelmanov and Semiat, 2013) Goethite-rich iron ore (Behera et al., 2012) Geothite and hydrous ferric oxide (Manceau and Charlet, 1994) Geothite (Rahnemaie et al., 2006) Geothite and hematite (Rovira et al., 2008) Hematite (Duc et al., 2006) Iron oxide nanomaterial (Gonzalez et al., 2012)
Alumina and Al based adsorbents	Alumina (Parida and Gorai, 2010; Wu et al., 2000) Aluminum oxide (Peak, 2006) Activated alumina (Su et al., 2008) Aluminium oxide coated sand (Kuan et al., 1998) Aluminum-based water treatment residuals (Ippolito et al., 2009)
Silica based adsorbents	Silica based nano hybrid maerials (Karatchevtseva et al., 2010) Silica (Sahin et al., 2003; Xiong et al., 2008)
TiO_2 based adsorbents	TiO_2, Rutile (Svecova et al., 2011) Nano TiO_2 (Zhang et al., 2009) Hydrous titanium oxide (Nilore, 1997) Anatase (Jordan et al., 2013a)
Other metal oxide (Mn,	Iron oxyhydroxide and Mn-dioxide (Balistrieri and Chao,

Mg, Al, Zn, Fe) based adsorbents	1990) Fe–Mn hydrous oxides (Szlachta and Chubar, 2013; Szlachta et al., 2012) Metal oxides (Sheha and El-Shazly, 2010) Binary oxide systems (Chan et al., 2009) Al-oxides, Fe-oxides (Bleiman and Mishael, 2010) Ion exchangers based on double Mg–Al hydrous oxides (Chubar, 2011) Mg/Fe hydrotalcite-like-compound (Das et al., 2002) Manganese nodule leached residues (Dash and Parida, 2007) Layered double hydroxides (Goh et al., 2008; Liu et al., 2009; Mandal et al., 2009) Mg–Al and Zn–Al layered double hydroxides (You et al., 2001) Manganese oxide nanomaterial (Gonzalez et al., 2011) Magnetic iron/manganese oxide nanomaterial (Gonzalez et al., 2010)
Apatites	Apatites and iron oxides (Duc et al., 2003) Nanocrystalline hydroxyapatite from fish scale waste (Kongsri et al., 2013) Hydroxyapatite (Monteil-Rivera et al., 2000)
Soils, granite, Other	Tropical soil (Goh and Lim, 2004)

	South Dakota Soils (Lee et al., 2011) Crushed granite (Jan et al., 2008) Thiourea-Formaldehyde Resin (Gezer et al., 2011) Mackinawite (FeS) (Han et al., 2011) Chitosan-clay composites (Bleiman and Mishael, 2010)

Activated carbon/charcoal is an efficient and economic method for adsorption of trace elements from various aqueous media (Latva et al., 2003a). Activated carbons have a large specific surface area and microporous structure, high adsorption capacity, surface reactivity due to presence of functional groups, and can be easily modified chemically or thermally to meet the requirements of a specific application (Dobrowolski and Otto, 2013). Selective adsorption of various ions by activated carbon occurs through ion exchange, precipitation, chelation and electrostatic attraction (coovalent bonds, van der waal's bonds etc.) (Dobrowolski and Otto, 2013).

Adsorption of selenium onto the untreated activated carbons does not give appreciable adsorption capacities (Latva et al., 2003a), however, chemically treated activated carbon increases adsorption capacities. e.g., (1) L-ascorbic acid can be used to reduce selenite to elemental Se and, hydrazine can be used to reduce both selenite and selenate prior to activated carbon addition (Bertolino et al., 2006); (2) modification of activated carbon surface with complexing reagents such as tetrabutylammonium hydroxide (TBAH) (Tsoi and Leung, 2011), and adding complexing reagents such as 3,3-diaminobenzidine (DAB)

(Izgi et al., 2006) in to the solution for selenium pre-concentration before adding the activated carbon has generated great results; (3) adsorption of selenium species directly by complex formation with metal coated/impregnated activated carbon also has been reported; Mg and Fe loaded activated charcoal (Latva et al., 2003b), Fe loaded activated carbon (Dobrowolski and Otto, 2013), Zr loaded activated charcoal (Peraniemi and Ahlgrén, 1995), Fe coated granular activated carbon (Zhang et al., 2008), Activated carbon treated with $FeCl_3$ (Wasewar et al., 2009b), Bagasse fly ash treated with $FeCl_3$ (Wasewar et al., 2009a).

Biomass ash and charcoal which obtained as byproducts from combustion of wood residue and other carbonaceous fuels in boilers at cogeneration plants in the pulp and paper industry may be a suitable adsorbent for Se(IV) and Se(VI) removal from aqueous media. Application of adsorbents derived from these waste biomass ash/char for selenium removal can be considered a very economical and eco-friendly method of treatment, if proven effective/successful.

3.4 Batch Equilibrium Studies on Se(IV) and Se(VI) Removal by Adsorption

This section reviews a number of batch equilibrium adsorption studies in detail to understand the effect of change in different conditions such as adsorbent dosage, solution pH, initial concentration of selenium, contact time and temperature on the removal of selenite/ selenate by different types of adsorbents.

Adsorption percentage and adsorption capacity have been calculated using following equations.

$$\text{Adsorption capacity}\left(\frac{mg}{g}\right) = \frac{(C_i - C_e)\ x\ V}{m} \qquad (3\text{-}1)$$

$$\text{Adsorption \%} = \frac{(C_i - C_e)\ x\ 100}{C_i} \qquad (3\text{-}2)$$

C_i = Initial concentration of adsorbate (mg/L)

C_e = Equilibrium adsorbate concentration (mg/L)

V = Volume of the solution (L)

m = Mass of the adsorbent(g)

3.4.1 Selenite, Se(IV)

In Nettem, 2013, Ganoderma lucidum biomass was used as an adsorbent (Nettem and Almusallam, 2013). The experimental conditions covered pH 2-8 (solution), adsorbent dosage 1- 10 g/L, initial selenite concentration 100 mg/L, contact time 5-180 minutes, temperature 293 K, mixing speed 250 rpm, 100 mL solutions. The adsorption increased with solution pH from 2 to 5 and then decreased with further increase in pH up to 8 (Figure 3-2). An optimum pH was selected as pH 5. As the biosorbent dosage was increased from 1 to 7 g/L at 293 K sorption increased from 19.9 % to 97.13%. Beyond this dose there were no noticeable increase in biosorption percentage (Figure 3-2). Equilibrium was achieved at 90 minutes at all temperatures (293, 303, 313 K). As

temperature increased from 293 to 303 K, the biosorption decreased from 97% to 74%. This confirms that biosorption by Ganoderma lucidum biomass is kinetically controlled by an exothermic process.

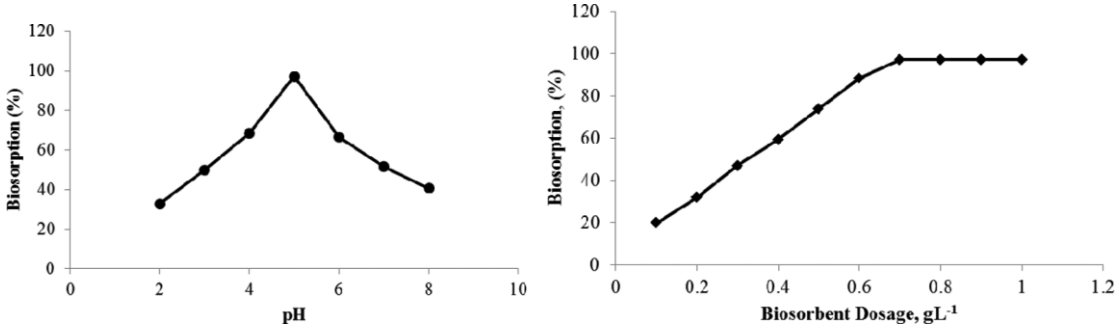

Figure 3-2: Effect of pH and biosorbent dosage on biosorption of selenite on to Ganoderma lucidum biomass (Nettem and Almusallam, 2013)

Li et al., (2013) investigated Aspergillus sp. J2 microorganism as sorption medium. Solution pH was varied from 2 - 11, adsorbent dosage 20 g/L, initial selenite concentration 5 mg/L, contact time 18 h, temperature 28 ^{o}C, and mixing speed 120 rpm. Selenite sorbed (mg/g) was not affected by the initial solution pH in the range 4 - 10.7, hence electrostatic attraction is not the adsorption mechanism in this range. Sorption of selenite decreased when initial pH was less than 3.8 and when initial pH is greater than 10.7. Therefore, pH 5.5 was selected as the optimum pH for further experiments. Equilibrium sorption increased when the initial selenite concentration was increased from 5 mg/L to 10 mg/L and equilibrium was reached after 15 h. Biosorption increased with

temperature (18, 28, 38 ^{o}C). The higher uptake at higher temperature indicates the selenium biosorption by Aspergillus sp. J2 is endothermic in nature (Li et al., 2013).

In Tuzen and Sarı (2010) dead green algae (cladophora hutchinsiae) biomass was tested at solution pH of 2 - 8, adsorbent dosage 1-20 g/L, initial selenite concentration 10 mg/L, contact time 5 - 120 min, temperature 20 ^{o}C, mixing speed 120 rpm. The maximum sorption of 96% was achieved at pH 5 and lowest (70%) at pH=2 (Figure 3). The high sorption at pH of 5 is due to the abundance of protons allowing more reduction of Se(IV) to elemental selenium on the adsorbent surface. Below pH 3.5, selenius acid dominates (H_2SeO_3) and this neutral species cannot undergo electrostatic interaction with the biosorbent, hence the low sorption at pH 2. Sorption significantly increases with the increase in biomass dose up to 8 g/L due to availability of more sorption sites (sorption at a dose of 8 g/L was 96% and at 20 g/L it increased to 98%) (Figure 3-3). The sorption was fast, equilibrium was achieved in 60 min of contact time at the studied temperatures (20, 30, 40, 50 ^{o}C). Sorption decreased from 96% to 60% with the increase in temperature from 20 to 50 ^{o}C. The decrease in adsorption with increase in temperature may be due to, exothermic nature of selenium biosorption onto C.hutchinsiae biomass; tendency of selenium ion escaping from solid phase to the bulk phase; destructing the active sites or deactivating the adsorbent surface at high temperature; weakness of biosorptive forces between the active sites on the adsorbent and the adsorbate (Tuzen and Sarı, 2010).

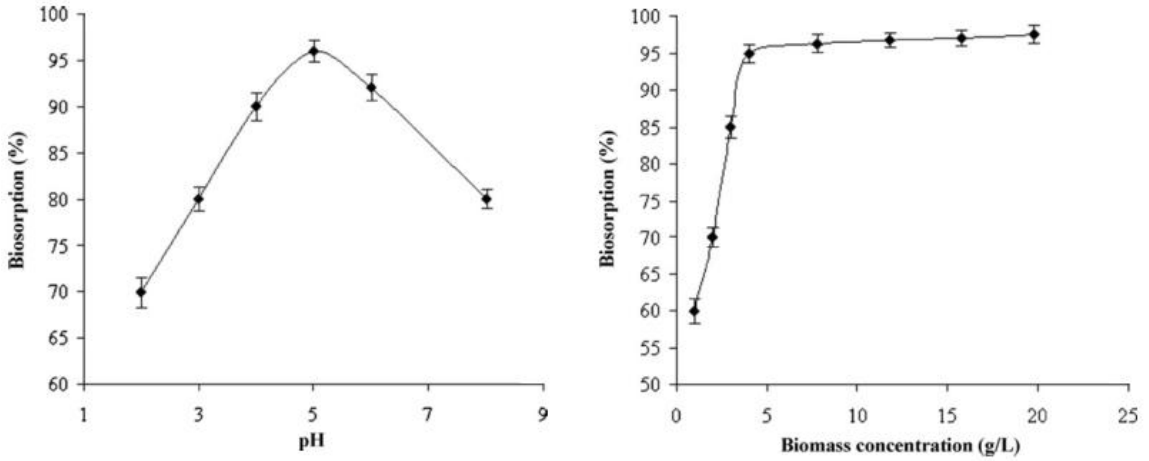

Figure 3-3: Effect of pH and adsorbent dose (biomass concentration) on sorption of selenite onto Cladophora hutchinsiae biomass (Tuzen and Sarı, 2010)

Sheha and El-Shazly (2010) used metal oxides, iron and silicon oxides (Fe_2O_3 and SiO_2) as sorbents. The pH was varied from 2-11, adsorbent dosage 10 g/L, initial selenite concentration 20 mg/L, contact time 6 h, temperature 29 +/- 1 ^oC , 100 mL solutions. Over a pH range of 2-8 high removal efficiency was achieved and the efficiency decreased at pH values higher than 8 (Figure 3-4). Therefore, pH value of 4 +/- 0.5 was selected for further experiments. The adsorption process was very fast and more than 90% sorption was achieved after 3 h (89% using SiO_2 and 94% using Fe_2O_3). The adsorption capacity decreased with the increase in temperature (303, 313, 323 K). This was due to change in surface properties of the adsorbent, solubility of the solute species, exothermic nature of the adsorption process (Sheha and El-Shazly, 2010).

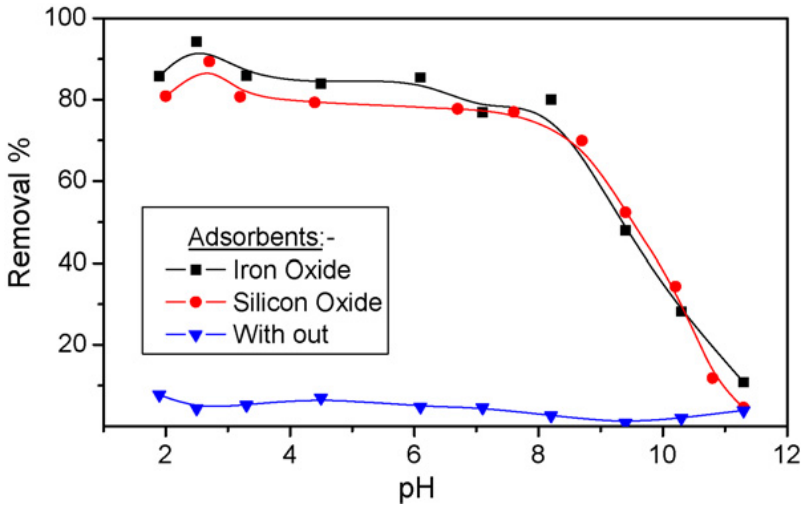

Figure 3-4: Effect of pH on sorption of selenite on to iron and silicon oxides (Fe_2O_3 and SiO_2) (Sheha and El-Shazly, 2010)

El-Shafey (2007) treated peanut shells with sulphuric acid and tested sorption over a pH range of 1.5-7, adsorbent dosage 2 g/L, initial selenite concentration 25-250 mg/L, contact time 330 h, temperature 25 ^{o}C, mixing speed 100 rpm, 50 mL solutions. Se(IV) sorption increased at low pH values but decreased with increase in initial Se(IV) concentration. Using wet sorbent at 50 mg/L initial concentration, Se(IV) sorption % was 41.7% at pH 1.5 and 21% at pH 5 and, at 100 mg/L initial concentration, sorption % was 31.9% at pH 1.5 and 17% at pH 5. Dry sorbent gives less sorption % of Se(IV) at the same conditions. The maximum sorption was achieved by the wet sorbent at 25 mg/L initial concentration which was 58.2% at 25 ^{o}C and increased up to 62.5 % at 45^{o}C. At 100 mg/L Se(IV) concentration and a pH of 1.5, equilibrium was reached within 260 h for wet sorbent and within 330 h for dry sorbent. Increased adsorption with increase in temperature from 25 - 45 ^{o}C was noticed, which may be due to the expansion of

adsorption sites with temperature (El-Shafey, 2007a). In a related study (El-Shafey, 2007b), carbonaceous sorbent was prepared from rice husk via sulphuric acid treatment. The pH was varied from 1.5-7, adsorbent dosage 2 g/L, initial selenite concentration 100 mg/L, contact time 200 h, temperature 25 ^{o}C, mixing speed 100 rpm, 50 mL solutions. As in the previous work, the sorption was high at low pH values, 1.5 and decreased with increase in pH until pH of 7. The final pH of the solutions increased which may be due to the proton consumption during the adsorption process. In general the wet adsorbent performed better than the dry adsorbent and the quilibrium sorption was reached within ~ 200 h at pH 1.5. Higher sorption was associated with increases in temperature (25,35,45 ^{o}C).

In Kongsri et al. (2013), nanocrystalline hydroxyapatite from fish scale waste (FHAp) was used as an adsorbent. pH was varied from 3 to 10, adsorbent dosage 4 g/L, 25 mL solutions, initial selenite concentration 0.01 mg/L, contact time 90 mins, temperature 30 ^{o}C, and mixing speed 250 rpm. Adsorption decreased at pH above 6. The pH at the point of zero charge was determined as 7.86, hence the surface becomes positively charged at pH below this pH and negatively charged above this pH. Adsorption decreases at high pH, due to repulsion forces between the negatively charged surface of FHAp nanopowders. As dosage was changed from 0.02-0.1 g the adsorption increased rapidly and came to a maximum at 0.1 g. This may be due to the increase in the number of adsorption sites with the increase in the dosage. The maximum value of equilibrium sorption capacity was at 0.02 mg/L initial selenite concentration at pH 5 and 0.08 g

adsorbent dosage which was 1.58 mg/g. At 0.01 mg/L initial selenium concentration, adsorption reached equilibrium at 90 mins for FHAp, the rate of adsorption was very fast initially and decreased gradually until equilibrium. This is likely due to selenium being adsorbed on exterior surfaces of the adsorbent initially and then diffusion of selenium into the pores and adsorption at the interior surface of the adsorbents (Kongsri et al., 2013).

3.4.2 Selenate, Se(VI)

Recently, Dobrowolski and Otto (2013) used activated carbon impregnated with iron(III) nitrate(V) for Se(VI) adsorption. The pH was varied from 1.3 to 11.5, adsorbent dosage 1-10 g/L, initial selenite concentration 100 mg/L, contact time 20 minutess, temperature 25 +/- 1 ^{o}C, mixing speed 250 rpm. The sorption capacity increased with pH until a pH of 4.8 and decreased as pH exceeded 5.0. pH 3.2 was selected as optimum for activated carbon sample labelled 10C which was prepared by impregnating with 10% $Fe(NO_3)_3$ solution and heating at 200 ^{o}C. Equilibrium was achieved after 20 min at a pH 3.2 and 25 ^{o}C with 20.96 mg/L initial concentration for 10C activated carbon (Dobrowolski and Otto, 2013).

Jordan et al. (2013), studied anatase TiO_2 at a solution pH range of 3.5 - 7 (Figure 3-5), adsorbent dosage 0.5 g/L, an initial selenate concentration of 10^{-5} mol/L (0.8 mg/L), contact time 48 h, and range of temperature 293- 333 K. Se(VI) sorption was maximized at acidic conditions and decreased as solution pH was increased. The isoelectric point (pH_{IEP}) of anatase at 298 K is at pH 6.3 and decreased with temperature (to pH 5.5 at 333

K). At a pH lower than the pH_{IEP}, sorption of negatively charged Se(VI) ions on to positively charged surface groups of anatase is promoted. Sorption decreased with an increase in temperature therefore the process is exothermic (Jordan et al., 2013a).

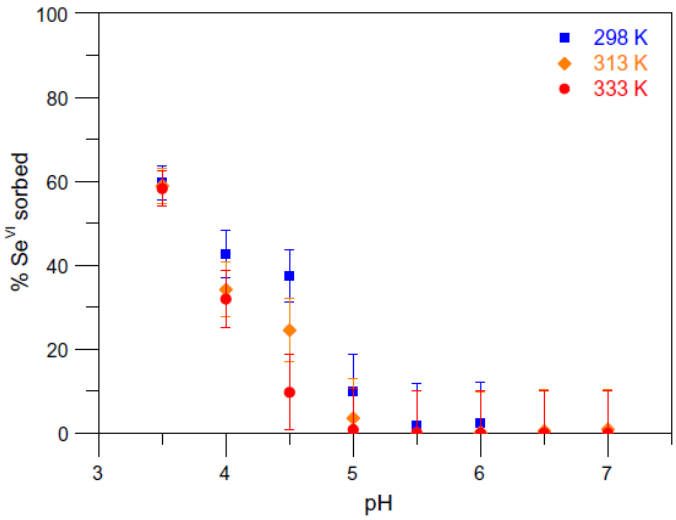

Figure 3-5: Effect of pH on sorption of selenate, Se(VI) on to anatase (Jordan et al., 2013a)

The results of these equilibrium studies indicate the type and composition of the adsorbent is critical in the sorption capacity and operating conditions (e.g. pH and temperature). However, it is clear that pH, electrostatic properties, mineral compositions etc. of the adsorbent are critical factors in designing an adsorbent process.

3.5 Adsorbent Characterization

Physicochemical characterization of adsorbents before and after selenium adsorption have been carried out using the following techniques in the above discussed studies; BET specific surface area and total pore volume (Jordan et al., 2013a; Kongsri et al., 2013), point of zero charge pH (pH_{PZC}) (Sheha and El-Shazly, 2010), SEM-EDX (Scanning Electron Microscopy with Energy Dispersive X-Ray detector) (Dobrowolski and Otto, 2013; El-Shafey, 2007a, 2007b; Kongsri et al., 2013; Nettem and Almusallam, 2013), FT-IR(Fourier Transform Infrared Spectroscopy) (Jordan et al., 2013a; Kongsri et al., 2013; Li et al., 2013; Nettem and Almusallam, 2013; Tuzen and Sarı, 2010), XRD (X-ray Diffraction) (El-Shafey, 2007a, 2007b; Jordan et al., 2013a; Kongsri et al., 2013), TGA (Thermal Gravimetric Analysis) (Kongsri et al., 2013) and XPS (X-ray Photoelectron Spectroscopy) (Dobrowolski and Otto, 2013). The results of the characterizations are outlined in subsequent sections.

3.6 Sorption Mechanism

Biosorption of Se(IV) ions on to Aspergillus sp. J2 microorganism was slow which may be due to intra-particle diffusion. FT-IR results indicate that sulfonyl and sulfonamide groups present in the bioadsorbent may have been affected by Se(IV) ions. Since, sulphur and selenium compound ions have similar chemical properties and binding behaviour, they can isomorphously replace each other (Li et al., 2013).

SEM (Figure 3-6) and FT-IR analysis confirmed that presence of amino, carboxyl, hydroxyl and carbonyl groups in the Ganoderma lucidum biomass. These groups are responsible for Se(IV) removal. The isoelectric point of the treated biomass shifted to pH 4.7 from pH 4.2. This shift can be attributed to the fact that at pH 4.7 specific sorption of selenite occurs on the biosorbent (Nettem and Almusallam, 2013).

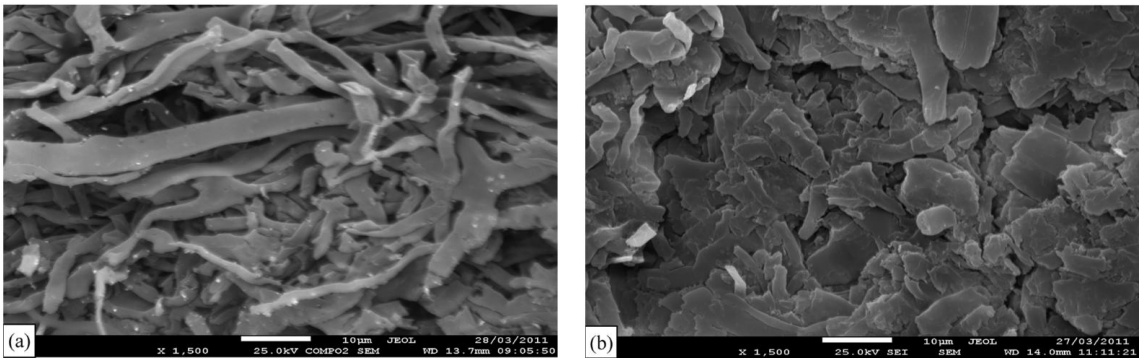

Figure 3-6: SEM images of (a) original samples of Ganoderma lucidum biomass (b) Se(IV) loaded Ganoderma lucidum biomass (Nettem and Almusallam, 2013)

Marine algae (seaweeds) have been reported to have high metal binding capacities due to the presence of polysaccharides, proteins or lipid on the cell wall which contains functional groups such as amino, hydroxyl, carboxyl and sulphate. These functional groups can act as binding sites for metals. FT-IR analysis was used to understand the nature of possible cell-metal ion interactions in the adsorption of Se(IV) ions onto dead green algae (cladophora hutchinsiae) biomass. The resulting shifts in stretching vibration bands of carboxyl, hydroxyl and amide groups after biosorption indicate that biosorption may have been occurred due to the chemical interactions between the metal ions and the

hydrogen atoms of carboxyl, hydroxyl and amide groups of biomass (Tuzen and Sarı, 2010).

Ligand-exchange interations and/or inner sphere complexation (covalent binding) was considered as the method of Se(IV) immobilization onto the surface of iron and silicon oxides (Fe_2O_3 and SiO_2) in the study conducted by Sheha and El-Shazly(2010). The specific surface areas of SiO_2 and Fe_2O_3 are 198.5 and 98.2 m^2/g respectively. Generally, the surface of silica is very acidic and has very low point of zero charges (pH_{PZC} of 2 - 3), therefore below this low pH, ionized surface sites of silica are positive. Iron oxides are also good adsorbents for selenite and selenate as their pH_{PZC} is generally around pH 8 - 10 making them positively charged over a wide range of pH. Measured pH_{PZC} values in this study for SiO_2, Fe_2O_3 are 3.1 and 6.4 respectively. Therefore, the surface sites are highly protonated at low pH which favors adsorption of Se(IV) and Se(VI) anions (Sheha and El-Shazly, 2010).

In the study of Se(IV) ions sorption onto sulphuric acid treated peanut shell, the sorbent acidity, cation exchange capacity (CEC) and surface functionality (by Boehm titrations) increased after the reaction with the Se(IV) in the solution. This indicates oxidation processes taking place on the sorbent surface. The surface area of the dry sorbent was 72 m^2/g and the pH of the sorbent before reaction was pH 2.4. SEM and XRD studies confirmed the presence of elemental selenium particles on the sorbent surface as a result of Se(IV) reduction into Se(0) which is accompanied by the surface oxidation (Figure 3-

7) (El-Shafey, 2007a). In the study of Se(IV) ions sorption onto carbonaceous sorbents prepared from rice husk via sulphuric acid treatment, similar results were reported. The surface area of the dry sorbent (modified rice husk) was 66 m^2/g and pH of the sorbent before reaction was pH 2.65 (El-Shafey, 2007b).

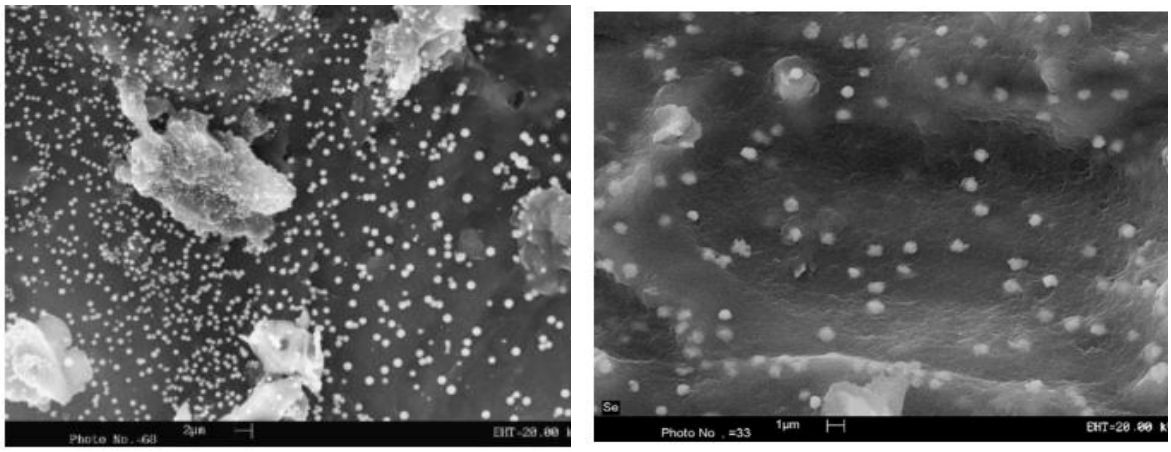

Figure 3-7: SEM images of precipitated elemental selenium on the sulphuric acid treated peanut shell and modified rice husk adsorbents (El-Shafey, 2007a, 2007b).

In sorption onto nanocrystalline hydroxyapatite from fish scale waste (FHAp) the BET specific surface area of FHAp was 110.56 m^2/g. In the acidic solution, adsorbent surface is positively charged, hence adsorption is promoted by ligand exchange. The possible interactions between selenite and FHAp can be surface complexation, dissolution and precipitation, ion exchange, electrostatic interaction (Kongsri et al., 2013).

When 10C activated carbon impregnated with 10% $Fe(NO_3)_3$ solution is heated at 200 ^oC, the resulting adsorbent had a BET surface area of 1170 m^2/g and point of zero charge

(pH_{PZC}) is 4.07. Adsorption reactions of selenate with iron oxide minerals and amorphous iron hydroxide coatings which are naturally occurring may be significant in soils that are slightly acidic (with pH_{PZC} of 6-7) (Dobrowolski and Otto, 2013).

ATR (Attenuate Total Reflectance)-FTIR results confirmed the formation of outer sphere complexes with no significant structural changes in the study of Se(VI) sorption onto Anatase ($TiO_{2)}$. BET surface area of anatase was 267 m^2/g. At pH lower than the isoelectric point(pH_{IEP}), the positively charged surface groups of anatase and negatively charged selenate ions enhances adsorption zeta potential and the isoelectric point of anatase were shifted to lower values at higher temperatures, which may have caused the decrease in selenium(VI) adsorption. This decrease in adsorption may also be due to changes in the speciation of selenium in the aqueous solution; exothermic nature of the sorption process; instability of complexes formed in adsorption of selenate onto anatase at high temperatures hence releasing the selenate ions into the solution; decrease of available absorption sites on anatase due to changes in the adsorbent such as dissolution (Jordan et al., 2013a).

3.7 Thermodynamic Parameters

The ΔG (Gibbs free energy change of adsorption), ΔH (enthalpy change), ΔS (entropy change) are typically assessed in all processes to determine the thermodynamic nature of the process (e.g. tendency to occur at given conditions).

The Distribution Coefficient at different temperatures can be calculated using the following relations;

$$K_D = \frac{q_e}{C_e} \qquad (3\text{-}3)$$

K_D = Distribution coefficient

q_e = Amount of selenium adsorbed by the adsorbent at equilibrium

C_e = Equilibrium concentration of selenium in the solution

The values of free energy change (ΔG) at different temperatures can be calculated from the following relation:

$$\Delta G = -RT\ ln\ K_D \qquad (3\text{-}4)$$

R = Universal gas constant (8.314 $Jmol^{-1}K^{-1}$)

T = Temperature(K)

K_D = Distribution coefficient

Van't Hoff equation can be applied to calculate the enthalpy change (ΔH) and entropy change (ΔS). ΔS and ΔH can be calculated from the intercept and slope of the linear plot of ln K_D versus 1/T .

$$ln\ K_D = \frac{\Delta S}{R} - \frac{\Delta H}{R} \times \frac{1}{T} \qquad (3\text{-}5)$$

When Ganoderma lucidum was used as an adsorbent (Nettem and Almusallam, 2013), the ΔG at 293 K was -3.728 $kJmol^{-1}$ indicating the adsorption process will occur at these condition. Positive ΔG values obtained at 303, 313 K of 0.224 kJ/mol and 2.308 kJ/mol indicate the process is not thermodynamically favored. Overall for the adsorption on iron and silicon oxide the ΔG were negative, however the values increased from -17.61 to -15.88 kJ/mol for iron oxide and from -16.76 to -15.56 kJ/mol for silicon oxide as temperature increases, which indicates that lower temperatures favors Se(IV) adsorption (Sheha and El-Shazly, 2010). In sorption using anatase, ΔG values increased with increasing pH and temperature which indicates that at high pH and temperature values adsorption process is less favorable and less feasible (Jordan et al., 2013a).

In all three studies discussed above, calculated ΔH values were negative which indicates the exothermic nature of adsorption. The calculated ΔS values were also negative which indicates the reduced degree of randomness at the adsorbent/solution interface.

3.8 Adsorption Isotherm Modelling

Isotherm constants indicate the surface properties and affinity of the adsorbent. These constants can be used to compare sorption capacities of different adsorbents. The equilibrium sorption behaviour can be characterized via different isotherm models including; Langmuir isotherm model, Freundlich isotherm model and Dubinin-Radushkevich isotherm model. The basic assumption of the Langmuir model is that sorption takes place at specific homogeneous sites within the sorbent. The Freundlich model assumes a heterogeneous adsorption surface and active sites with different energies while the Dubinin–Radushkevich isotherm model is used to determine the nature of adsorption process as physical or chemical.

Langmuir isotherm model $$q_e = \frac{q_m K_L C_e}{1+K_L C_e} \quad (3\text{-}6)$$

q_e = Amount of metal adsorbed per unit weight of adsorbent (mg/g dry weight)

C_e = Equilibrium Se(IV) concentration in the solution (mg/L)

K_L = Langmuir constant related to the affinity of the binding sites (L/mg)

q_m = Maximum metal uptake or monolayer biosorption capacity of the sorbent (mg/g)

Freundlich isotherm model $$q_e = K_f C_e^{\frac{1}{n}} \quad (3\text{-}7)$$

K_f = Constant relating to biosorption capacity

1/n = Empirical parameter relating to biosorption intensity, varies with the heterogeneity of material

Dubinin-Radushkevich isotherm model $\ln q_{ed} = \ln q_{max} - \beta\varepsilon^2$ (3-8)

q_{ed} = Amount of metal ions sorbed per unit weight of biomass (mol/g)

q_{max} = Maximum biosorption capacity (mol/g)

β = Activity coefficient related to biosorption mean free energy(mol^2/J^2)

ε = Polanyi potential ; $\varepsilon = RT \ln(1+1/C_e)$

Both the Langmuir and Freundlich isotherm models were very good fits for adsorption onto Ganoderma lucidum biomass. Monolayer adsorption capacity from Langmuir isotherm was 126.99 mg/g. The 1/n value calculated from the Freundlich isotherm model was 0.599, which indicates that biosorption is favorable (Nettem and Almusallam, 2013). The Langmuir model gives a better fit than the Freundlich model for the investigation of Aspergillus sp J2 as an adsorbent. Sorption capacity increased with the concentration and reached a plateau at the initial selenite concentration of 8 mg/L. Maximum uptake capacities from Langmuir model (q_m) at 18, 28, 38 ^oC were 4.14 mg/g, 5.33 mg/g, 5.67 mg/g respectively. K_L values increased with temperature which indicates the strong affinity of Aspergillus sp. J2 for selenite at higher temperatures (Li et al., 2013). The Langmuir isotherm model was also a good fit for sorption onto C.hutchinsiae biomass. The maximum biosorption capacity (q_m) was 74.9 mg/g. The 1/n value was found to be

0.53 which indicates favorable biosorption at the studied conditions. The Dubinin-Radushkevich isotherm model also showed a good fit to the equilibrium data. Calculated mean biosorption energy value of 10.9 kJ/mol from the D-R model indicates the involvement of chemical ion-exchange (chemisorption) in the sorption of C.hutchinsiae biomass (Tuzen and Sarı, 2010).

The Langmuir isotherm constants (q_m and K_L) for the sorption onto iron oxide and silicon oxide were 8.47 mg/g Fe_2O_3 and 7.06 mg/g SiO_2 at 303 K. The Langmuir constants decreased with increase in temperature indicating the exothermic nature of adsorption process. The calculated separation factor values are less than unity indicating adsorption is favoured. This was further strengthened by the fact the 1/n values were between 0.69 and 0.99. The K_f values of adsorption of Se(IV) ions onto iron oxide are higher than the values obtained for silicon oxide. i.e. iron oxide has greater adsorption tendency than the silicon oxide. The mean free energy of adsorption (E), calculated from the Dubinin-Radushkevich isotherm model was in the range 5.72 - 7.29 kJ/mol for both metal oxides. Since the values are less than 8 kJ/mol, it can be concluded that the overall adsorption mechanism is physical (Sheha and El-Shazly, 2010).

The Langmuir isotherm model was the best fit for Se(IV) sorption to sulphuric acid treated peanut shell with a maximum sorption capacity for 42.96 mg/g for wet sorbent and 32.15 mg/g for dry sorbent at 45^{o}C. Separation factor values were within 0.11 - 0.66 indicating good adsorption (El-Shafey, 2007a). The sorption of Se(IV) onto modified rice

husk also fitted well with the Langmuir isotherm model. Higher sorption was achieved with an increase in temperature. Monolayer sorption capacity ($q_{m)}$ was 34.13 mg/g for dry sorbent and 40.92 mg/g for wet sorbent at 45 ^{o}C. The 1/n values calculated from the Freundlich isotherm model vary between 0.4 - 0.5 which indicates a favourable adsorption (El-Shafey, 2007b).

Se(IV) sorption onto FHAp (Fish scale hydroxyapapite) followed the Freundlich isotherm model. The monolayer adsorption capacity for FHAp was 1.94 mg/g and 1/n values for was 0.32 which indicates high affinity of Se(IV) towards the FHAp nanocrystals (Kongsri et al., 2013).

Activated Carbon sample labeled 10C impregnated by iron(III) nitrate(V) follows the Langmuir isotherm. The maximum adsorption capacity was 21 mg/g (Dobrowolski and Otto, 2013).

The monolayer sorption capacities (q_m) of Se(IV) and Se(VI) sorption onto various adsorbents are listed in Table 3-2 with the specific experimental conditions (pH, Temperature).

Table 3-2: Se(IV) and Se(VI) monolayer sorption capacities (q_m) of various adsorbents

Selenium species	Adsorbent	q_m (mg/g)	pH, Temperature
Selenite, Se (IV)	Ganoderma lucidum	126.99	pH 5, 20 ^{o}C

(Nettem and Almusallam, 2013)	biomass		
Selenite, Se (IV) (Li et al., 2013)	Aspergillus sp. J2 microorganism	4.14	pH 5.5, 18 ^{o}C
Selenite, Se (IV) (Li et al., 2013)	Aspergillus sp. J2 microorganism	5.67	pH 5.5, 38 ^{o}C
Selenite, Se (IV) (Tuzen and Sarı, 2010)	dead green algae (cladophora hutchinsiae) biomass	74.9	pH 5, 20 ^{o}C
Selenite, Se (IV) (Sheha and El-Shazly, 2010)	Metal oxides -Fe_2O_3	8.47	pH 4+/- 0.5, 30 ^{o}C
Selenite, Se (IV) (Sheha and El-Shazly, 2010)	Metal oxides - SiO_2	7.06	pH 4+/- 0.5, 30 ^{o}C
Selenite, Se (IV) (El-Shafey, 2007a)	Sulphuric acid treated peanut shell, wet sorbents	42.96	pH 1.5, 45^{o}C
Selenite, Se (IV) (El-Shafey, 2007a)	Sulphuric acid treated peanut shell, dry sorbents	32.15	pH 1.5, 45^{o}C
Selenite, Se (IV) (El-Shafey, 2007b)	Modified rice husk, wet sorbent	40.92	pH 1.5, 45^{o}C
Selenite, Se (IV)	Modified rice husk, dry	34.13	pH 1.5, 45^{o}C

(El-Shafey, 2007b)	sorbent		
Selenite, Se (IV) (Kongsri et al., 2013)	nanocrystalline hydroxyapatite from fish scale waste(FHAp)	1.94	pH 5, 30 ^{o}C
Selenite, Se (IV) (Kuan et al., 1998)	Aluminium oxide coated sand	1.08	pH 4.8
Selenite, Se (IV) (Lo and Chen, 1997)	Iron oxide coated sand	1.32	pH 4
Selenite, Se (IV) (Hasan and Ranjan, 2010)	Wheat bran	0.089	pH 2, 20 ^{o}C
Selenite, Se (IV) (Zhang et al., 2008)	iron-coated granular activated carbons	2.58	pH 5+/- 0.3 , 25 ^{o}C
Selenite, Se (IV) (Gulipalli et al., 2011)	$FeCl_3$ coated rice husk ash	0.28	pH 2 - 3, 20 ^{o}C
Selenate, Se (VI) (Dobrowolski and Otto, 2013)	AC impregnated by iron(III) nitrate(V) -10C	21	pH 3.2, 25 ^{o}C
Selenate, Se (VI) (Kuan et al., 1998)	Aluminium oxide coated sand	0.92	pH 4.8
Selenate, Se (VI) (Lo and Chen, 1997)	Iron oxide coated sand	1.11	pH 6.5

Selenate, Se (VI) (Hasan and Ranjan, 2010)	Wheat bran	0.081	pH 2, 20 ^{o}C

3.9 Adsorption Kinetic Modelling

The rate of adsorption is typically determined by comparing experimental data to the following models: pseudo first order kinetic model (Lagrangian), pseudo second order kinetic model, intra-particle diffusion model (Webber-Morris) and liquid film diffusion model. The models are outlined below:

Pseudo first order kinetic model $$\log(q_e - q_t) = \log q_e - \frac{K_1 t}{2.303} \quad (3\text{-}9)$$

Pseudo second order kinetic model $$\frac{t}{q_t} = \frac{1}{K_2 q_e^2} + \frac{t}{q_e} \quad (3\text{-}10)$$

Intra-particle diffusion model $$q_t = K_{id} t^{0.5} + C \quad (3\text{-}11)$$

Liquid film diffusion model $$\log(1 - F) = -\frac{K_{fd} t}{2.303} \quad (3\text{-}12)$$

q_e = Metal adsorbed on the surface at equilibrium (mg/g)

q_t = Metal adsorbed on the surface at time t (mg/g)

K_1 = First order rate constant of adsorption (1/min)

K_2 = Pseudo-second order rate constant. (g/mg min)

K_{id} = Rate constant of intra particle diffusion(mg/g.min0.5)

h = Initial adsorption rate $K_2 q_e$ in the pseudo second order model

C = Constant of intra-particle diffusion model relating to boundary layer effect.

F = Fractional attainment of equilibrium (q_t/ q_e)

K_{fd} = Film diffusion rate constant

Li et al. (2013) conducted kinetic studies with Se(IV) concentrations of 5 mg/L and 10 mg/L. Both pseudo first and second order kinetic models mentioned to have given good fits to the data. Calculated equilibrium adsorption values with 5 and 10 mg/L initial selenite concentrations were 4.03 and 4.84 mg/g based on the pseudo first order model and 5.32 and 6.31 mg/g based on the pseudo second order model. Experimental equilibrium sorption data at 5 and 10 mg/L initial selenite concentrations were not given (Li et al., 2013).

When Ganoderma lucidum biomass was used as adsorbent, a pseudo first order kinetic model gave the best fit (highest correlation coefficients, R^2) compared to the pseudo second order and the intra-particle diffusion models at all three temperatures studied 293, 303, 313 K (Nettem and Almusallam, 2013).

In a study of C.hutchinsiae biomass, the pseudo second order kinetic model provided a good correlation than the pseudo first order kinetic model. Experimental values for equilibrium sorption capacities obtained at 20, 30, 40, 50 ^{o}C was 3.08, 2.88. 2.76, 2.54 mg/g and the equilibrium sorption values calculated based on the pseudo second order

model were 3.02, 2.85, 2.70 and 2.50 respectively at each temperature (Tuzen and Sarı, 2010).

Sorption kinetic data from the study of Se(IV) adsorption onto carbonaceous sorbent prepared from rice husk via sulphuric acid treatment also followed the pseudo second order model (El-Shafey, 2007b).

The equilibrium sorption capacity (q_e) for sorption of Se(IV) with SiO_2 was 1.796 mg/g and with Fe_2O_3 was 1.853 mg/g. A pseudo second order model was a very good fit and suggested that chemisorption, through sharing or exchange of electrons between Se(IV) species and the metal oxides, is the rate limiting step. Analysis using the liquid film diffusion model confirmed that the sorption process was not solely controlled by diffusion through the liquid film surrounding the solid adsorbents due to the non zero intercepts from the model graph for both oxides (Sheha and El-Shazly, 2010).

Fish scale hydroxyapapite (FHAp) as an adsorbent showed pseudo second order kinetics. Experimental equilibrium sorption capacity was 1.59 mg/g and calculated sorption capacity from the pseudo second order kinetic model was 1.61 mg/g. The intra-particle diffusion plot showed that both surface adsorption (boundary layer effect) and the intra-particle diffusion (pore diffusion) impacted adsorption of Se(IV) on to FHAp. Also, the value of intra particle diffusion constant (C) was higher for FHAp which indicates that the surface sorption of selenium on the adsorbent is significant (Kongsri et al., 2013).

Activated carbon sample labeled 10C, impregnated by iron(III) nitrate(V) also showed a good fit to the pseudo second order model (Dobrowolski and Otto, 2013).

3.10 Analytical Determination of Selenium in Aqueous Media

The key in determining the effectiveness of the adsorption of selenium is analyzing the treated effluent and/or the adsorbent material. This is challenging given both the low levels of Se in mining wastewaters and the regulatory limit. Hydride generation - atomic absorption spectrometry (HG-AAS) is a widely used method in analytical determination of Se(IV) and Se(VI) in aqueous media (Nettem and Almusallam, 2013; Sheha and El-Shazly, 2010; Tuzen and Sarı, 2010). Kongsri et al., 2013 used flow injection-hydride generation equipped with quartz tube furnace atomic absorption spectrometry (QTFAAS) with AAWinlab software for Se(IV) determination (Kongsri et al., 2013). Carbon slurry sampling graphite furnace atomic absorption spectrometry technique (GFAAS) and standard calibration method has been used for Se(VI) determination (Dobrowolski and Otto, 2013). Ion chromotography has also been used in Se(IV) and Se(VI) determination (Kuan et al., 1998). UV-visible spectrophotometry is another commonly used method that can be used for Se(IV) determination (El-Shafey, 2007a, 2007b; Li et al., 2013). Analyses using Inductively coupled plasma mass spectrometry (ICP-MS) (Gonzalez et al., 2010) and inductively coupled plasma optical emission spectrometry (ICP-OES) (Szlachta and Chubar, 2013) have also been reported in the literature.

3.11 Conclusion

This review gives an overall understanding on the different types of adsorbents used in batch equilibrium studies for treatment of selenite, Se(IV) and selenate, Se(VI) in aqueous solutions. Published work on selenate is not as abundant as the study of selenite. High selenium removal was achieved at low pH values and removal amount decreased with increase in pH for both selenite and selenate in a temperature range of 20 oC - 50 oC. On a selenium species basis, high monolayer adsorption capacities were observed in the selenite adsorption studies while monolayer capacities obtained for selenate were comparatively low. Overall, biomass derived adsorbents have shown greater adsorption capacities than other adsorbents like metal oxide coated sand, metal oxide coated activated carbon. Also, kinetic data from most of the studies followed pseudo second order kinetics and, isotherm data in general followed Langmuir isotherm model.

Bibliography - Chapter 3

Afkhami, A. and Madrakian, T.: Kinetic-spectrophotometric determination of selenium in natural water after preconcentration of elemental selenium on activated carbon., Talanta, 58(2), 311–7 [online] Available from: http://www.ncbi.nlm.nih.gov/pubmed/18968755, 2002.

Aurelio, G., Fernández-Martínez, a., Cuello, G. J., Román-Ross, G., Alliot, I. and Charlet, L.: Structural study of selenium(IV) substitutions in calcite, Chem. Geol., 270(1-4), 249–256, doi:10.1016/j.chemgeo.2009.12.004, 2010.

Balistrieri, L. S. and Chao, T. .: Adsorption of selenium by amorphous iron oxyhydroxide and manganese dioxide, Geochim. Cosmochim. Acta, 54(3), 739–751, doi:10.1016/0016-7037(90)90369-V, 1990.

Behera, R. K., Rout, K., Nayak, B. and Das, N. N.: Removal of Selenium and Arsenic Oxyanions using Natural Goethite-Rich Iron Ore from Daitari, Orissa, India: Effect of Heat Treatment, Adsorpt. Sci. Technol., 30(10), 867–880, doi:10.1260/0263-6174.30.10.867, 2012.

Bertolino, F. A., Torriero, A. A. J., Salinas, E., Olsina, R., Martinez, L. D. and Raba, J.: Speciation analysis of selenium in natural water using square-wave voltammetry after preconcentration on activated carbon., Anal. Chim. Acta, 572(1), 32–8, doi:10.1016/j.aca.2006.05.021, 2006.

Bleiman, N. and Mishael, Y. G.: Selenium removal from drinking water by adsorption to chitosan-clay composites and oxides: batch and columns tests., J. Hazard. Mater., 183(1-3), 590–5, doi:10.1016/j.jhazmat.2010.07.065, 2010.

Chan, Y. T., Kuan, W. H., Chen, T. Y. and Wang, M. K.: Adsorption mechanism of selenate and selenite on the binary oxide systems., Water Res., 43(17), 4412–20, doi:10.1016/j.watres.2009.06.056, 2009.

Chen, M. L. and An, M. Il: Selenium adsorption and speciation with Mg-FeCO3 layered double hydroxides loaded cellulose fibre., Talanta, 95, 31–5, doi:10.1016/j.talanta.2012.03.038, 2012.

Chen, M., Yang, T. and Wang, J.: Precipitate coating on cellulose fibre as sorption medium for selenium preconcentration and speciation with hydride generation atomic fluorescence spectrometry., Anal. Chim. Acta, 631(1), 74–9, doi:10.1016/j.aca.2008.10.019, 2009.

Chubar, N.: New inorganic (an)ion exchangers based on Mg-Al hydrous oxides: (alkoxide-free) sol-gel synthesis and characterisation., J. Colloid Interface Sci., 357(1), 198–209, doi:10.1016/j.jcis.2011.01.098, 2011.

Das, J., Das, D., Dash, G. P. and Parida, K. M.: Studies on Mg/Fe hydrotalcite-like-compound (HTlc) I. Removal of inorganic selenite (SeO3(2-)) from aqueous medium., J. Colloid Interface Sci., 251(1), 26–32, doi:10.1006/jcis.2002.8319, 2002.

Dash, S. S. and Parida, K. M.: Studies on selenite adsorption using manganese nodule leached residues., J. Colloid Interface Sci., 307(2), 333–9, doi:10.1016/j.jcis.2006.12.007, 2007.

Dobrowolski, R. and Otto, M.: Preparation and evaluation of Fe-loaded activated carbon for enrichment of selenium for analytical and environmental purposes., Chemosphere, 90(2), 683–90, doi:10.1016/j.chemosphere.2012.09.049, 2013.

Duc, M., Lefèvre, G. and Fédoroff, M.: Sorption of selenite ions on hematite., J. Colloid Interface Sci., 298(2), 556–63, doi:10.1016/j.jcis.2006.01.029, 2006.

Duc, M., Lefevre, G., Fedoroff, M., Jeanjean, J., Rouchaud, J. C., Monteil-Rivera, F., Dumonceau, J. and Milonjic, S.: Sorption of selenium anionic species on apatites and iron oxides from aqueous solutions., J. Environ. Radioact., 70(1-2), 61–72, doi:10.1016/S0265-931X(03)00125-5, 2003.

El-Shafey, E. I.: Removal of Se(IV) from aqueous solution using sulphuric acid-treated peanut shell., J. Environ. Manage., 84(4), 620–7, doi:10.1016/j.jenvman.2007.03.021, 2007a.

El-Shafey, E. I.: Sorption of Cd(II) and Se(IV) from aqueous solution using modified rice husk., J. Hazard. Mater., 147(1-2), 546–55, doi:10.1016/j.jhazmat.2007.01.051, 2007b.

Envirogen Technologies: Treatment of Selenium-Containing Coal Mining Wastewater with Fluidized Bed Reactor Technology. [online] Available from: http://www.envirogen.com/files/files/ETI_Selenium_GrayPaper_V_FINAL.pdf, 2011.

Environment protection Division Ministry of Environment Government of British Columbia: Ambient Water Quality Guidelines for Selenium, [online] Available from: http://www.env.gov.bc.ca/wat/wq/BCguidelines/selenium/selenium.html, 2001.

Gezer, N., Gulfen, M. and Aydin, A. O.: Adsorption of Selenite and Selenate Ions onto Thiourea-Formaldehyde Resin, J. Appl. Polym. Sci., 122, 1134–1141, doi:10.1002/app, 2011.

Goh, K. H. and Lim, T. T.: Geochemistry of inorganic arsenic and selenium in a tropical soil: effect of reaction time, pH, and competitive anions on arsenic and selenium adsorption., Chemosphere, 55(6), 849–59, doi:10.1016/j.chemosphere.2003.11.041, 2004.

Goh, K. H., Lim, T. T. and Dong, Z.: Application of layered double hydroxides for removal of oxyanions: a review., Water Res., 42(6-7), 1343–68, doi:10.1016/j.watres.2007.10.043, 2008.

Gonzalez, C. M., Hernandez, J., Parsons, J. G. and Gardea-Torresdey, J. L.: A study of the removal of selenite and selenate from aqueous solutions using a magnetic iron/manganese oxide nanomaterial and ICP-MS, Microchem. J., 96(2), 324–329, doi:10.1016/j.microc.2010.05.005, 2010.

Gonzalez, C. M., Hernandez, J., Parsons, J. G. and Gardea-Torresdey, J. L.: Adsorption of Selenite and Selenate By a High- and Low-Pressure Aged Manganese Oxide Nanomaterial, Instrum. Sci. Technol., 39(1), 1–19, doi:10.1080/10739149.2010.537721, 2011.

Gonzalez, C. M., Hernandez, J., Peralta-Videa, J. R., Botez, C. E., Parsons, J. G. and Gardea-Torresdey, J. L.: Sorption kinetic study of selenite and selenate onto a high and low pressure aged iron oxide nanomaterial., J. Hazard. Mater., 211-212, 138–45, doi:10.1016/j.jhazmat.2011.08.023, 2012.

Gulipalli, C. H. S., Prasad, B. and Wasewar, K. L.: Batch Study, Equilibrium and Kinetics of Adsorption of Selenium using Rice Husk Ash (RHA), J. Eng. Sci. Technol., 6(5), 586–605 [online] Available from: http://jestec.taylors.edu.my/Vol 6 Issue 5 October 11/Vol_6_5_586_605_WASEWAR.pdf, 2011.

Han, D. S., Batchelor, B. and Abdel-Wahab, A.: Sorption of selenium(IV) and selenium(VI) to mackinawite (FeS): effect of contact time, extent of removal, sorption envelopes., J. Hazard. Mater., 186(1), 451–7, doi:10.1016/j.jhazmat.2010.11.017, 2011.

Hasan, S. H. and Ranjan, D.: Agro-Industrial Waste : A Low-Cost Option for the Biosorptive Remediation of Selenium Anions, Ind. Eng. Chem. Res., 49(19), 8927–8934, doi:10.102/ie100622c, 2010.

Ippolito, J. A., Scheckel, K. G. and Barbarick, K. A.: Selenium adsorption to aluminum-based water treatment residuals., J. Colloid Interface Sci., 338(1), 48–55, doi:10.1016/j.jcis.2009.06.023, 2009.

Izgi, B., Gucer, S. and Jaćimović, R.: Determination of selenium in garlic (Allium sativum) and onion (Allium cepa) by electro thermal atomic absorption spectrometry, Food Chem., 99(3), 630–637, doi:10.1016/j.foodchem.2005.08.033, 2006.

Jan, Y. L., Wang, T. H., Li, M. H., Tsai, S. C., Wei, Y. Y. and Teng, S. P.: Adsorption of Se species on crushed granite: a direct linkage with its internal iron-related minerals., Appl. Radiat. Isot., 66(1), 14–23, doi:10.1016/j.apradiso.2007.08.007, 2008.

Jordan, N., Lomenech, C., Marmier, N., Giffaut, E. and Ehrhardt, J.-J.: Sorption of selenium(IV) onto magnetite in the presence of silicic acid., J. Colloid Interface Sci., 329(1), 17–23, doi:10.1016/j.jcis.2008.09.052, 2009.

Jordan, N., Müller, K., Franzen, C. and Brendler, V.: Temperature impact on the sorption of selenium(VI) onto anatase., J. Colloid Interface Sci., 390(1), 170–5, doi:10.1016/j.jcis.2012.09.021, 2013a.

Jordan, N., Ritter, A., Foerstendorf, H., Scheinost, A. C., Weiß, S., Heim, K., Grenzer, J., Mücklich, A. and Reuther, H.: Adsorption mechanism of selenium(VI) onto maghemite, Geochim. Cosmochim. Acta, 103, 63–75, doi:10.1016/j.gca.2012.09.048, 2013b.

Karatchevtseva, I., Astoux, M., Cassidy, D. J., Yee, P., Bartlett, J. R. and Griffith, C. S.: Synthesis and characterization of functionalized silica-based nanohybrid materials for oxyanions adsorption., Langmuir, 26(11), 8327–35, doi:10.1021/la904747m, 2010.

Kim, S. S., Min, J. H., Lee, J. K., Baik, M. H., Choi, J.-W. and Shin, H. S.: Effects of pH and anions on the sorption of selenium ions onto magnetite., J. Environ. Radioact., 104, 1–6, doi:10.1016/j.jenvrad.2011.09.013, 2012.

Kongsri, S., Janpradit, K., Buapa, K., Techawongstien, S. and Chanthai, S.: Nanocrystalline hydroxyapatite from fish scale waste: Preparation, characterization and application for selenium adsorption in aqueous solution, Chem. Eng. J., 215-216, 522–532, doi:10.1016/j.cej.2012.11.054, 2013.

Kuan, W. H., Lo, S. L., Wang, M. K. and Lin, C. F.: Removal of Se(IV) and Se(VI) from water by aluminum-oxide-coated sand, Water Res., 32(3), 915–923, doi:10.1016/S0043-1354(97)00228-5, 1998.

Kubota, T., Suzuki, K. and Okutani, T.: Determination of total selenium content in sediments and natural water by graphite furnace-atomic absorption spectroscopy after collection as a selenium(IV) complex on activated carbon., Talanta, 42(7), 949–55 [online] Available from: http://www.ncbi.nlm.nih.gov/pubmed/18966316, 1995.

Latva, S., Peräniemi, S. and Ahlgrén, M.: Study of metal-loaded activated charcoals for the separation and determination of selenium species by energy dispersive X-ray fluorescence analysis, Anal. Chim. Acta, 478(2), 229–235, doi:10.1016/S0003-2670(02)01524-6, 2003a.

Latva, S., Peräniemi, S. and Ahlgrén, M.: Study of metal-loaded activated charcoals for the separation and determination of selenium species by energy dispersive X-ray fluorescence analysis, Anal. Chim. Acta, 478(2), 229–235, doi:10.1016/S0003-2670(02)01524-6, 2003b.

Lee, S., Doolittle, J. J. and Woodard, H. J.: Selenite Adsorption and Desorption in Selected South Dakota Soils as a Function of pH and Other Oxyanions, Soil Sci., 176(2), 73–79, doi:10.1097/SS.0b013e31820a0ff6, 2011.

Li, Z., Li, H., Yang, X., Zhang, H., Liu, C. and Cao, B.: Characterization of Se(IV) removal from aqueous solution by Aspergillus sp. J2, Chem. Eng. J., 220(3), 67–71, doi:10.1016/j.cej.2012.11.136, 2013.

Liu, R., Frost, R. L. and Martens, W. N.: Absorption of the selenite anion from aqueous solutions by thermally activated layered double hydroxide., Water Res., 43(5), 1323–9, doi:10.1016/j.watres.2008.12.030, 2009.

Lo, S. and Chen, T.: Adsorption of Se(IV) and Se(VI) on an Iron-Coated Sand from Water, Chemosphere, 35(5), 919–930, doi:10.1016/S0045-6535(97)00190-2, 1997.

Manceau, A. and Charlet, L.: The Mechanism of Selenate Adsorption on Geothite and Hydrous Ferric Oxide, J. Colloid Interface Sci., 168, 87–63, doi:10.1006/jcis.1994.1396, 1994.

Mandal, S., Mayadevi, S. and Kulkarni, B. D.: Adsorption of Aqueous Selenite [Se(IV)] Species on Synthetic Layered Double Hydroxide Materials, Ind. Eng. Chem. Res., 48(17), 7893–7898, doi:10.1021/ie900136s, 2009.

Martínez, M., Giménez, J., de Pablo, J., Rovira, M. and Duro, L.: Sorption of selenium(IV) and selenium(VI) onto magnetite, Appl. Surf. Sci., 252(10), 3767–3773, doi:10.1016/j.apsusc.2005.05.067, 2006.

Missana, T., Alonso, U., Scheinost, a. C., Granizo, N. and García-Gutiérrez, M.: Selenite retention by nanocrystalline magnetite: Role of adsorption, reduction and dissolution/co-precipitation processes, Geochim. Cosmochim. Acta, 73(20), 6205–6217, doi:10.1016/j.gca.2009.07.005, 2009.

Monteil-Rivera, F., Fedoroff, M., Jeanjean, J., Minel, L., Barthes, M. and Dumonceau, J.: Sorption of Selenite (SeO(3)(2-)) on Hydroxyapatite: An Exchange Process., J. Colloid Interface Sci., 221(2), 291–300, doi:10.1006/jcis.1999.6566, 2000.

Nettem, K. and Almusallam, A. S.: Equilibrium, Kinetic and Thermodynamic Studies on the Biosorption of Selenium (IV) Ions onto Ganoderma Lucidum Biomass, Sep. Sci. Technol., (June), doi:10.1080/01496395.2013.791318, 2013.

Nilore, P. O.: Sorption of Selenium at Micromolar Levels onto Hydrous Titanium Oxide from Aqueous Solutions using Radiotracer Technique, Appl. Radiat. Isot., 48(5), 595–600, doi:10.1016/S0969-8043(96)00325-9, 1997.

Parida, K., Gorai, B., Das, N. and Rao, S.: Studies on Ferric Oxide Hydroxides, J. Colloid Interface Sci., 185(2), 355–62 [online] Available from: http://www.ncbi.nlm.nih.gov/pubmed/22448881, 1997.

Parida, K. M. and Gorai, B.: Removal of Aqueous Selenite Using Alumina, Int. J. Environ. Stud., (June 2013), 37–41, doi:10.1080/00207230304749, 2010.

Peak, D.: Adsorption mechanisms of selenium oxyanions at the aluminum oxide/water interface., J. Colloid Interface Sci., 303(2), 337–45, doi:10.1016/j.jcis.2006.08.014, 2006.

Peak, D. and Sparks, D. L.: Mechanisms of selenate adsorption on iron oxides and hydroxides., Environ. Sci. Technol., 36(7), 1460–6 [online] Available from: http://www.ncbi.nlm.nih.gov/pubmed/11999051, 2002.

Peraniemi, S. and Ahlgrén, M.: Optimized arsenic , selenium and mercury determinations in aqueous solutions by energy dispersive x-ray fluorescence after preconcentration onto zirconium-loaded activated charcoal, Anal. Chim. Acta, 2670(94), doi:10.1016/0003-2670(94)00439-S, 1995.

Rahnemaie, R., Hiemstra, T. and van Riemsdijk, W. H.: Inner- and outer-sphere complexation of ions at the goethite-solution interface., J. Colloid Interface Sci., 297(2), 379–88, doi:10.1016/j.jcis.2005.11.003, 2006.

Rovira, M., Giménez, J., Martínez, M., Martínez-Lladó, X., de Pablo, J., Martí, V. and Duro, L.: Sorption of selenium(IV) and selenium(VI) onto natural iron oxides: goethite and hematite., J. Hazard. Mater., 150(2), 279–84, doi:10.1016/j.jhazmat.2007.04.098, 2008.

Sahin, F., Volkan, M., Howard, A. G. and Ataman, O. Y.: Selective pre-concentration of selenite from aqueous samples using mercapto-silica., Talanta, 60(5), 1003–9, doi:10.1016/S0039-9140(03)00154-1, 2003.

Sheha, R. R. and El-Shazly, E. a.: Kinetics and equilibrium modeling of Se(IV) removal from aqueous solutions using metal oxides, Chem. Eng. J., 160(1), 63–71, doi:10.1016/j.cej.2010.03.004, 2010.

Su, T., Guan, X., Gu, G. and Wang, J.: Adsorption characteristics of As(V), Se(IV), and V(V) onto activated alumina: effects of pH, surface loading, and ionic strength., J. Colloid Interface Sci., 326(2), 347–53, doi:10.1016/j.jcis.2008.07.026, 2008.

Svecova, L., Dossot, M., Cremel, S., Simonnot, M.-O., Sardin, M., Humbert, B., Den Auwer, C. and Michot, L. J.: Sorption of selenium oxyanions on TiO2 (rutile) studied by batch or column experiments and spectroscopic methods., J. Hazard. Mater., 189(3), 764–72, doi:10.1016/j.jhazmat.2011.02.090, 2011.

Szlachta, M. and Chubar, N.: The application of Fe–Mn hydrous oxides based adsorbent for removing selenium species from water, Chem. Eng. J., 217, 159–168, doi:10.1016/j.cej.2012.11.100, 2013.

Szlachta, M., Gerda, V. and Chubar, N.: Adsorption of arsenite and selenite using an inorganic ion exchanger based on Fe-Mn hydrous oxide., J. Colloid Interface Sci., 365(1), 213–21, doi:10.1016/j.jcis.2011.09.023, 2012.

Tsoi, Y.-K. and Leung, K. S.-Y.: Toward the use of surface modified activated carbon in speciation: selective preconcentration of selenite and selenate in environmental waters., J. Chromatogr. A, 1218(16), 2160–4, doi:10.1016/j.chroma.2011.02.016, 2011.

Tuzen, M. and Sarı, A.: Biosorption of selenium from aqueous solution by green algae (Cladophora hutchinsiae) biomass: Equilibrium, thermodynamic and kinetic studies, Chem. Eng. J., 158(2), 200–206, doi:10.1016/j.cej.2009.12.041, 2010.

US EPA: Basic Information about Selenium in Drinking Water, [online] Available from: http://water.epa.gov/drink/contaminants/basicinformation/selenium.cfm#four, 1992.

Wasewar, K. L., Prasad, B. and Gulipalli, S.: Adsorption of Selenium Using Bagasse Fly Ash, CLEAN - Soil, Air, Water, 37(7), 534–543, doi:10.1002/clen.200800183, 2009a.

Wasewar, K. L., Prasad, B. and Gulipalli, S.: Removal of Selenium by Adsorption onto Granular Activated Carbon (GAC) and Powdered Activated Carbon (PAC), CLEAN - Soil, Air, Water, 37(11), 872–883, doi:10.1002/clen.200900188, 2009b.

World Health Organization: Background document for preparation of WHO Guidelines for drinking-water quality, (WHO/SDE/WSH/03.04/13), 2003.

Wu, C., Lo, S. and Lin, C.: Competitive adsorption of molybdate , chromate , sulfate , selenate , and selenite on g-Al 2 O 3, Colloids Surfaces A Physicochem. Eng. Asp., 166, 251–259, doi:10.1016/S0927-7757(99)00404-5, 2000.

Xiong, C., He, M. and Hu, B.: On-line separation and preconcentration of inorganic arsenic and selenium species in natural water samples with CTAB-modified alkyl silica microcolumn and determination by inductively coupled plasma-optical emission spectrometry., Talanta, 76(4), 772–9, doi:10.1016/j.talanta.2008.04.031, 2008.

Yan, D., Gang, D. D., Zhang, N. and Lin, L.: Iron Oxide-Coated GAC Adsorbents: Diffusion-Controlled Sorption of Selenite, Ind. Eng. Chem. Res., 50(4), 2214–2219, doi:10.1021/ie100932r, 2011.

You, Y., Vance, G. F. and Zhao, H.: Selenium adsorption on Mg–Al and Zn–Al layered double hydroxides, Appl. Clay Sci., 20(1-2), 13–25, doi:10.1016/S0169-1317(00)00043-0, 2001.

Zelmanov, G. and Semiat, R.: Selenium removal from water and its recovery using iron (Fe3+) oxide/hydroxide-based nanoparticles sol (NanoFe) as an adsorbent, Sep. Purif. Technol., 103, 167–172, doi:10.1016/j.seppur.2012.10.037, 2013.

Zhang, L., Liu, N., Yang, L. and Lin, Q.: Sorption behavior of nano-TiO2 for the removal of selenium ions from aqueous solution., J. Hazard. Mater., 170(2-3), 1197–203, doi:10.1016/j.jhazmat.2009.05.098, 2009.

Zhang, N., Gang, D., Asce, M. and Lin, L.: Adsorptive Removal of Parts per Million Level Selenate Using Iron-Coated GAC Adsorbents, J. Environ. Eng., (October), 1089–1095, doi:10.1061/ ASCE EE.1943-7870.0000245, 2010.

Zhang, N., Lin, L.-S. and Gang, D.: Adsorptive selenite removal from water using iron-coated GAC adsorbents., Water Res., 42(14), 3809–16, doi:10.1016/j.watres.2008.07.025, 2008.

Chapter 4 : Characterization of Biomass Ash/Char from Pulp and Paper Mill Boilers

Bhagya M.K. Range, Kelly A. Hawboldt

Faculty of Engineering and Applied Science, Memorial University of Newfoundland,

St John's, NL, Canada. A1B3X5

Abstract

Combustion of forestry residue and other plant biomass in power boilers is gaining increasing interest as a low cost method of energy generation. In this process, carbon rich ash is produced as a by-product which can represent a disposal issue. The chemical makeup of the ash may make it reusable for a number of applications from adsorbents to concrete amendment. Characterization of these ash/char plays an important role as it is necessary to understand the properties of biomass ash/char in order to find possible applications. In this study, biomass ash/char collected from three pulp and paper mill boilers are characterized chemically, physically, thermally, and structurally by inductively coupled plasma mass spectrometry and optical emission spectrometry (ICP-MS, ICP-OES), CNS elemental analysis, mineral liberation analysis (MLA), X-ray diffraction (XRD), Fourier transform infrared spectroscopy (ATR-FTIR), scanning electron microscopy (SEM), specific surface area, pore volume, bulk density, pH, total alkalinity, thermo-gravimetric analysis (TGA).

4.1 Introduction

Low cost fuel sources such as coal, heavy oils, forestry residue and other plant biomass are burned in furnaces to produce heat to drive steam turbines in thermal power plants, utility and steam plants. In the process, ash is generated as a combustion by-product. The pulp and paper industry use cogeneration plants where power boilers utilize a significant percentage of forest residue (wood refuse) and/or fossil fuels as a heat source. The wood refuse, commonly referred to as hog fuel, consists of wood wastes such as saw dust, sticks, wood chips, cut offs, bark as well as wood harvest residues (Adeoti, 2011). Two kinds of ash are produced during the combustion process: fly ash and bottom ash. Fly ash is generally trapped by electrostatic precipitators before they are released to the environment. Bottom ash is collected as residue in the boiler bottom. The relative amounts of fly and bottom ash generated depend on the type of boiler used and fuel source (e.g. power boiler, fluidized boiler, grate boiler) (Berra et al., 2011). Ash is also generated in coal power plants as a by-product of combustion of pulverized coal, incinerator ash produced from burning garbage and municipal solid wastes, and tire ash generated by pyrolysis/combustion of waste tires (Adeoti, 2011).

It is estimated that approximately 476 million tons of biomass ash is generated worldwide annually based on burning 7 billion tons of biomass with 6.8% mean ash yield on dry basis, which is more than half of the quantity of coal ash produced per year (780 million tons) (Vassilev et al., 2013a). Generally, these biomass ash/char are sent to landfills for disposal, however, due to the limited availability of landfills as well as the strict

environmental regulations, it has become necessary to find alternative uses for these ashes.

Table 4-1 summarizes the literature on characterization of biomass ash/char with details on the different techniques used for characterization. Methods/techniques used for characterization of biomass ash/char include: chemical composition analysis by XRF; elemental analysis by ICP-MS, ICP-OES and CHN elemental analyzer; morphology and microstructure by SEM; specific surface area, pore volume, average pore diameter by BET method; functional groups by FT-IR; minerals/phases by XRD; pH; porosity; density.

Table 4-1: Literature related to characterization of biomass ash/char

Reference	**Ash/char details**
Vassilev et al., 2013	Biomass ash from beech wood chips, corn cobs, marine macroalgae, weathered plum pits, rice husks, switchgrass, sunflower shells, walnut shells
Berra et al., 2010, Berra et al., 2011	Woody biomass fly ash from Italian chipped-wood burning plant
Adeoti, 2011	Pulp and paper mill boiler ash
Pan and Eberhardt, 2011	Carbon-rich fly ash from southern yellow pine wood chips: wood ash; combusted fly ash; and fly ash
Gupta and Sharma, 2003;	Bagasse fly ash

Tailor et al., 2012	
Sasithorn et al., 2010	Rice husk fly ash
Pengthamkeerati et al., 2008, 2010	Biomass fly ash from combustion of Eucalyptus trims and chips and rice husks
Chowdhury et al., 2011	Oil palm ash
Giro et al., 2012	Biomass fly ash from Eucalyptus bark
Eberhardt and Pan, 2012	Chars isolated from carbon rich ash from gasification of pinewood chips
Liu et al., 2011	Biochars derived from corncobs and rice
Li et al., 2010	Range of biochars derived from rosewood, pinewood, bamboo, rice husk, rice straw
Shang et al., 2012	Biochar from camphor tree
Arami-Niya et al., 2012	Biochar from palmshell
Zheng et al., 2010	Greenwaste biochar samples
Liu et al., 2010	Char from pinewood pyrolysis and hydrothermal treatment

Biomass ash is a heterogeneous multi-component mixture of inorganic and organic compounds. The compositions of these biomass ashes vary depending on several factors: source of biomass; combustion conditions of biomass; particle size of biomass; combination of fuels burned etc. Major elements and phases identified in a biomass ash system may include: glass, silicates and oxyhydroxides containing Si–Al–Fe–Na–Ti; carbonates, oxyhydroxides, glass, silicates phosphates and sulphates containing Ca–Mg–

Mn; phosphates, sulphates, chlorides, glass, silicates and carbonates containing K–P–S–Cl (Vassilev et al., 2013a). Biomass char has a high carbon content, low density, high porosity, high specific surface area and char extracted from combustion residue is less expensive than activated carbon. Due to the large surface area and the surface chemistry, char is widely used as a low cost adsorbent in wastewater treatment and gas purification applications (Pastor-Villegas et al., 2006).

In this study, biomass ash/char was obtained from three different pulp and paper mills. These ash/char was characterized to determine physical, chemical and thermal properties. The characterization methodology and results from the analyses are detailed in subsequent sections.

4.2 Biomass Ash/Char Samples Used in This Study

4.2.1 Source Information

The biomass ash samples characterized in this study were obtained from three pulp and paper mills located in Quebec, British Columbia and Corner Brook in Canada.

4.2.1.1 Kruger Brompton Mill (KBM)

Kruger Brompton Mill is located in Sherbrooke, Quebec, Canada. This mill has a 23 MW biomass cogeneration plant. It has a secondary effluent treatment system to ensure its compliance with environmental laws and regulations. The hog fuel boiler burns about 600

dry metric tons of paper mill sludge, bark, other wood residue per day (Kruger Inc., 2013a). The ash sample used for characterization was collected in January 2012.

4.2.1.2 Corner Brook Mill (CBM)

Corner Brook Pulp and Paper Limited (CBPPL) is located in Corner Brook, NL Canada. This mill has a 15 MW biomass cogeneration plant. This mill also has a secondary effluent treatment system to ensure its compliance with environmental laws and regulations (Kruger Inc., 2013b).

The CBPPL Ash Diversion Project Report (November 2010) indicates the plant burns a mix of biomass and waste oil, approximately 90% biomass (75-80% hog fuel, 10-15% dried secondary sludge) and 10% waste oil. Hog fuel consists of bark, wood, construction wood waste and saw mill waste. CBPPL's goal is to divert as much ash as possible from the landfill site. The mill is collecting 10,000 - 15,000 tonnes of total ash each year. The majority of this ash is fly ash (60-70%). The ash is disposed at the Wild Cove Landfill site at an approximate annual cost of $250,000 (Churchill and Kirby, 2010).

Three samples were collected from CBPPL. The first sample (CBM) was collected from the Corner Brook mill's boiler in January 2012. The second sample (CBM-D) was collected from the cogeneration plant in dry form before it was impounded in water. The third char sample (CBM-W) was collected from the top of the water impounded conveyor where char floats on top of water.

4.2.1.3 Zelstoff Celgar Mill (CLM)

Zellstoff Celgar Limited Partnership (ZCLP) is located in Castlegar, BC Canada. Figure 4-1 gives an overview of their products, production process and raw materials.

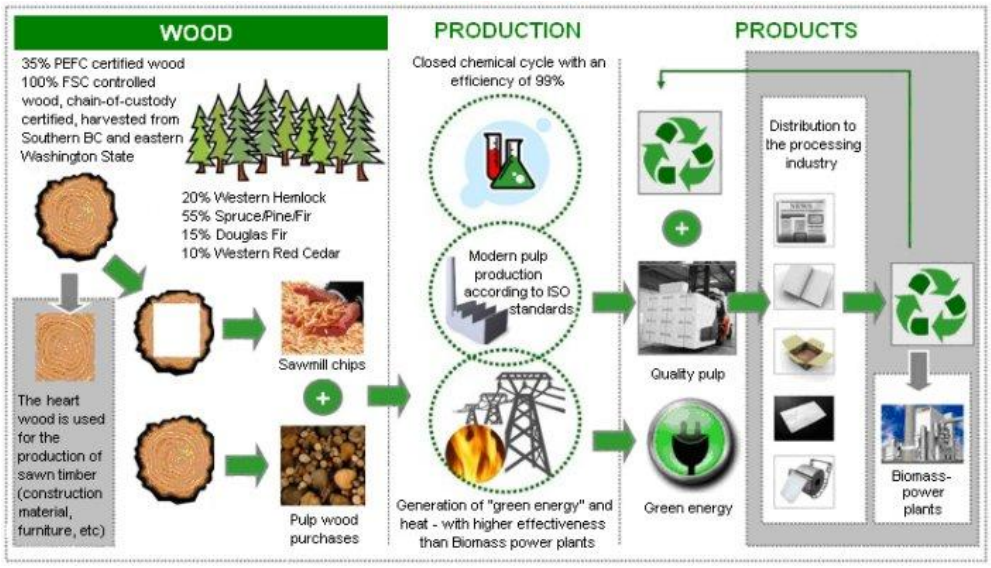

Figure 4-1: Overview of products, production process and raw materials of ZCLP (Zellstoff Celgar Limited Partnership, 2013)

Ash is generated as an unwanted combustion by-product of burning hog fuel in their power boiler. Hog fuel consists of wood particles (sawdust and pine chips), bark, sludge from the effluent bio-treatment facility and other impurities. The sludge from the effluent bio-treatment facility is primarily made of organic matter, fibre, and lime. Ash is the single largest contributor of material that goes into the mill's landfill which was estimated at 6500 m^3/year (Personal communication). Finding alternative uses for these ash is beneficial to the ZCLP as it may reduce the costs involved in ash handling and disposal

such as fuel, manpower, and obtaining permits for the landfill and it will also address the safety concerns such as landfill fires that may be caused due to the heat of the ash. The ash sample (CLM) used in this study was collected from the bunker below power boiler in January 2013.

4.2.2 Sample Details

All samples (CBM, KBM, CBM-D, CBM-W, CLM) were dried at 105^{o}C for 24 hours and sieved using a W.S. Tyler 8570 Ro-Tap sieve shaker with USA standard testing sieves (ASTM E-11 specification). The fraction of the CLM sample that was retained in the 1.18 mm sieve was crushed again to obtain only two size fractions (CLM1: d < 500 µm and CLM2: 500 µm < d < 1.18 mm). Very small amounts of CBM, CBM-W and KBM2 samples were retained in the 4 mm mesh size and this retained fraction composed mainly of unburned wood particles and was not further analyzed. The details of the samples that were characterized in this study are given in Table 4-2 and the images of the samples are given in Figure 4-2.

Table 4-2: Sample details (source and size fractions)

Sample Name	Description	Sieve mesh size
CBM	Corner Brook Mill first sample	1.18 mm < d < 4 mm
KBM2	Kruger Brompton Mill sample	1.18 mm < d < 4 mm
KBM1	Kruger Brompton Mill sample	d < 1.18 mm

CBM-D2	Corner Brook Mill second sample	500 µm < d < 1.18 mm
CBM-D1	Corner Brook Mill second sample	d < 500 µm
CBM-W	Corner Brook Mill third sample	1.18 mm < d < 4 mm
CLM2	Zelstoff Celgar Mill sample	500 µm < d < 1.18 mm
CLM1	Zelstoff Celgar Mill sample	d < 500 µm

CBM

KBM2

KBM1

CBM-D2

CBM-D1

CBM-W

CLM2 CLM1

Figure 4-2: Images of the biomass ash/char samples used in this study

4.3 Biomass Ash/Char Characterization Methodology

4.3.1 Elemental Composition Using ICP-OES and ICP-MS

Elemental analysis of the ash/char samples were done at TERRA (The Earth Resources Research and Analysis) Facility at Memorial University. Samples dissolution procedure is as described in the next paragraphs.

Sample dissolution procedure for ICP-OES analysis: All the samples were finely ground and 0.1000 g of each sample was weighed into a clean dry teflon screw cap jar and weight was recorded. 2 mL of clean 8 N HNO_3 and 1 mL of HF was added. The capped teflon jars were heated on a hot plate at 70 ^{o}C for 24 hours followed by the addition of 4 mL of aqua regia (3:1 conc. HCl:HNO_3) to each sample and jars were heated for another 48 hours. 10 mL of saturated boric acid was added to the solution in the jars. The contents were then transferred into a clean 50 mL graduated tube and

nanopure water was added to make the solution up to 50 mL mark. The solution was filtered into another clean tube using a funnel and No.01 Whatman filter paper and analyzed by ICP-OES instrument.

Sample dissolution procedure for ICP-MS analysis: All the samples were finely ground and 0.1000 g of sample was weighed into a clean dry teflon screw cap jar and weight was recorded. 2 mL of clean 8 N HNO_3 and 1 mL of HF were added and the samples were heated on a hot plate at 70 ^oC for 48 hours. The cover was removed and rinsed with 8N HNO_3 into the teflon jar and the sample was evaporated to dryness at 100 ^oC. Then, 3 mL of aqua regia (3:1 conc. HCl:HNO_3) was added to each sample and the capped jars were heated for another 48 hours. The cap was removed and again rinsed with 8N HNO_3 into the teflon jar and evaporated to dryness. Then, 2 mL of 8N HNO_3 was added and evaporated to remove traces of HCl and HF. After adding another 2 mL of 8N HNO_3, the covered sample was heated for 5 more hours. The jar was then cooled before adding 1 mL of H_2O_2. Heating was continued until bubbling stopped and another 1 mL of H_2O_2 was added after cooling. After heating the sample for couple of more hours the contents were transferred into a clean dry labeled 120 mL snap seal container. Nanopure water was added until the solution weight was 30 g and the weight was recorded. Then the solution was filtered using a funnel and a No. 01 Whatman filter paper into another clean dry labeled 120 mL snap seal container. Then, 0.5 g of the solution was diluted with 9.5 g of 0.2 N Nitric acid in a centrifuge tube and analyzed by the ICP-MS instrument.

The samples were analyzed using ELAN-DRC-II (ICP-MS) and Perkin Elmer Optima 5300DV (ICP-OES) Instruments.

4.3.2 C, N, S Elemental Analysis

Ash/Char samples were analyzed in the Stable Isotope Lab at the TERRA Facility at Memorial University.

Analysis of Carbon (C) and Nitrogen (N): Carbon and Nitrogen percentages of the samples were analyzed using Carlo-Erba NA1500 Elemental Analyzer. The Carlo-Erba NA1500 Elemental Analyzer (EA) consists of an autosampler, oxidation and reduction ovens, water trap, gas chromatographic (GC) column and a thermal conductivity meter (TCD).

According to the analysis procedure, the entire EA system is continuously flushed with He (carrier gas) at a rate of 90 mL/min. The sample, sealed in a tin capsule, is loaded into the autosampler. The autosampler drops the capsule into the oxidation reactor (1050°C) just as a pulse of oxygen, flushed by He, arrives. Reaction of O_2 with the tin creates a flash combustion which totally oxidizes the sample into combustion products. The combustion gases pass through catalysts to ensure complete oxidation of the sample and also, to remove halides and SO_2. The gas mixture passes through the reduction reactor (650°C) which reduces nitrogen oxides to N_2 and also absorbs excess O_2. The gases pass through a water trap and the remaining gases (N_2, CO_2) enter the chromatographic

column. The individual gases are separated as they pass through the column and when they reach the TCD, they are detected as separate gas peaks: first N_2, then CO_2. The TCD output signal for each is proportional to the concentration of each combustion gas which allows elemental determination (%N, %C) based on sample weight.

Analysis of Sulphur (S): Sulphur percentages (by weight) of the samples were analyzed using Carlo-Erba NA1500 Series 2 Elemental Analyzer with ConFloII Interface and Finnigan MAT252 Isotope Ratio Mass Spectrometer.

4.3.3 Mineral Liberation Analysis (MLA)

Mineral Liberation Analyzer (MLA 650 FEG) is a Scanning Electron Microscope (SEM) based automated image analyzer based on FEI's Quanta platform and with a Field Emission Gun (FEG) source system ("FEI website", 2013). The Mineral Liberation Analysis of the samples using SEM allows inspection of samples in Backscattered Electron Emission (BSE) imaging mode and collection of Energy Dispersive X-ray-Spectra (EDS) of the particles. MLA uses DataView image analysis software to analyze the resulting data and it automatically identifies minerals and phases under the electron beam (energy 25 kV, current 10 nA) by using an X-ray spectral pattern matching algorithm to compare the x-ray spectrums to a library of reference spectra. However, MLA cannot provide a completely true identification of the actual compounds present in the analyzed areas and it's a semi quantitative analysis method.

CBM and KBM1 samples were further categorized for MLA, as listed in the Table 4-3. These were the first received samples. Hence, they were categorized into three more size fractions to understand the effect of mineral composition with change in particle size.

Table 4-3: Details of the samples used for MLA

Sample name (MLA)	Main sample description	Size fraction
CB 3	CBM	1.18 mm < d < 4 mm
CB 2		500 µm < d < 1.18 mm
CB 1		< 500 µm
KM 3 (same as KBM2)	KBM	1.18 mm < d < 4 mm
KM 2		500 µm < d < 1.18 mm
KM 1		< 500 µm
CBM-D2	CBM-D	500 µm < d < 1.18 mm
CBM-D1		d < 500 µm
CBM-W	CBM-W	1.18 mm < d < 4 mm
CLM2	CLM	500 µm < d < 1.18 mm
CLM1		d < 500 µm

The samples were analyzed at the CREAIT (Core Research Equipment & Instrument Training) Network's Micro-analysis Facility at Memorial University. Epoxy blocks were used to prepare the grain mounts. The regular epoxy resin used for mounting particles

contains carbon and hence accurate identification of minerals in carbon rich particles is difficult. Therefore, a brominated epoxy resin was prepared by mixing Kukdo brominated epoxy resin with Jeffamine hardener obtained from Hunstsman Corporation, Texas, USA. Analysis was done using both regular and brominated epoxy resins. The analytical surface of the epoxy block was grinded and polished to prepare the samples for the analysis. The minerals/phases of these samples were determined using the MLA 650 FEG instrument.

4.3.4 XRD Analysis

XRD (powder X-ray Diffraction) analysis was carried out at the TERRA facility at Memorial University. A small amount of sample was mounted on the aluminum plate trough and X-ray diffraction patterns were obtained using a Rigaku Ultima-IV X-ray diffractometer with Cu- Kα radiation (40 kV,44 mA) with 0.02^{o} step (angle 5^{o} - 100^{o}). Data were recorded and X-ray patterns were matched with ICSD-All and ICSD-Min databases (as a source of reference data) using Materials Data Inc.'s (MDI) Jade software.

4.3.5 ATR- FTIR Analysis

ATR-FTIR (Attenuated Total Reflectance - Fourier Transform Infrared Spectroscopy) analysis was done at the Centre for Chemical Analysis, Research and Training (C-CART) at Memorial University. Samples were finely ground to obtain a powder and analyzed using Bruker Tensor 27 FTIR spectrometer with OPUS data collection and analysis

program. ATR assembly uses a ZnSe crystal for reflection. IR spectrum is obtained in the wavelength range of 4000 cm^{-1} to 650 cm^{-1}.

4.3.6 SEM Analysis

SEM (Scanning Electron Microscopy) analysis was done at the CREAIT Network's Micro-analysis Facility. All the ash/char samples were mounted on double sided tape on SEM stub samplers. These samples were analyzed using Quanta scanning electron microscope with FEG source system and Large Field Detector (LFD). Recorded SEM micrographs are analyzed in detail in the results section.

4.3.7 Specific Surface Area, Pore Volume and Mean Pore Diameter

All the samples were analyzed using the Belsorp-max instrument (by BEL Japan Inc.) at the Material Surface Characterization Laboratory in the Department of Chemical Engineering at University of New Brunswick.

The Belsorp-max (used for BET surface area measurement) is an automatic gas adsorption/desorption measuring unit and measures adsorption isotherm in the relative pressure (P/P0) range of 10^{-8} - 0.997. Liquid nitrogen (77 K) is used to determine the specific surface area and pore size distribution of samples. The samples were pre-treated for 4 hours using a furnace at 200 ^{o}C (Personal communication). Pre-treatment is important to remove moisture, gases or contaminants from the surface and pores of

samples before starting the measurement. Analysis software by BEL Japan Inc. is used to analyze the data measured by the Belsorp adsorption apparatus, and the BET plot was used to evaluate the specific surface area and pore size distribution.

CLM1 and CBM-D2 samples were also analyzed at Micromeritics Analytical Services, Particle testing authority, Georgia, USA (www.particletesting.com). The samples were pre-treated under vacuum for 240 minutes and analyzed using Micromeritics ASAP 2020 (Accelerated Surface Area and Porosimetry) system. Analysis adsorptive used in this testing was CO_2 at 273 K. The specific surface area and pore volumes were calculated using Density Functional Theory, Dubinin-Radushkevich method and Dubinin-Astakhov method.

BET (Brunauer, Emmett and Teller) is the best-known and most commonly used method for evaluating specific surface areas of porous materials. Although, it is easy to apply and widely accepted, accurate measurement of the true surface area of microporous materials is not possible by this method (Quantachrome Instruments, 2013). On the other hand, application of methods derived from the Dubinin - Radushkevich approach and methods based on Density Functional Theory are more useful when determining the surface area of microporous carbons (Tascon, 2012). Dubinin equations are based on micropore volume filling theory and characteristic energy of adsorption. Dubinin-Radushkevich equation generally applies only to solids with a uniform micropore structure where as Dubinin-Astakhov equation applies to non-homogenous microporous structures (e.g.

carbon) (Gil and Grange, 1996). Density Functional Theory (DFT) looks at sorption phenomena in micro and mesopores at a molecular level using statistical mechanics. DFT uses complex mathematical modeling of gas-solid interations plus pore geometry to develop density profiles of adsorbed fluids as a function of pressure or temperature. From these density profiles, the amount adsorbed can be calculated (Quantachrome Instruments, 2013).

Further, CO_2 at 273 K (0^oC) is a more suitable adsorptive than N_2 at 77 K (-196^oC) for surface area and pore volume analysis of microporous materials. The diffusion rate of N_2 molecules into micropores of char at -196^oC is extremely slow and these pores are inaccessible to N_2 molecules. On the other hand, the CO_2 molecules at 0^oC can easily access the micropores of the same material. Therefore, CO_2 at 0^oC is a better adsorbent for highly microporous carbons, providing more reliable measurements than N_2 at -196^oC because of higher testing temperature (McLaughlin et al., 2012)

4.3.8 Bulk Density

True density of a porous solid is the ratio of the mass to the volume occupied by that mass. Therefore, when measuring true density, volume of pores and inter-particle spaces must be excluded. Helium pycnometry is generally used as a method for true density measurement of porous solids as helium is a non interactive fluid which is able to completely fill the pores.

Bulk density includes both volume of pores and inter-particle spaces and it is calculated as follows. Bulk density of the dried samples were measured using a 100 mL (V) measuring cylinder. First step is to measure the weight of the empty measuring cylinder (M_1) using a digital balance. It was then filled with the closely packed sample up to the 100 mL mark and the weight was measured again (M_2). Sample weight (M_2 - M_1) was divided by the volume (V) to calculate the bulk density.

4.3.9 pH Values

The pH of the ash/char samples was measured by mixing them with de-ionized water at 1:20 (kg/L) solid/solution ratio and taking the pH reading from a Oakton pH 2100 bench top meter using a combined pH electrode after 10 minutes of initial mixing at 180 rpm in a VWR shaker (Luo et al., 2011). A 3-point calibration was performed using pH buffer solutions at pH 4.0, 7.0 and 10.0 before taking the pH measurements.

4.3.10 Total Alkalinity

Total Alkalinity is a measure of resistance of water to change in pH. It can also be called as buffering capacity of water. Materials such as carbonate, bicarbonate, hydroxides can contribute towards increased alkalinity in water. Total Alkalinity is defined as the amount of acid required to lower the pH of the sample to a pH value of 4.5 (endpoint) at which all carbonate and bicarbonate ions are converted to carbonic acid (H_2CO_3). Total alkalinity can be measured by titrating a water sample with HCl or H_2SO_4 acid of known concentration.

Analysis procedure: Fly ash leaching tests were performed at a liquid to solid ratio of 20 L/kg. 10 g of solid sample and 200 mL of de-ionized water was mixed in a 250 mL Erlenmeyer flask. The flasks were then agitated by using a VWR series shaker for 24 hours at 10 rpm. The mixtures were then filtered through a Whatman No 42 filter paper.

50 mL of the sample was titrated with 0.2 N H_2SO_4 solution, leaving sufficient time for the neutralization reaction to happen and a Oakton pH 2100 bench top meter was used to monitor and record pH. The volume of H_2SO_4 needed for the pH of the solution to drop to 4.5 was recorded at three replicate titrations. Then the total alkalinity is calculated as follows.

Alkalinity, mg/L $CaCO_3$ = (mL titrant* normality of acid* 50000)/ mL of sample

= mL of H_2SO_4 acid used* 0.2 N*50000/ 50 mL

4.3.11 Thermal Analysis by TGA

Thermal properties of the samples were analyzed using the Thermo Gravimetric Analyzer (TGA Q500 V20.10 Build 36) at the Centre for Chemical Analysis, Research and Training (C-CART) at Memorial University. Samples were dried at 105^{o}C overnight and finely ground. A very small quantity of the sample (<15 mg) was placed in the platinum pan and loaded into tarred equipment. Samples were heated to 1000^{o}C at the ramping rate of 20^{o}C/min under inert (N_2) atmosphere at 50 mL/min sample gas flow. Balance gas flow was maintained at 40 mL/min sample gas flow. Weight percentage and the derivative weight percentage with temperature was analyzed.

4.4 Biomass Ash/Char Characterization Results and Discussion

4.4.1 Elemental Composition from ICP-OES and ICP-MS Analysis

Table 4-4 summarizes the results from the elemental analysis of the ash/char samples. The actual concentration of the elements in ash/char samples may be slightly higher than the mentioned values as the samples were not completely dissolved in the solution. K, Na, Si were analyzed using ICP-OES while Mg, Al, P, Ca, Ti, Fe, Mn were analyzed using both ICP-OES and MS. The values obtained from the ICP-OES analysis are given in the table. All the other elementals present in concentrations less than 100 ppm were analyzed using ICP-MS. Elements such as Be, Se, Ag, Cd, Cs, Hg, Tl, Bi, U were present in concentrations less than 5 ppm and these values are not given in the table.

Major elements present in the analyzed eight ash/char samples are Ca, Si, Al, Na, K, Fe, Mn, Mg, P, Ti. Very high Ca and Si elemental compositions are recorded in most of the samples; KBM1 sample has the highest Si content of 225,333 ppm and highest Ca content of 124,500 ppm. CBM-D2 and CBM-W samples have low Ca, K, Mg, Na values compared to other samples. Compounds rich in Ca, Na, K, Mg can be used to neutralize and increase pH of acidic effluent water streams such as AMD (Vassilev et al., 2013b). KBM1 and CBM-D1 samples contain the highest amount of Si and Al which is an important factor for zeolite synthesis (Adeoti, 2011; Vadapalli et al., 2012). Maximum concentrations of Ba, Sr, Cu, Zn, Pb, B in the samples are less than 2000 ppm. Heavy metal concentrations in the CBM-D2 and CBM-W samples are very low compared to other samples.

Table 4-4: Elemental analysis using ICP-MS and ICP-OES techniques

Element (ppm)	CBM	KBM2	KBM1	CBM-D2	CBM-D1	CBM-W	CLM2	CLM1
K	5,650	15,195	19,430	8,985	31,405	4,260	29,045	31,395
Na	1,400	6,750	18,443	1,263	15,008	993	50,083	55,820
Si	9,515	105,440	225,333	4,050	179,967	5,042	60,535	91,570
Mg	1,965	12,672	14,817	1,417	19,762	1,353	8,017	12,208
Al	3,333	34,838	69,655	1,490	45,455	2,085	14,903	21,210
P	2,370	938	1,748	1,290	29,048	1,043	4,355	5,678
Ca	110,575	45,998	124,500	18,395	124,300	22,610	75,168	101,325
Ti	233	6,608	10,712	112	3,197	125	527	833
Fe	3,663	14,934	20,158	1,514	49,530	1,833	6,854	11,264
Mn	3,880	615	1,117	2,875	36,363	2,825	4,923	7,242
Ba	713	765	852	226	1,943	232	817	1,138
Sr	129	485	554	61	484	71	461	612
Cu	23	524	564	16	174	18	46	57
Zn	265	966	1,701	42	563	72	347	489
Pb	12	411	527	2	17	5	24	31
Cr	21	236	206	7	164	5	101	64
As	1	139	106	0	4	0	3	3
B	36	340	799	22	70	22	89	86
Li	2	22	29	1	14	2	5	7
V	13	55	74	4	118	4	14	21
Co	1	16	16	1	17	1	2	3
Ni	10	47	43	6	93	5	60	18
Rb	15	73	67	21	70	11	74	84

Mo	12	3	3	1	11	1	4	3
Sn	6	20	36	5	10	5	9	11
Sb	1	33	43	0	3	0	1	2
La	3	18	27	1	28	1	7	11
Ce	4	45	63	2	41	2	13	20

4.4.2 C, N, S Elemental Composition

According to Table 4-5, CBM-D2 and CBM-W samples have the highest carbon content (%wt) of 77.47% and 79.47%. CBM-D1 sample has the lowest carbon of 3.61%. Nitrogen content is highest in the CBM-D2 sample. It is important to note that the sulphur percentages in CLM1 and CLM2 samples are higher than the other samples and some published data in literature (Li et al., 2010).

Table 4-5: C, N and S percentages in the samples by EA

Sample	%C	%N	%S
CBM	61.32	0.15	0.15
KBM2	53.60	0.16	0.19
KBM1	26.65	0.16	0.19
CBM-D2	77.47	0.22	0.04
CBM-D1	3.61	0.03	0.11
CBM-W	79.47	0.16	0.39
CLM2	40.79	0.09	0.99
CLM1	32.30	0.08	1.21

4.4.3 MLA Results

A list of the minerals/phases identified by MLA is given in Table 4-6. CB1, CB2, CB3 samples mainly consist of char, calcium carbonate, calcium rich slag, calcium rich char and slag rich in Ca-S-Al-Mg. CBM-D1 and KM2 samples were rich in SiO_2 and KM3 and KM1 samples were rich in carbon/char. It is interesting to note that main phase in both CBM-W and CBM-D2 samples is carbon; slag rich in Ca-S-Al-Mg and SiO_2 were identified as the other two main phases in these two samples. CLM1, CLM2 samples were similar to each other and the main minerals/phases present were alkali-feldspar, SiO_2, Ca-rich slag, Char, Ca-rich char, Ca-carbonate.

Table 4-6: Minerals/Phases identified in the samples by MLA

Sample name	Main mineral/phases	Other significant minerals/phases
CB 3	Char Calcium rich slag Calcium rich char Calcium carbonate Slag Ca-S-Al-Mg	Na-K chloride, Slag Ca-Fe-Mn-K-Si-Al-P-Ti, Slag Ca-P rich, Slag Ca-Si-Fe-P
CB 2	Char Calcium rich slag Calcium rich char Calcium carbonate	Al metal, Na-K chloride, Si-rich char, Slag Ca-rich silicate, Slag Si-Al-Ca-Fe-K, Silicon metal, SiO_2, Slag

	Slag Ca-S-Al-Mg	Pb-Zn-rich alkali, Slag Si-Al-K, Slag Ca-Si-Fe-P-Mn, Alkali silicate
CB 1	Char Calcium rich slag Calcium rich char Calcium carbonate Slag Ca-S-Al-Mg	Slag Ca-Si-Fe-P, SiO_2, Slag Ca-P rich, Slag Ca-Fe-Mn-K-Si-Al-P-Ti, Na-K chloride, Al-Silicate + Ca, Slag Si-Al-K, Slag Fe-Ca-P-K-Mn, Slag Si-rich alkali
KM 3 (same as KBM2)	Char Ca-rich char Na-K chloride Alkali-feldspar SiO_2-Muscovite Slag Si-Al-Ti	SiO_2, Muscovite-SiO_2, Slag Si-Al-K, Slag Ca-S-Al-Mg, Ti-oxide, Ca-rich slag, Slag Si-Al-Ca-Fe-K
KM 2	Alkali-feldspar Slag Si-Al-K SiO_2 Slag Ca-rich slicate	Slag Si-Al-Ca-Fe-K, SiO_2-Muscovite, Ca-rich slag, Slag Ca-S-Al-Mg, Ca-Mg rich carbonate, Mg-carbonate, Al-Silicate+Ca, Char, Epidote, Slag Ca-Si-Fe-P slag, Alkali silicate,

		Ca-rich char, Mg-rich clay, Ca-carbonate, Slag Si-Al-Fe-Mn-K-Ca, Slag Ca-Na silicate, Ca-rich slag, Plagioclase-feldspar, Fe-oxide
KM 1	Ca-rich slag Char Al-Silicate+Ca Ca-rich char Ca-carbonate	Slag Ca-rich slicate, SiO_2, Alkali-feldspar, Epidote, Slag Ca-Si-Fe-P slag, Mg-rich clay
CBM-D2	Char SiO_2 Slag Ca-S-Al-Mg	Alkali-feldspar, SiO_2-Muscovite, Ca-rich slag, Slag Ca-Fe-Mn-K-Si-Al-P-Ti, Slag Si-Al-K, Si-Al rich, Slag Ca-Fe-Mn-K-Si-Al-P, Slag Ca-Si-Fe-P slag, Al-Silicate+Ca, Slag Si-Al-Ca-Fe-K, Muscovite-SiO_2, Slag Ca-P rich, Ca-rich char, Si-rich char, Alkali silicate, Silicon metal, Ca-

		carbonate, Slag Si-rich alkali, Slag Ca-rich slicate
CBM-D1	SiO_2 Alkali-feldspar Slag Ca-Fe-Mn-K-Si-Al-P-Ti Slag Ca-Si-Fe-P slag	Char, Ca-rich slag, Slag Ca-Fe-Mn-K-Si-Al-P, Slag Si-Al-K, Slag Ca-S-Al-Mg, SiO_2-Muscovite, Si-Al rich, Slag Si-Al-Ca-Fe-K, Slag Ca-Fe-Mn rich. Plag-feldspar, Slag Si-Al-Fe-Mn-K-Ca, Slag Ca-P rich, Slag Si-rich alkali, Slag Ca-Fe-Mn rich, Ca-carbonate
CBM-W	Char Slag Ca-S-Al-Mg SiO_2	Ca-rich slag, Na-K chloride, Alkali-feldspar, Slag Ca-Fe-Mn-K-Si-Al-P-Ti, Silicon metal, Alkali silicate, Ca-rich char, Ca-carbonate
CLM2	Alkali-feldspar SiO_2 Ca-rich slag Char Ca-rich char	Plagioclase-feldspar, Slag Ca-Si-Fe-P slag, Slag Si-Mg-Al-Mn-Fe-Ca, Slag Ca-Si-Fe-Na-P-Mn-Mg, Slag Si-Mg-Al-Mn-Fe, Fe-oxide,

	Ca-carbonate	Si-rich char, Slag Si-Al-Fe-Mn-K-Ca, Slag Ca-Na silicate
CLM1	Alkali-feldspar SiO_2 Ca-rich slag Char Ca-rich char Ca-carbonate	Slag Ca-S-Al-Mg, Plag-feldspar, Slag Si-Mg-Al-Mn-Fe-Ca, Slag Ca-Si-Fe-P slag, Slag Ca-Si-Fe-Na-P-Mn-Mg, Slag Si-Mg-Al-Mn-Fe, Al-Silicate+Ca, Slag Si-Al-Ca-Fe-K, Slag Na-K-rich, Si-rich char, Na-K chloride, Slag Ca-Fe-Mn-K-Si-Al-P-Ti

4.4.4 XRD Results

Table 4-7 shows results from the XRD analysis. XRD patterns (**Appendix C**) show that these samples are partially crystalline (Berra et al., 2010) and these results are in agreement with the results (elements/minerals/phases) obtained from elemental analysis (ICP-MS, ICP-OES, CHN Elemental Analysis) and MLA. The XRD spectra for each sample is given in **Appendix C**.

Table 4-7: XRD results

Sample	Mineral/Phase	Chemical Formula
CBM	Calcite	$Ca(CO_3)$
	Portlandite	$Ca(OH)_2$
	Graphite	C
KBM2	Lead Bismuth Vanadium Oxide	Pb_4BiVO_8
	Calcite	$Ca(CO_3)$
	Barium Copper Oxide	$Ba_2Cu_2O_5$
	Biotite	$KFeMg_2(AlSi_3O_{10})(OH)_2$
KBM1	Quartz	SiO_2
	Strontium Sulphide	SrS
	Strontium Silicate	$SrSiO_3$
	Vanadium Oxide	VO_2
	Anglesite	$PbSO_4$
	Semseyite	$9PbS.4Sb_2S_3$
	Calcium Arsenide Bromide	Ca_2AsBr
	Lead Magnesium Carbonate	$PbMg(CO_3)_2$
CBM-D2	Calcium Carbonate	$Ca(CO_3)$
	Graphite 2H	C
CBM-D1	Silicon Dioxide - Quartz	SiO_2
	Cu-Ni-Co-Mn Oxide	$(Cu_{0.1}Ni_{0.61}Co_{0.2}Mn_{2.09})O_4$
	Albite	$Na(AlSi_3O_3)$

	Lime	CaO
	Calcium Catena-silicate	$Ca(SiO_3)$
	Anorthite	$Ca(Al_2Si_2O_8)$
	Iron Sulphate(IV)	$Fe(SO_3)$
CBM-W	Calcium Carbonate	$Ca(CO_3)$
	Graphite 2H	C
CLM2	Calcite	$Ca(CO_3)$
	Aluminium Arsenic Nickel	$(AlAsNi_3)_{0.8}$
	Copper Arsenide	$CuAs$
	Graphite	C
	Lithium Titanium Oxide	$(Li_2TiO_3)_{1.333}$
	Manganese Cobalt Silicon	Mn_2CoSi
	La-Sr-Mn-Ni Oxide	$(La_{1.5}Sr_{1.5})(Mn_{1.25}Ni_{0.75})O_{6.67}$
	Cadmium Zinc Sulphide	$(Cd_{0.15}\ Zn_{1.85})S_2$
CLM1	Calcite	$Ca(CO_3)$
	Silicon Dioxide - Alpha	SiO_2
	Aluminium Arsenic Nickel	$(Al_2As_2Ni_7)_{0.36}$
	Copper Arsenide	$CuAs$
	Graphite	C
	Vanadium(III) Phosphate Hydroxide Hydrate	$V_{1.23}(PO_4)(OH)_{0.69}(H_2O)_{0.64}$
	Aluminium Phosphate	$AlPO_4$

	Vanadium(IV) Oxide Cerium Oxide	VO_2 Ce_2O_3

4.4.5 Functional Groups from ATR- FTIR

FTIR analysis helps to identify the functional groups present in the ash/char samples. The ATR-FTIR spectrums in **Appendix A** show how the percentage transmittance varies with the frequency of the infra-red radiation for each ash/char sample. Table 4-8 identifies the possible functional groups that can be present in these samples based on the prominent stretch bands. XRD study confirms the presence of calcite, which is the potential source of C-O stretching in CBM, CLM2 and CLM1 samples. It also confirms the presence of SiO_2 in KBM1, CBM-D1, CLM1 which is the potential source of Si-O and Si-O-Si stretching. These explanations can be further validated using the results from MLA and elemental composition analysis. KBM2, CBM-D2 and CBM-W samples do not seem to contain any oxygen containing functional groups; hence, these samples are of hydrophobic nature (Liu et al., 2011, 2010).

Table 4-8: ATR - FTIR analysis results

Sample	Infra- red bands cm^{-1}	Possible functional groups (Smidt et al., 2011)
CBM	1400, 800	C-O stretching (carbonate at 1450-1410 and 875)
KBM2	-	No prominent stretch bands

KBM1	1400, 1000-800	C-O stretching (carbonate at 1450-1410 and 875) Si-O and Si-O-Si stretching(clay minerals and silica at 1030)
CBM-D2	-	No prominent stretch bands
CBM-D1	1100	Si-O stretching (clay minerals and and quartz at 1080) Si-O-Si stretching (silica at 1030)
CBM-W	-	No prominent stretch bands
CLM2	1400,1100, 800	C-O stretching (carbonate at 1450-1410 and 875, 713) S-O stretching (sulphate at 1140-1080) Si-O stretching (quartz at 1080)
CLM1	1400,1100, 800	C-O stretching (carbonate at 1450-1410 and 875, 713) S-O stretching (sulphate at 1140-1080) Si-O stretching (quartz at 1080)

4.4.6 SEM Results

Scanning electron micrographs of the eight samples are given below (Figures 4-3 to 4-10). KBM2, CBM-W, CBM-D2 samples mainly contain meso/macro porous carbon particles (Adeoti, 2011). A honeycomb structure is clearly visible in the images of CBM-W sample. The images also show the presence of a large number of fine particles on the carbon surface which may be a result of condensation of trace elements (amorphous slag caused during combustion and cooling) or due to the deposition of different species of alkali and other elements (Li et al., 2012). This can be further confirmed by the results

from the MLA which confirms the presence of calcium rich char, alkali-feldspar, silica, slag rich in Si, Al, Mg, S, Ca, Ti in these samples.

CBM, KBM1 and CBM-D1 samples are more heterogeneous. Both CBM and KBM1 samples contain carbon particles, silica and amorphous slag. KBM1 and CBM-D1 samples contain small irregular and skeletal shaped particles. Silica (quartz) in the CBM-D1 sample can be easily identified because of their low reflectance (Li et al., 2012).

CLM2 and CLM1 samples contain carbon particles rich in alkali species. Image of the CLM2 sample clearly shows alkali species (calcium rich slag and other species) deposited on carbon surface.

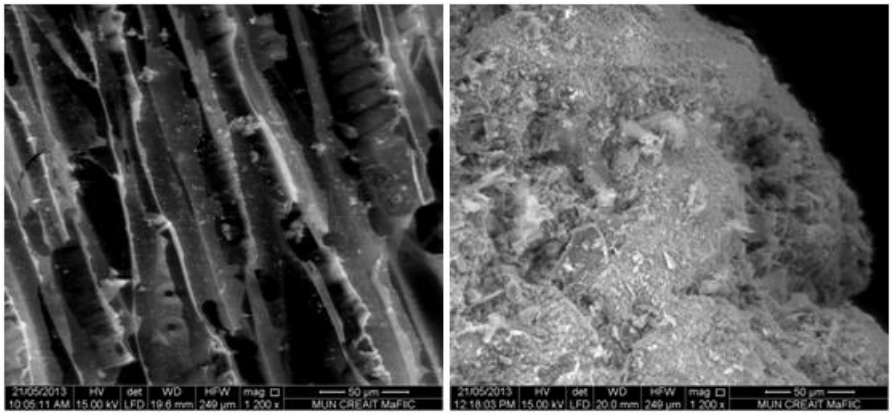

Figure 4-3: CBM (1.18 mm < d < 4 mm) SEM images

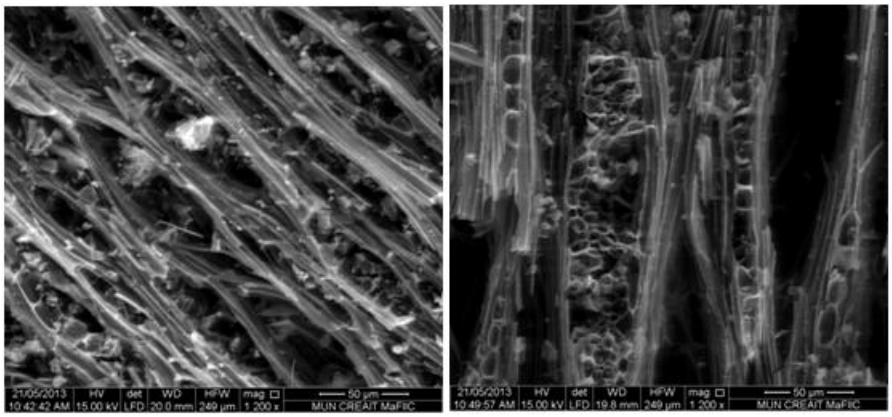

Figure 4-4: KBM2 (1.18 mm < d < 4 mm) SEM images

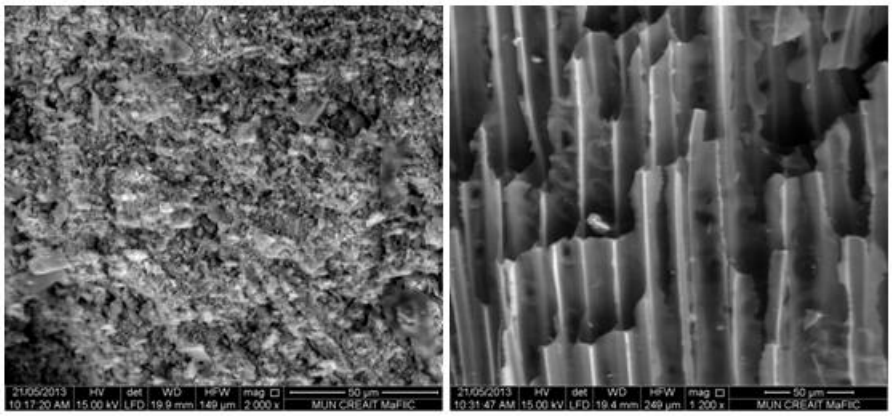

Figure 4-5: KBM1 (d<1.18 mm) SEM images

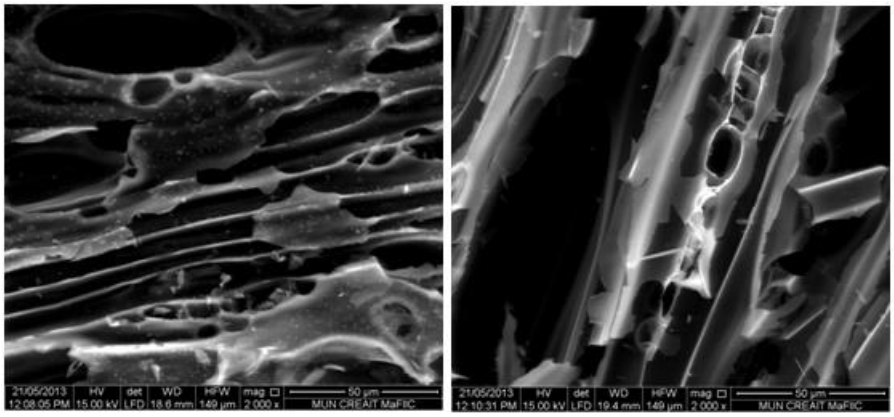

Figure 4-6: CBM-D2 (500 µm < d < 1.18 mm) SEM images

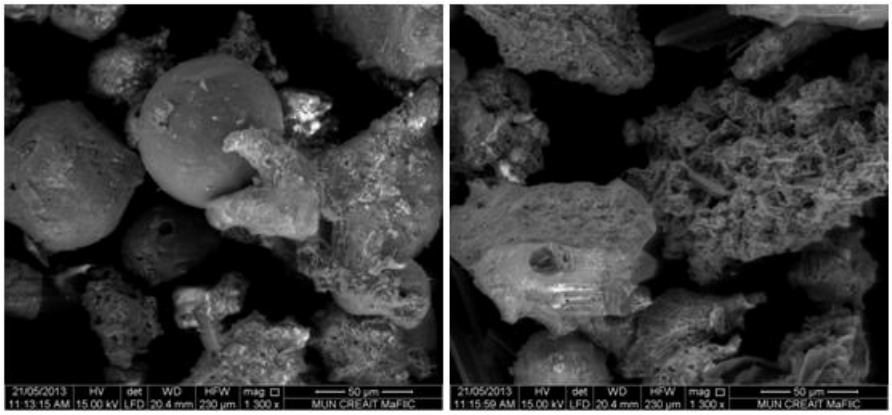

Figure 4-7: CBM-D1 (d < 500 µm) SEM images

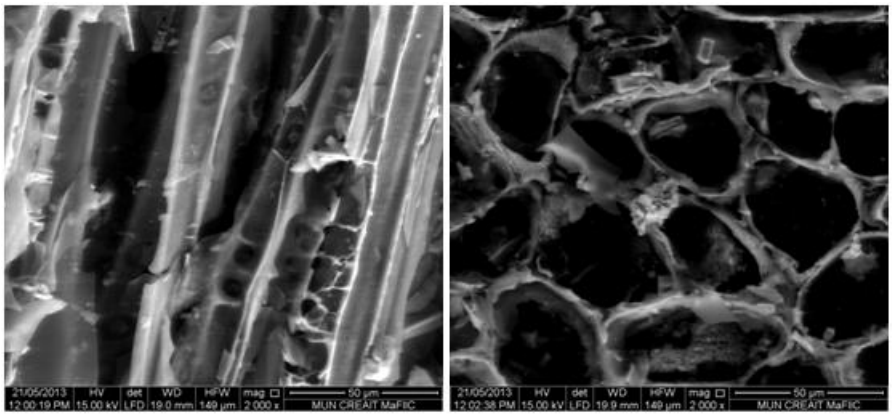

Figure 4-8: CBM-W (1.18mm < d < 4mm) SEM images

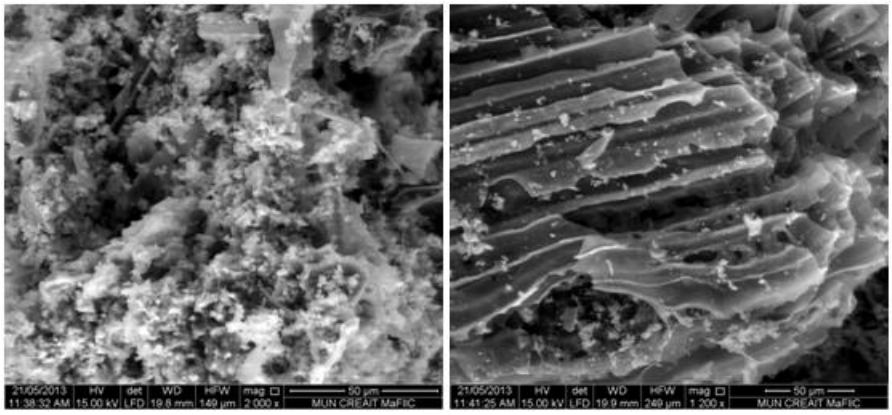

Figure 4-9: CLM2 (500 µm < d < 1.18 mm) SEM images

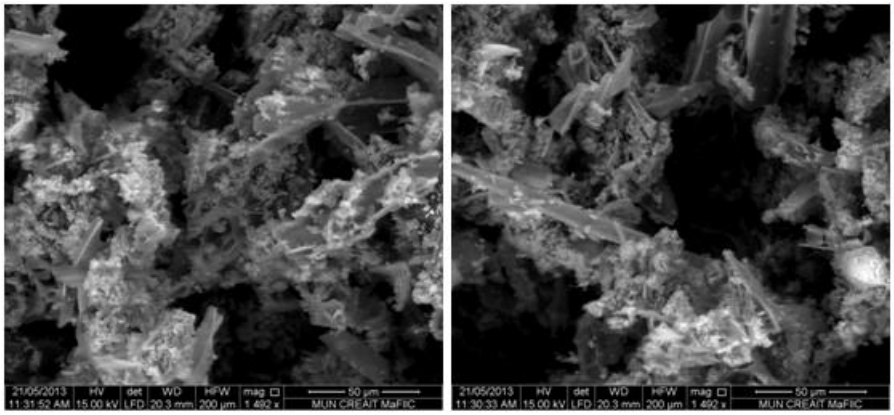

Figure 4-10: CLM1(d < 500 µm) SEM images

4.4.7 Specific Surface Area, Pore Volume and Mean Pore Diameter Results

KBM2, CBM-D2, CBM-W and CBM samples have high specific surface areas compared to other samples which can be attributed to the high carbon content in these samples (Table 4-9). Measured surface areas for CBM-D1 and CLM1 with CO_2 are higher than the values measured with N_2. The results are similar to Yao et al., 2011 and the reason is that micro pores are also taken into account with CO_2 measurement. Both specific surface area and pore volume values obtained for KBM1 and CBM-D1 samples are low compared to other six samples and similar to results obtained by (Adeoti, 2011; Li et al., 2010; Liu et al., 2010).

Table 4-9: Specific surface area, pore volume and mean pore diameter values

Results from University of New Brunswick (With N_2)			
Sample	Specific surface area (BET) [m^2 /g]	Total pore volume [cm^3/ g]	Mean pore diameter [nm]
CBM	361.480	0.1938	2.1440
KMB2	592.150	0.2974	2.0090
KMB1	41.456	0.0255	2.4649
CBM-D2	498.560	0.2150	1.7252
CBM-D1	17.842	0.0123	2.7668
CBM-W	425.330	0.1820	1.7114
CLM2	281.480	0.1667	2.3694
CLM1	178.170	0.1153	2.5877

Results from Micromeritics Analytical Services (With CO_2)				
Sample	Method	Specific surface area [m^2 /g]	Pore volume [cm^3/ g]	Mean pore diameter [nm]
CBM-D1	❶	43.946	0.0031	-
	❷	80.749	0.0323	-
	❸	231.942	0.1462	2.5212
CLM1	❶	247.522	0.0428	-
	❷	240.8768	0.0965	-

	❸	348.6429	0.1564	1.7949

Notes: ❶ Density Functional Theory, ❷ Dubinin-Radushkevich method, ❸ Dubinin-Astakhov method

4.4.8 Bulk Density

The highest bulk density values are obtained for CBM-D1 sample which contains smaller but heavy particles (Table 4-10). CBM-D2 and CBM-W samples with larger particles of mostly unburned carbon gave the lowest bulk density values.

Table 4-10: Bulk density of ash/char samples

Sample	Bulk density (g/cm^3)
CBM-D2	0.101
CBM-D1	0.956
CBM-W	0.101
CLM2	0.263
CLM1	0.448

4.4.9 pH Values

Typically, high pH values are obtained for biomass ash than for char derived from biomass (Adeoti, 2011; Liu et al., 2010; Pan and Eberhardt, 2011; Shang et al., 2012). All

the samples analyzed are highly alkaline and the lowest pH obtained was for CBM-W char sample at pH 9.6 (Table 4-11).

Table 4-11: pH of ash/char samples

Sample	pH at 25^{o}C
CBM	11.6
KBM2	10.7
KBM1	11.6
CBM-D2	11.4
CBM-D1	12.0
CBM-W	9.6
CLM2	11.1
CLM1	11.2

4.4.10 Total Alkalinity Values

Total alkalinity of CLM2 and CLM1 samples are high which explains that these samples have a higher ability than CBM-D2 or CBM-W samples to increase the pH and reduce the acidity of effluent water streams such as AMD (Table 4-12).

Table 4-12: Total alkalinity of ash/char samples

Samples	Volume of H_2SO_4 (endpoint pH=4.5)	Total Alkalinity (mg/L $CaCO_3$)
CBM-D2	2.1 mL	420
CBM-D1	5 mL	1000
CBM-W	0.5 mL	100
CLM2	13.6 mL	2720
CLM1	11.8 mL	2360

4.4.11 TGA Results

Thermo gravimetric Analysis (TGA) determines the presence of unburned carbon (weight loss in the range of 300–500 ^{o}C) and inorganic carbon (weight loss in the range of 630–750 ^{o}C) in the ash/char samples (Berra et al., 2011). Weight % and Derivative weight (%/^{o}C) vs. Temperature graphs from TGA are given in **Appendix B.** The residual weight percentages of CBM-D2 and CBM-W are the lowest showing more than 90% weight loss when heated up to 1000^{o}C under inert atmosphere (Table 4-13). This can be related to the high carbon content present in these samples as per the results from the CNS elemental analysis. Residual weight percentage of CBM-D1 and KBM1 samples are very high at approximately 95% with about 5% weight loss occurring in the temperature range of 450 ^{o}C to 700 ^{o}C. It is important to note that during 650 ^{o}C - 850 ^{o}C, rate of weight loss increased significantly for CLM2, CLM2 samples which may be due to decomposition of calcite in this temperature range (Rajamma et al., 2009).

Table 4-13: Residue weight percentages from TGA

Sample	Residue weight %
CBM	28.05
KBM2	21.79
KBM1	94.56
CBM-D2	8.69
CBM-D1	93.94
CBM-W	7.24
CLM2	33.51
CLM1	45.26

4.5 Conclusion

From the characterization analysis, it can be concluded that the behavior of CBM, KBM2, CBM-D2, CBM-W is similar to typical biomass derived char; KBM1 and CBM-D1 samples have characteristics similar to typical biomass derived ash; CLM2, CLM1 samples are complex mixtures of both ash and small particles of unburned carbon, thus have moderate characteristics compared to all other analyzed samples.

Major elements present in the eight samples analyzed were Ca, Si, Al, Na, K, Fe, Mn, Mg, P, Ti. CBM-D2 and CBM-W had low concentrations of most elements analyzed by the ICP-MS and ICP-OES techniques compared to other six samples. However, these two

samples had the highest C percentages (77.47 and 79.47%). CLM1 and CLM2 samples have considerably high sulphur percentages. MLA results showed that these samples mainly consist of char, silica, alkali-feldspar, calcium carbonate, aluminium silicate, slag rich in various elements like Ca, S, Ti, Al, Fe, Mn, S, P, Na, K,Mg. Results from the XRD analysis were in agreement with the MLA results. Although, ATR-FTIR analysis showed no prominent stretch bands for CBM-D2, KBM2, CBM-W samples, the following functional groups were found to be present in other samples: Si-O (quartz), S-O (sulphate), C-O (carbonate) in CLM2 and CLM1 samples; C-O (carbonate) in CBM sample; Si-O (quartz), Si-O-Si (silica), C-O (carbonate) in KBM1 sample; Si-O (quartz), Si-O-Si (silica) in CBM-D1 sample. SEM micrographs were useful in understanding the morphology of these samples. Highest BET specific surface area was obtained for KMB2 sample (592.150 m^2/g) and the lowest BET surface area was found in CBM-D1 sample (17.842 m^2/g).

CBM-D1 sample had the highest bulk density value (0.956 g/cm^3) where as CBM-W and the CBM-D2 samples had the lowest bulk density (0.101 g/cm^3). CBM-W sample had the lowest pH value (pH 9.6) and CBM-D1 sample gave the highest pH value (pH 12). Total alkalinity of CBM-W (100 mg/L $CaCO_3$) and CBM-D2 (420 mg/L $CaCO_3$) samples were very low compared to high total alkalinity of CLM1 and CLM2 samples, 2360 and 2720 mg/L $CaCO_3$ respectively. High weight loss % given by the TGA analysis for CBM-D2 and CBM-W samples confirmed that the high unburned carbon content in CBM-D2 and

CBM-W samples is the reason for high BET surface area and low density of these samples.

The next step after characterization is to identify utilization options for these ash/char samples. Potential utilization directions for these biomass ash/char based on characterization results are: soil amendment (liming, neutralization, stabilization) and fertilization; adsorbents for water treatment and gas purification; mine backfilling and excavation work, neutralization of acid water and waste; recovery of char; recovery of Fe fraction enriched in some trace elements; recovery of other valuable elements and compounds; refractory materials (silica minerals, calcium silicates, lime); synthesis of zeolites; construction materials (Vassilev et al., 2013b). However, preliminary tests need to be carried out in order to confirm the suitability of using these ash/char sample for any specific application in order to understand the feasibility, cost implications and other environmental concerns.

Bibliography - Chapter 4

Adeoti, I. A.: Characterization and Alternative Use Study of Fly Ash, 160 pp., Memorial University of Newfoundland., 2011.

Anon: FEI website, [online] Available from: http://www.fei-natural-resources.com/geosciences/products.aspx, 2013.

Arami-Niya, A., Abnisa, F., Shafeeyan, M. S., Daud, W. M. A. W. and Sahu, J. N.: Optimization of synthesis and characterization of palm shell-based bio-char as a by-product of bio-oil production process, , 7, 246–264, 2012.

Berra, M., Casa, G. De, Orso, M. D., Galeotti, L., Mangialardi, T., Paolini, A. E. and Piga, L.: Reuse of Woody Biomass Fly Ash in Cement-Based Materials : Leaching Tests, in Recycling of Biomass Ashes, edited by H. Insam and B. A. Knapp, pp. 133–146, Springer Berlin Heidelberg., 2011.

Berra, M., Dell'orso, M., Mangialardi, T., Paolini, A. E. and Piga, L.: Chemical and Environmental Characterization of Fly Ash from Woody Biomass Combustion, in Internation Symposium on Energy from Biomass and Waste, CISA, Environmental Sanitary Engineering Centre, Venice., Italy., 2010.

Chowdhury, Z. Z., Zain, S. M. and Khan, R. A.: Equilibrium Kinetics and Isotherm Studies of Cu (II) Adsorption from Waste Water onto Alkali Activated Oil Palm Ash, , 8(3), 230–237, 2011.

Churchill, D. and Kirby, A.: CB Pulp and Paper Ash Diversion, Phase 1: Initial Ash Testing, Project No 09-14., 2010.

Eberhardt, T. L. and Pan, H.: Elemental analyses of chars isolated from a biomass gasifier fly ash, Fuel, 96, 600–603, doi:10.1016/j.fuel.2012.01.010, 2012.

Gil, A. and Grange, P.: Application of the Dubinin-Radushkevich and Dubinin-Astakhov equations in the characterization of microporous solids, Colloids Surfaces A Physicochem. Eng. Asp., 113(1-2), 39–50, doi:10.1016/0927-7757(96)81455-5, 1996.

Giro, R. P., Sua, I., Ruiz, B., Fuente, E. and Gil, R. R.: Fly Ash from the Combustion of Forest Biomass (Eucalyptus globulus Bark): Composition and Physicochemical Properties, Energy & Fuels, 2012.

Gupta, V. K. and Sharma, S.: Removal of Zinc from Aqueous Solutions Using Bagasse Fly Ash - a Low Cost Adsorbent, , (Cl), 6619–6624, 2003.

Kruger Inc.: Brompton Biomass Cogeneration Plant, [online] Available from: http://www.krugerenergy.com/html/en/cogeneration/ke_cogen_brompton_en.html (Accessed 23 May 2013a), 2013.

Kruger Inc.: Corner Brook Biomass Cogeneration Plant, [online] Available from: http://www.krugerenergy.com/html/en/cogeneration/ke_cogen_cornerbrook_en.html (Accessed 23 May 2013b), 2013.

Li, L., Yu, C., Bai, J., Wang, Q. and Luo, Z.: Heavy metal characterization of circulating fluidized bed derived biomass ash., J. Hazard. Mater., 233-234, 41–7, doi:10.1016/j.jhazmat.2012.06.053, 2012.

Li, X., Guo, X., Wang, S., Wang, K., Luo, Z. and Wang, Q.: Characterization and Analysis of Char Produced by Biomass Fast Pyrolysis, 2010 Asia-Pacific Power Energy Eng. Conf., 1–4, doi:10.1109/APPEEC.2010.5448524, 2010.

Liu, W. J., Zeng, F. X., Jiang, H. and Zhang, X. S.: Preparation of high adsorption capacity bio-chars from waste biomass., Bioresour. Technol., 102(17), 8247–52, doi:10.1016/j.biortech.2011.06.014, 2011.

Liu, Z., Zhang, F.-S. and Wu, J.: Characterization and application of chars produced from pinewood pyrolysis and hydrothermal treatment, Fuel, 89(2), 510–514, doi:10.1016/j.fuel.2009.08.042, 2010.

Luo, Y., Giammar, D. E., Huhmann, B. L. and Catalano, J. G.: Speciation of Selenium, Arsenic, and Zinc in Class C Fly Ash, Energy & Fuels, 25(7), 2980–2987, doi:10.1021/ef2005496, 2011.

McLaughlin, H., Shields, F., Jagiello, J. and Thiele, G.: Analytical Options for Biochar Adsorption and Surface Area Authors, in 2012 US Biochar Conference session on Char Characterization, pp. 1–19. [online] Available from: http://www.micromeritics.com/Repository/Files/Analytical_Options_for_Biochar_full_paper_2012.pdf, 2012.

Pan, H. and Eberhardt, T.: Characterization of Fly Ash from the Gasification of Wood and Assessment for Its Application as a Soil Amendment., 2011.

Pastor-Villegas, J., Pastor-Valle, J. F., Rodríguez, J. M. M. and García, M. G.: Study of commercial wood charcoals for the preparation of carbon adsorbents, J. Anal. Appl. Pyrolysis, 76(1-2), 103–108, doi:10.1016/j.jaap.2005.08.002, 2006.

Pengthamkeerati, P., Satapanajaru, T., Chatsatapattayakul, N., Chairattanamanokorn, P. and Sananwai, N.: Alkaline treatment of biomass fly ash for reactive dye removal from aqueous solution, Desalination, 261(1-2), 34–40, doi:10.1016/j.desal.2010.05.050, 2010.

Pengthamkeerati, P., Satapanajaru, T. and Singchan, O.: Sorption of reactive dye from aqueous solution on biomass fly ash., J. Hazard. Mater., 153(3), 1149–56, doi:10.1016/j.jhazmat.2007.09.074, 2008.

Quantachrome Instruments: An Introduction to Calculation Methods for Surface Area and Pore Size from Gas Sorption Data, [online] Available from: http://www.atomikateknik.com/pdf/Porous Materials Primer gas sorption calculation methods.pdf (Accessed 30 December 2013), 2013.

Rajamma, R., Ball, R. J., Tarelho, L. a C., Allen, G. C., Labrincha, J. a and Ferreira, V. M.: Characterisation and use of biomass fly ash in cement-based materials., J. Hazard. Mater., 172(2-3), 1049–60, doi:10.1016/j.jhazmat.2009.07.109, 2009.

Sasithorn, J., Wiwattanadate, D. and Sangsuk, S.: Utilization of Fly Ash from Power Plant for Adsorption of Hydrocarbon Contamination in Water, J. Met. Mater. Miner., 20(1), 5–10, 2010.

Shang, G., Shen, G., Wang, T. and Chen, Q.: Effectiveness and mechanisms of hydrogen sulfide adsorption by camphor-derived biochar, J. Air Waste Manage. Assoc., 62(8), 873–879, doi:10.1080/10962247.2012.686441, 2012.

Smidt, E., Böhm, K. and Schwanninger, M.: Fourier Transforms - New Analytical Approaches and FTIR Strategies, edited by G. Nikolic, InTech., 2011.

Tailor, R., Shah, B. and Shah, A.: Sorptive Removal of Phenol by Zeolitic Bagasse Fly Ash: Equilibrium, Kinetics, and Column Studies, J. Chem. Eng. Data, 57(5), 1437–1448, doi:10.1021/je300399y, 2012.

Tascon, J. M. D.: Novel Carbon Adsorbents, First Edit., Elsevier, Oxford, UK., 2012.

Vadapalli, V. R. K., Gitari, M. W., Petrik, L. F., Etchebers, O. and Ellendt, A.: Integrated acid mine drainage management using fly ash, J. Environ. Sci. Health. A. Tox. Hazard. Subst. Environ. Eng., 47(1), 60–9, doi:10.1080/10934529.2012.629582, 2012.

Vassilev, S. V., Baxter, D., Andersen, L. K. and Vassileva, C. G.: An overview of the composition and application of biomass ash. Part 1. Phase–mineral and chemical composition and classification, Fuel, 105, 40–76, doi:10.1016/j.fuel.2012.09.041, 2013a.

Vassilev, S. V., Baxter, D., Andersen, L. K. and Vassileva, C. G.: An overview of the composition and application of biomass ash. Part 2. Potential utilisation, technologcal and ecological advantages and challenges, Fuel, 105, 19–39, doi:10.1016/j.fuel.2012.10.001, 2013b.

Yao, Y., Gao, B., Inyang, M., Zimmerman, A. R., Cao, X., Pullammanappallil, P. and Yang, L.: Removal of phosphate from aqueous solution by biochar derived from anaerobically digested sugar beet tailings., J. Hazard. Mater., 190(1-3), 501–7, doi:10.1016/j.jhazmat.2011.03.083, 2011.

Zellstoff Celgar Limited Partnership: Zellstoff Celgar Resources, [online] Available from: http://www.celgar.com/Resources.aspx (Accessed 23 May 2013), 2013.

Zheng, W., Guo, M., Chow, T., Bennett, D. N. and Rajagopalan, N.: Sorption properties of greenwaste biochar for two triazine pesticides., J. Hazard. Mater., 181(1-3), 121–6, doi:10.1016/j.jhazmat.2010.04.103, 2010.

Chapter 5 : Adsorption of Thiosulphate, Trithionate, Tetrathionate Using Biomass Ash/Char

Bhagya M.K. Range, Kelly A. Hawboldt

Faculty of Engineering and Applied Science, Memorial University of Newfoundland, St John's, NL, Canada. A1B3X5

Abstract

Thiosalts (sulphur oxy-anions) are generated in the process of mining of sulphide ores such as pyrite. Although thiosalts have relatively low toxicity, Sulphuric acid formed as the final product in the oxidation of these sulphide ores, leads to pH depression in the receiving water bodies creating toxic conditions for aquatic plant and animal life. In the present study, suitability of using biomass ash/char as an adsorbent to remove three thiosalt species, thiosulphate ($S_2O_3^{2-}$), trithionate ($S_3O_6^{2-}$) and tetrathionate ($S_4O_6^{2-}$) from aqueous solutions was investigated. The biomass ash used in this study was obtained from two pulp and paper mills and physico-chemical, mineralogical and thermal properties were determined as outlined in Chapter 4. Batch mixing experiments were conducted with three different types of biomass ash/char (CBM-D1, CBM-W, CLM1) where initial solution pH (2, 4, 7, 9), adsorbent dose (20, 50, 80 g/L) and temperature (5, 21, 35 ^{o}C) were varied. The highest adsorption capacities were recorded at the highest adsorption dose (80 g/L) which were 10.82, 10.29, 14.24 mg/g of CBM-W char for thiosulphate, trithionate and tetrathionate respectively. Variation in pH and temperature did not have a measureable effect on sulphur adsorption. The biomass had a moderate

neutralization effect on solutions as the final pH ranged from 6.6 - 9.4 depending on dosage and initial pH. The Freundlich isotherm equation was found to be a better fit than the Langmuir isotherm equation in modeling the experimental isotherm data at the given experimental conditions.

5.1 Introduction

Partially oxidized sulphur compounds which are also known as thiosalts are formed during mining and mineral processing activities during oxidation of sulphide ores (e.g. pyrite, pyrrhotite) (Negeri et al., 1999). The thiosalts generated and dissolved in wastewater during mineral processing can further oxidize to form sulphuric acid leading to low pH values in natural water bodies, impacting aquatic plants and animals (Chanda et al., 1984). Some of the other adverse effects include depletion of dissolved oxygen, reduction of buffering capacity and dissolution of metals from the sediment (Dinardo and Sally, 1998). Thiosalt species identified in mining effluent water include thiosulphate ($S_2O_3^{2-}$), trithionate ($S_3O_6^{2-}$), tetrathionate ($S_4O_6^{2-}$) and also low concentrations of higher polythionates (Dinardo and Sally, 1998; Miranda-Trevino et al., 2012). The reactivity of thiosalts is complex and depends on many factors such as temperature, pH, dissolved oxygen content, microorganisms and presence of heavy metals. At typical tailing pond conditions most sulphur compounds oxidize to sulphate, however, thiosalts are slow to oxidize and are present in the tailings pond (Miranda-Trevino et al., 2012; Wasserlauf and Dutrizac, 1982).

The Environmental Code of Practice for Metal Mines in Canada states that thiosalt management practices should be in place at sites where there is a risk of thiosalts occurring in wastewater from ore processing. These include minimizing the concentration of thiosalts in the discharged wastewater from the mining site, ensuring degradation of thiosalts on site, monitoring concentrations of thiosalts in wastewater and checking for pH depression downstream to avoid harmful effects on aquatic species and drinking water (Environment Canada, 2009).

Treatment of mining effluent streams by adsorption could be a cost effective method if combustion by-products such as biomass ash and char are used as adsorbents. The pulp and paper industry has cogeneration plants where power boilers utilize a significant percentage of forestry residue (wood refuse) and/or fossil fuels as a heat source. In this process, carbon rich ash is generated as a combustion by-product. If the ash can be used as an adsorbent to treat thiosalts, it would reduce the demand for landfill space required for ash disposal. It will also address other concerns such as cost of transportation and manpower required for ash handling and landfill fires which can occur due to heat of ash. Using these ash as adsorbents is a sustainable approach to waste handling as one waste stream is used to treat another waste stream. Therefore, in this study, we investigate the possibility of using biomass ash/char from pulp and paper mill boilers to treat three thioslat species: thiosulphate ($S_2O_3^{2-}$), trithionate ($S_3O_6^{2-}$), tetrathionate ($S_4O_6^{2-}$).

5.2 Sulphur Pourbaix (Eh-pH) Diagrams

Pourbaix or Eh-pH diagrams developed by the Belgian Chemist, Marcel Pourbaix, depict the thermodynamic stability of an element as a function of electrode potential and pH in an aqueous electrochemical system. These diagrams illustrate the oxidizing and reducing abilities of the major stable species of an element and are widely used in corrosion, geochemical, environmental applications (McCafferty, 2010). However, these diagrams do not provide information on chemical kinetics. In a Pourbaix diagram, there are three possible straight lines: horizontal lines which are for reactions involving electrode potential; vertical lines which are for reactions involving only pH; and slanted lines which are for reactions including both electrode potential and pH. The regions between various lines represents where specific species are thermodynamically stable (McCafferty, 2010). Understanding the form in which an element is present at a certain pH/ potential is very useful in designing treatment processes for removal of these elements from effluent water systems.

The following Eh-pH diagram (Figure 5-1), generated by HSC Chemistry 7.1 software, shows the thermodynamic stability areas of different sulphur species that may be present in the solutions of sodium thiosulphate ($Na_2S_2O_3$), sodium trithionate ($Na_2S_3O_6$), potassium tetrathionate ($K_2S_4O_6$) used in this study at 21 ^oC. Sulphur species considered in this Eh-pH analysis are elemental sulphur (S), H_2S(a), HS^-(a), S^{2-}(a), HSO_3^-(a), HSO_4^-(a), H_2SO_4(a), H_2SO_3(a), SO_4^{2-}(a), SO_3^{2-}(a), $S_2O_3^{2-}$(a), $S_3O_6^{2-}$(a), and $S_4O_6^{2-}$(a). The region in between the dotted lines in the diagrams are the stability area for water (H_2O).

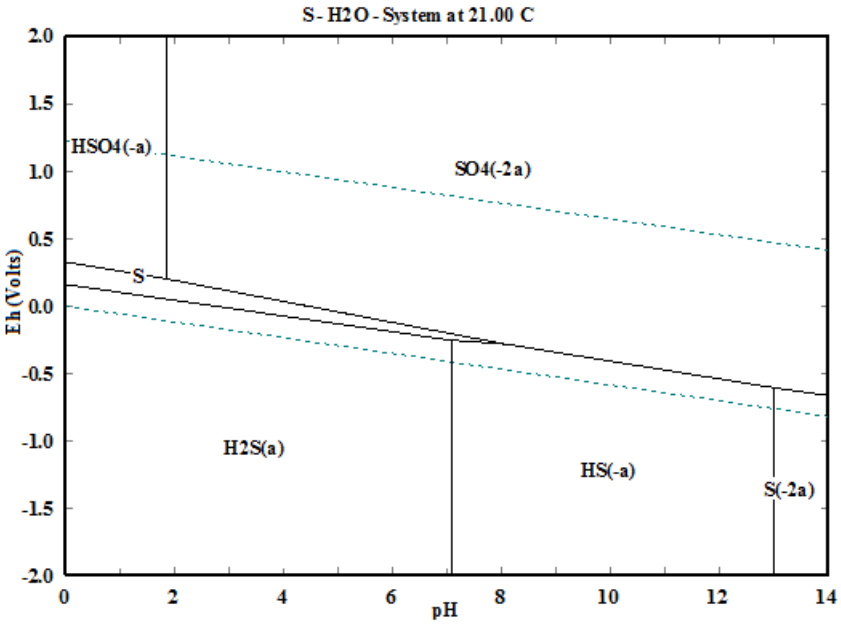

Figure 5-1: Pourbaix diagram for the S-O-H system at temperature 21 ^{o}C, molality 0.25 mol/kg H_2O, pressure 1 atm

5.3 Materials and Experimental Methodology

5.3.1 Characterization of Biomass Ash/Char

Three biomass ash/char samples were used in this study; CBM-D1, CBM-W and CLM1. CBM-D1 and CBM-W samples were obtained from Corner Brook Pulp and Paper Limited (CBPPL) located in Corner Brook, NL Canada. CLM1 sample was obtained from Zellstoff Celgar Limited Partnership (ZCLP) located in Castlegar, BC Canada. The CBM-D1 sample was collected from CBPPL's cogeneration plant in dry form prior to water impoundment. CBM-W was collected from the water impounded conveyor where char

floats on top of water. CLM1 was collected from ZCLP's power boiler and it is the ash residue left in the boiler after combustion. All the samples were dried at 105 ^{o}C for 24 hours and sieved to obtain the required size fractions as given in Table 5-1 (Please refer Chapter 4 for more details on samples).

Table 5-1: Sample details (source and size fractions)

Sample name	Description	Sieve mesh size
CBM-D1	Corner Brook Mill dry sample	d < 500 µm
CBM-W	Corner Brook Mill wet sample	1.18 mm < d < 4 mm
CLM1	Zelstoff Celgar Mill sample	d < 500 µm

The biomass ash/char samples were characterized by: inductively coupled plasma and optical emission spectrometry (ICP-MS, ICP-OES), CNS (carbon, nitrogen, sulphur) analysis, mineral liberation analysis (MLA), X-ray diffraction (XRD), Fourier transform infrared spectroscopy (ATR-FT-IR), scanning electron microscopy (SEM) analysis, specific surface area, pore volume, bulk density, pH, total alkalinity, thermo-gravimetric analysis (TGA).

The complete characterization methodology and discussion of results for the three ash/char samples (CBM-D1, CBM-W and CLM1) is outlined in Chapter 4. Initial adsorption tests indicated that the highest sulphur adsorption percentage/capacity occurred with CBM-W as an adsorbent in all three solutions (i.e. thiosulphate, trithionate

and tetrathionate) and therefore, CBM-W sample was selected for further adsorption experiments. The properties of CBM-W samples are briefly outlined in the 'Results and Discussion' section in this chapter.

5.3.2 Materials/ Chemicals

Sodium thiosulphate (Reagentplus 99%) $Na_2S_2O_3$ and potassium tetrathionate, $K_2S_4O_6$, were ordered from Sigma-Aldrich Canada Co. Sodium trithionate, $Na_2S_3O_6$ was synthesized in the laboratory using the method followed by Vongporm, 2008. The method is outlined below.

Trithionate Synthesis Methodology: 15.6 g of sodium thiosulphate pentahydrate was weighed and dissolved in 9 mL of deionized water with the aid of a sonicator. The solution was then placed in ice and cooled to 1 ^{o}C with continuous stirring. 14 mL of 30% (w/v) hydrogen peroxide was added to the cold thiosulphate solution dropwise by using a dropping pipette while maintaining continuous stirring and not letting the temperature rise above 20 ^{o}C. Stirring was stopped after all the hydrogen peroxide was added and the solution was maintained in ice for 2 more hours. Sodium sulphate that was crystallized during this period, was removed by suction filtration and the crystals were washed with 10 mL ethanol (95%) which was added to the filtrate. The filtrate was then transferred to a 200 mL beaker and cooled to 3 ^{o}C and then 25 mL of ice-cold ethanol was added and the mixture was left for another 1 hour at 0 - 3 ^{o}C. Sodium sulphate crystals formed, were again removed by suction filtration and washed with 20 mL of ice-cold

ethanol which also joined the filtrate. The filtrate and additional 10 mL of ethanol which was used to rinse the flask was transferred to another beaker containing 100 mL of cold ethanol. This mixture was stirred and left at 3 ^{o}C for another 2 hours. During this time, sodium trithionate crystallizes and is isolated by suction filtration. The solid was washed with 5 mL of ethanol, 5 mL of acetone and dried in a desiccator (Vongporm, 2008). The purity was determined to be 96 - 100 % by characterizing with UV-Visible spectrometry and X-ray Diffraction (XRD).

5.3.3 Batch Adsorption Experiments

Batch experiments were conducted by mixing (at 120 rpm) different doses of ash/char samples (20, 50, 80 g/L) with 100 mL of individual thiosulphate, trithionate and tetrathionate at different pH (2, 4, 7, 9) and temperature (5, 21, 35 ^{o}C) until equilibrium is achieved (24 hrs). The total sulphur concentrations in the solutions were 2000 mg/L with initial concentrations of 3500 mg/L $S_2O_3^{2-}$, 4000 mg/L $S_3O_6^{2-}$, 3500 mg/L $S_4O_6^{2-}$ in the individual solutions. Batch isotherm adsorption experiments were conducted by changing the initial concentration of individual thiosalt solutions; thiosulphate (175 - 3500 mg/L $S_2O_3^{2-}$); trithionate (200 - 4000 mg/L $S_3O_6^{2-}$) and; tetrathionate (175 - 3500 mg/L $S_4O_6^{2-}$). at 21^{o}C (room temperature) and pH 2 (to represent pH of acidic mining effluent waters). Solution pH values were adjusted by using dilute HNO_3 acid before mixing the ash. After mixing for 24 hours, all the samples were filtered through No 42 Whatman filter papers and the spent adsorbent samples were completely dried (at 60^{o}C for 48 hours), crushed and sent to the Stable Isotopes for Innovative Research Lab of Department of Geological

Sciences at University of Manitoba for elemental analysis (total sulphur percentage analysis). The sulphur percent adsorbed onto ash and the equilibrium sulphur concentration in the solution was calculated from the results. Although, the standard deviation of sulphur elemental analysis measurements was less than 0.05wt% (or +/- 25 mg sulphur/L or +/- 1.25% of 2000 mg sulphur/L) at a biomass ash dose of 50 g/L, due to the heterogeneous nature of the ash/char samples used as the adsorbent, the error can be higher than this. Use of other sulphur analytical techniques such as inductively coupled plasma mass spectrometry (ICP-MS), iodine titration for thiosulphate and capillary electrophoresis for analytical determination of thiosalts were considered, but found to be challenging mainly due to the matrix effect. Matrix effect is the combined effect of all the components of the aqueous sample (e.g. dissolved components from biomass ash) other than the analyte (sulphur species) on the measurement of the quantity (IUPAC, 2009).

The percentage of sulphur absorbed and adsorption capacity were calculated using the following equations.

$$\text{Adsorption capacity}\left(\frac{\text{mg}}{\text{g}}\right) = \frac{(C_i - C_e)\ \text{x}\ V}{m} \qquad (5\text{-}1)$$

$$\text{Adsorption \%} = \frac{(C_i - C_e)\ \text{x}\ 100}{C_i} \qquad (5\text{-}2)$$

C_i = Initial concentration of sulphur in the individual solutions of thiosulphate, trithionate and tetrathionate (mg/L)

C_e = Equilibrium sulphur concentration (mg/L)

V = Volume of the solution (L)

m = Mass of the biomass ash/char used as the adsorbent(g)

5.3.4 Adsorption Isotherm Studies

The equilibrium sorption behavior can be characterized via different isotherm models and in this study experimental data were compared to Langmuir and Freundlich isotherm equations. For design and optimization of an adsorption process, it is important to establish the most appropriate adsorption equilibrium correlation (Monier et al., 2012) as isotherm constants indicate the surface properties and affinity of the adsorbent. These constants can also be used to compare sorption capacities of different adsorbents.

The basic assumption of the Langmuir model is that sorption takes place at specific homogeneous sites within the sorbent with no interaction between adsorbate molecules (Monier et al., 2012).

Langmuir isotherm model $q_e = \frac{q_m K_L C_e}{1+K_L C_e}$ (5-3)

q_e = Amount of S adsorbed per unit weight of adsorbent (mg/g dry weight)

C_e = Equilibrium S concentration in the solution (mg/L)

K_L = Langmuir constant related to the affinity of the binding sites (L/mg)

q_m = Maximum S uptake or monolayer biosorption capacity of the sorbent (mg/g)

The dimensionless parameter R_L defined below, gives information on the nature of adsorption according to the Langmuir isotherm. C_o is the initial adsorbate concentration.

$$R_L = \frac{1}{1+K_L C_0} \qquad (5\text{-}4)$$

If R_L is within 0 and 1 adsorption is considered favorable (Karagozoglu et al., 2007; Nethaji and Sivasamy, 2011). If R_L values are greater than 1, adsorption is unfavorable. If R_L equal to 0 adsorption is irreversible and if it is equal to 1 adsorption is linear (El-Shafey, 2007a).

The Freundlich model assumes a heterogeneous adsorption surface and active sites with different energies where as Langmuir isotherm assumes that the surface is homogenous where each site can hold one molecule (mono layer adsorption) having no interactions with the adjacent sites (Monier et al., 2012). Therefore, Freundlich isotherm may be more suitable for modelling with highly heterogeneous adsorbents (Nethaji and Sivasamy, 2011).

Freundlich isotherm model $q_e = K_f C_e^{\frac{1}{n}}$ (5-5)

q_e = Amount of S adsorbed per unit weight of adsorbent (mg/g dry weight)

C_e = Equilibrium S concentration in the solution (mg/L)

K_f = Constant relating to sorption capacity

1/n = Empirical parameter relating to biosorption intensity, varies with the heterogeneity of material

The data were fitted to linear forms of Langmuir (C_e/q_e vs C_e plot) and Freundlich isotherms (ln q_e vs ln C_e plot) to determine which isotherm best fits the data. Linear form of the two equations are given below.

Langmuir isotherm equation $$\frac{\mathbf{C_e}}{\mathbf{q_e}} = \frac{\mathbf{C_e}}{\mathbf{q_m}} + \frac{\mathbf{1}}{\mathbf{q_m K_L}} \quad (5\text{-}6)$$

Freundlich isotherm equation $$\ln q_e = \frac{1}{n} \ln C_e + \ln K_f \quad (5\text{-}7)$$

Thermodynamic parameters (ΔG, ΔH, ΔS) were calculated using equations (5-8), (5-9) and (5-10). The Distribution Coefficients at different temperatures were calculated using the following relation;

$$K_D = \frac{q_s}{C_s} \quad (5\text{-}8)$$

K_D = Distribution coefficient (mL/g)

q_e = Amount of selenium adsorbed by the adsorbent at equilibrium (mg/g)

C_e = Equilibrium concentration of selenium in the solution (C_e in mg/mL only for this equation)

The free energy change (ΔG) at different temperatures were calculated from the following relation:

$$\Delta G = -RT \ln K_D \quad (5\text{-}9)$$

R = Universal gas constant (8.314 $Jmol^{-1}K^{-1}$)

T = Absolute temperature (K)

The Van't Hoff equation was applied to calculate the enthalpy change (ΔH) and entropy change (ΔS). ΔS ($Jmol^{-1}K^{-1}$) and ΔH ($Jmol^{-1}$) can be calculated from the intercept and slope of the linear plot of ln K_D versus 1/T .

$$\ln K_D = \frac{\Delta S}{R} - \frac{\Delta H}{R} \times \frac{1}{T} \quad (5\text{-}10)$$

5.4 Results and Discussion

5.4.1 Biomass Ash/Char Characteristics (CBM-W Sample)

Major elements present in the CBM-W sample were Ca (22,610 ppm), Si (5,042 ppm) and K (4,260 ppm). Mg, Al, Fe, Mn concentrations vary between 1000 to 3000 ppm. CBM-W sample has the ability to neutralize and increase pH of acidic effluent water streams such as AMD due to presence of Ca, K, Na, Mg (Vassilev et al., 2013b). Carbon, nitrogen and sulphur percentages (by weight) were 79.47 %, 0.16% and 0.39% respectively.

The main minerals/phases identified by MLA were mainly char and also SiO_2, calcium rich char, Na-K chloride and slag rich in Ca, S, Al, Mg were present. The XRD patterns indicated the presence of calcium carbonate, graphite (carbon) and these results are in agreement with the results (elements/minerals/phases) obtained from elemental analysis (ICP-MS, ICP-OES, CNS Elemental Analysis) and MLA. However, prominent stretch bands relating to specific functional groups were not identified in the ATR-FTIR analysis of CBM-W sample. If there are functional groups present, they may contribute towards the adsorption (chemi-sorption) process.

An image taken from SEM of CBM-W sample is given in Figure 5-2. The sample mainly contain carbon particles. A honeycomb structure is clearly visible in the second image which confirms the presence of graphite (Adeoti, 2011). The image also shows the presence of fine foreign particles on the carbon surface which may have been caused as a

result of condensation of trace elements (slag) or due to the deposition of alkali species (calcite) and other elements (Li et al., 2012).

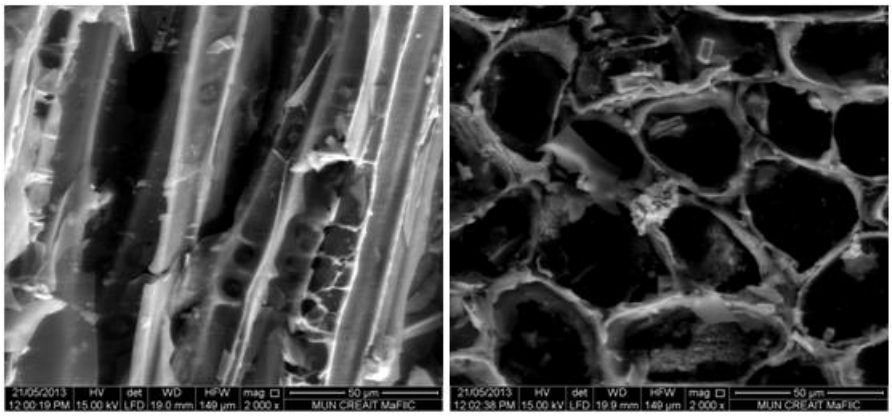

Figure 5-2: CBM-W (1.18mm < d < 4mm) SEM images

Nitrogen gas adsorption measurement at liquid nitrogen temperature (77 K) was used to determine the BET surface area and pore size distribution of the CBM-W sample. The BET surface area was 425.330 m^2 /g, total pore volume was 0.1820 cm^3/ g and the mean pore diameter was 1.7114 nm. Bulk density of a porous solid is the ratio of the bulk mass to the bulk volume. The low bulk density value of 0.101 g/cm^3 of CBM-W sample is mainly due to the presence of large char particles in the samples. Typically, biomass derived ash/char is alkaline in nature (Adeoti, 2011; Liu et al., 2010; Pan and Eberhardt, 2011; Shang et al., 2012) and CBM-W samples were also found to be alkaline with a pH value of 9.6 at 25 ^oC.

Total alkalinity (buffering capacity) is a measure of the ability of a solution to resist changes in pH. Materials such as carbonate, bicarbonate, hydroxides can contribute towards increased alkalinity in water. The total alkalinity of CBM-W sample was found to be lower (100 mg/L $CaCO_3$) than the CBM-D1 (1000 mg/L $CaCO_3$) and CLM1 (2360 mg/L $CaCO_3$) samples indicating that the ash has low potential to reduce the acidity in effluent streams such as AMD compared to the other two samples.

Thermal properties of the samples were analyzed by heating the sample to 1000 ^oC under inert (N_2) atmosphere. Weight loss (%) with increase in temperature was analyzed. Thermo gravimetric analysis (TGA) determines unburned carbon (weight loss in the range of 300 - 500 ^oC) and inorganic carbon (weight loss in the range of 630 - 750 ^oC) in the ash samples (Berra et al., 2011). Residue weight percentage for CBM-W was 7.24% with a large weight loss (approximately 80%) during the temperature range, 450 - 650 ^oC which is due to decomposition of char in the sample.

5.4.2 Effect of Different Ash/Char Samples

Batch mixing experiments were conducted using the three ash/char samples (CBM-D1, CBM-W, CLM1) to select the sample which has the highest affinity towards sulphur. 10 g of CBM-D1 and CLM1 samples and 5 g of CBM-W sample was mixed with 100 mL solutions of 5,000 mg/L Sodium Thiosulphate $Na_2S_2O_3$, Potassium Tetrathionate, $K_2S_4O_6$, Sodium Trithionate, $Na_2S_3O_6$ in Erlenmeyer flasks. Initial total sulphur (S) concentrations in the three solutions were 2025 mg/L, 2017 mg/L and 2119 mg/L

respectively. These sulphur concentrations were selected to represent the actual concentrations of sulphur oxy-anions present in mining effluent streams. All the flasks were covered with black rubber stoppers and mixed for 24 hours until equilibrium at room temperature (21^{o}C).

Table 5-2: Sulphur adsorption on to different biomass ash/char samples

Ash/Char sample	Adsorbent dose (g/L)	Thiosalt species	Initial S conc. (mg/L)	S removed (mg/L)	S adsorption (%)	S adsorption capacity (mg/g)
CBM-D1	100	Thiosulphate	2025	77.07	3.8	0.77
	100	Tetrathionate	2119	129.86	6.1	1.30
CBM-W	50	Thiosulphate	2025	250.78	12.4	5.02
	50	Trithionate	2017	288.97	14.3	5.78
	50	Tetrathionate	2119	311.72	14.7	6.23

Note: Standard deviation of sulphur elemental analysis measurements was less than 0.05wt% (i.e +/- 25 mg sulphur/L with CBM-W sample, +/- 50 mg/L with CBM-D1 sample)

CBM-W sample gave the highest sulphur removal in all three solutions (thiosulphate, trithionate, tetrathionate) as presented in Table 5-2. The particle size of CBM-W sample was larger (1.18 - 4 mm) compared with the particle size of CBM-D1 and CLM1 samples (0.5 mm seive size) (Table 5-1). Therefore, only 50 g/L dose of CBM-W sample was

used to enable effective mixing and the used dose of other samples were 100 g/L. CLM1 sample is not a suitable adsorbent as sulphur present in this ash sample appeared to be leaching in to the solution and not removing sulphur from the solution. The sulphur percentage in the original sample was 1.21 wt% and the sulphur percentage in the treated CLM1 samples were 0.35-0.45 wt%. sulphur adsorption capacity of CBM-D1 sample was lower than the CBM-W sample. Therefore, CBM-W carbon-rich sample was selected for further experiments. The low removal efficiency may be due to the reason that all the waste biomass ash/char samples used in this study were not pretreated and and used as received without any chemical/thermal modification.

5.4.3 Effect of pH

The next set of experiments were conducted to determine if there is an optimum pH to maximize sulphur adsorption from the three individual solutions of thiosalt species (thiosulphate, trithionate, tetrathionate). The solutions were prepared with an initial sulphur (S) concentration of 2000 mg/L and CBM-W char dose was kept constant at 50 g/L to ensure proper mixing and contact. Batch mixing experiments were initially conducted at room temperature (21 ^{o}C). Initial solution pH was adjusted (pH 2, 4, 7, 9) using dilute HNO_3 acid before mixing the ash.

Table 5-3 shows the percentages of sulphur adsorbed from the three thiosalt solutions at different pH values. Although, adsorption of sulphur from thiosulphate and tetrathionate solutions at pH 2 is higher than the adsorption values at other pH values, considering the standard deviation in measurement of +/- 25 mg sulphur/L, the difference in amount of adsorption is not significant (Figure 5-4). There appears to be very little effect of pH on sulphur adsorption from trithionate solutions. Given the minimal impact of pH and that most mining effluents are acidic in nature, the initial solution pH was maintained at pH 2 for further experiments.

Table 5-3: Effect of pH on sulphur adsorption on to CBM-W from thiosalt solutions

Sample	Initial pH	Final pH	S removed (mg/L)	S adsorption (%)	S adsorption capacity(mg/g)
Thiosulphate					
S2 - PH2	2.1	8.4	251.42	12.6	5.03
S2 - PH4	4.0	9.3	214.08	10.7	4.28
S2 - PH7	7.0	9.4	207.33	10.4	4.15
S2 - PH9	9.0	9.4	230.82	11.5	4.62
Trithionate					
S3 - PH2	2.0	7.4	206.70	10.3	4.13
S3 - PH4	4.0	8.0	219.28	11.0	4.39
S3 - PH7	7.1	8.0	223.40	11.2	4.47
S3 - PH9	9.1	8.1	200.05	10.0	4.00

Tetrathionate					
S4 - PH2	2.0	7.5	271.86	13.6	5.44
S4 - PH4	3.9	8.4	245.63	12.3	4.91
S4 - PH7	6.5	8.4	238.65	11.9	4.78
S4 - PH9	9.0	8.5	236.26	11.8	4.73

Note: Standard deviation of sulphur elemental analysis measurements was less than 0.05wt% (Same as +/- 25 mg sulphur/L or +/- 1.25% of 2000 mg sulphur/L solution)

Figure 5-3 shows the initial and final pH values of thiosalt solutions. It is important to note that, at initial pH values of 4, 7, 9 the final pH of all three solutions tend to move towards constant pH value and stabilize: pH 9.4 for thiosulphate; pH 8.1 for trithionate, pH 8.5 for tetrathionate.

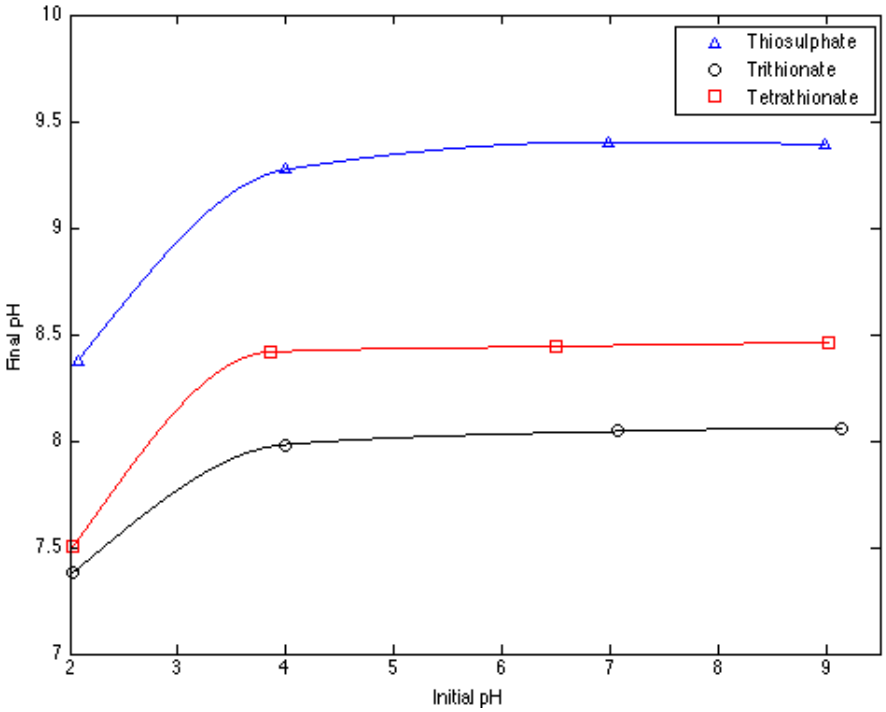

Figure 5-3: Initial pH vs. Final pH

Also, sulphur adsorption capacities from all three thiosalt solutions fall in the range, 4.00 - 5.43 mg/g of biomass char (Table 5-3, Figure 5-4).

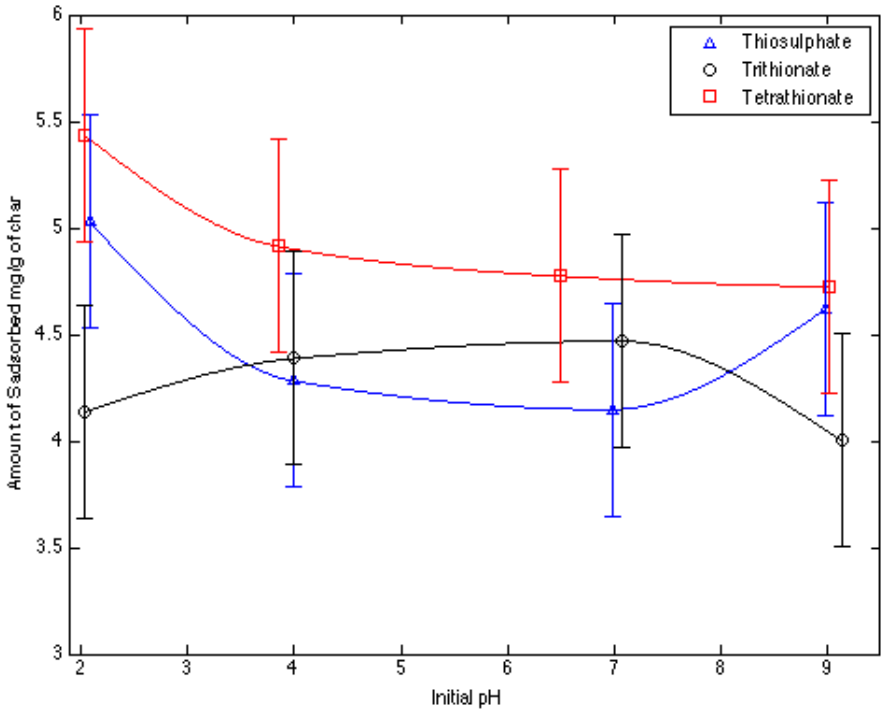

Figure 5-4: Amount of sulphur adsorbed (mg/g of CBM-W) at different initial pH

5.4.4 Effect of Adsorbent Dose

The next set of experiments were performed with varying adsorbent (CBM-W sample) dose (20, 50, 80 g/L). A maximum of 80 g/L char dose was selected, as at higher doses, mixing of the adsorbent in the thiosalt solutions was difficult. The char floats on top due to low density where most of the particles were not making proper contact with the thiosalt solutions. The results are given in the Table 5-4 and the results indicate that sulphur adsorption percentage and adsorption capacity increase with increasing adsorbent dose (Figure 5-5). At 80 g/L, sulphur adsorption percentages and adsorption capacities from thiosulphate, trithionate and tetrathionate solutions were 27.1, 25.7, 35.6% and 10.82, 10.29, 14.24 mg/g of char respectively. Further, final pH value of the solution

(filtrate) was in the range pH 6.6 - 8 where at high adsorbent doses the final pH of the solution was slightly higher than at low adsorbent doses.

Table 5-4: Effect of adsorbent dose on sulphur adsorption from thiosalt solutions

Sample	Adsorbent dose (g/L)	S removed (mg/L)	S adsorption (%)	S adsorption capacity (mg/g)
Thiosulphate				
S2 - 20D	20	202.29	10.1	4.05
S2 - 50D	50	342.54	17.1	6.85
S2 - 80D	80	541.11	27.1	10.82
Trithionate				
S3 - 20D	20	131.79	6.6	2.64
S3 - 50D	50	269.98	13.5	5.40
S3 - 80D	80	514.55	25.7	10.29
Tetrathionate				
S4 - 20D	20	140.43	7.0	2.81
S4 - 50D	50	306.95	15.3	6.14
S4 - 80D	80	711.76	35.6	14.24

Note: Standard deviation of sulphur elemental analysis measurements was less than 0.05wt% . Same as +/- 0.5% of 2000 mg sulphur/L solution for 20g/L dose, +/- 1.25% for 50g/L dose and +/- 2% for 80g/L dose

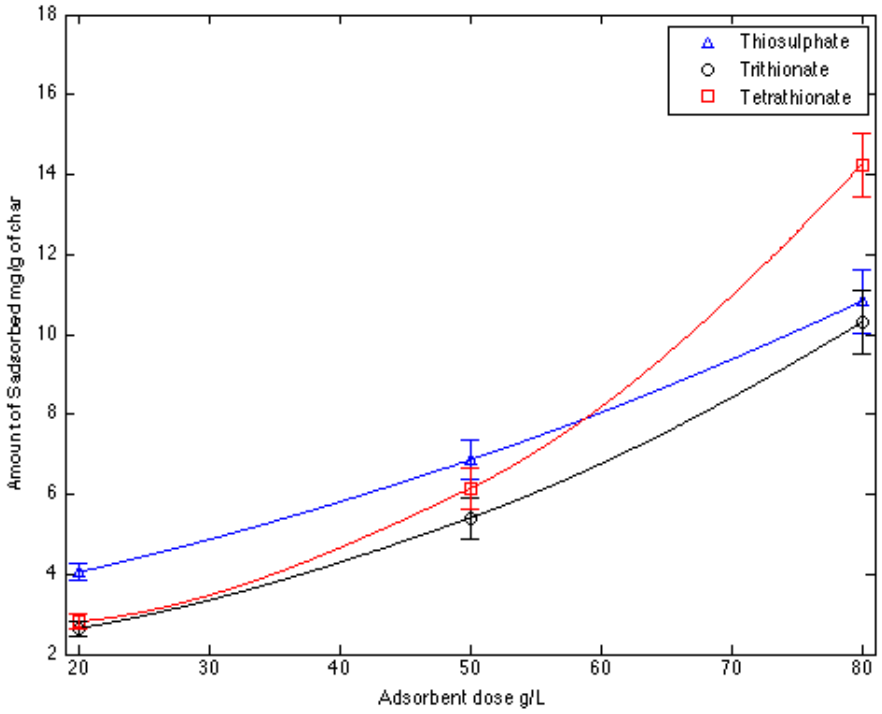

Figure 5-5: Biomass ash dose (g/L) vs. amount of sulphur adsorbed (mg/g of char)

5.4.5 Effect of Temperature

The experiments were run at different temperatures (5, 21, 35 ^{o}C) maintaining the adsorbent dose and the initial sulphur concentration at 50 g/L and 2000 mg/L respectively. Although, slightly higher adsorption percentages from thiosulphate and trithionate solutions were recorded at 35 ^{o}C (Table 5-5, Figure 5-6), the values are well within the measurement error values (+/- 1.25%). Therefore, it is difficult to arrive at a conclusion regarding the effect, increasing temperature has on adsorption of sulphur onto CBM-W sample. For future work, it is recommended to conduct experiments representing a wide temperature range or use another method of sulphur analysis with less

experimental error, so that the effect of temperature on thiosalt adsorption can be evaluated.

Table 5-5: Effect of temperature on sulphur adsorption from thiosalt solutions

Sample	Temperature (^{o}C)	S removed (mg/L)	S adsorption (%)	S adsorption capacity (mg/)
Thiosulphate				
S2 - 35C	35	356.42	17.8	7.13
S2 - 21C	21	342.54	17.1	6.85
S2 - 5C	5	296.88	14.8	5.94
Trithionate				
S3 - 35C	35	317.16	15.9	6.34
S3 - 21C	21	269.98	13.5	5.40
S3 - 5C	5	289.15	14.5	5.78
Tetrathionate				
S4 - 35C	35	318.66	15.9	6.37
S4 - 21C	21	306.95	15.3	6.14
S4 - 5C	5	343.21	17.2	6.86

Note: Standard deviation of sulphur elemental analysis measurements was less than 0.05wt% (Same as +/- 25 mg sulphur/L or +/- 1.25% of 2000 mg sulphur/L solution)

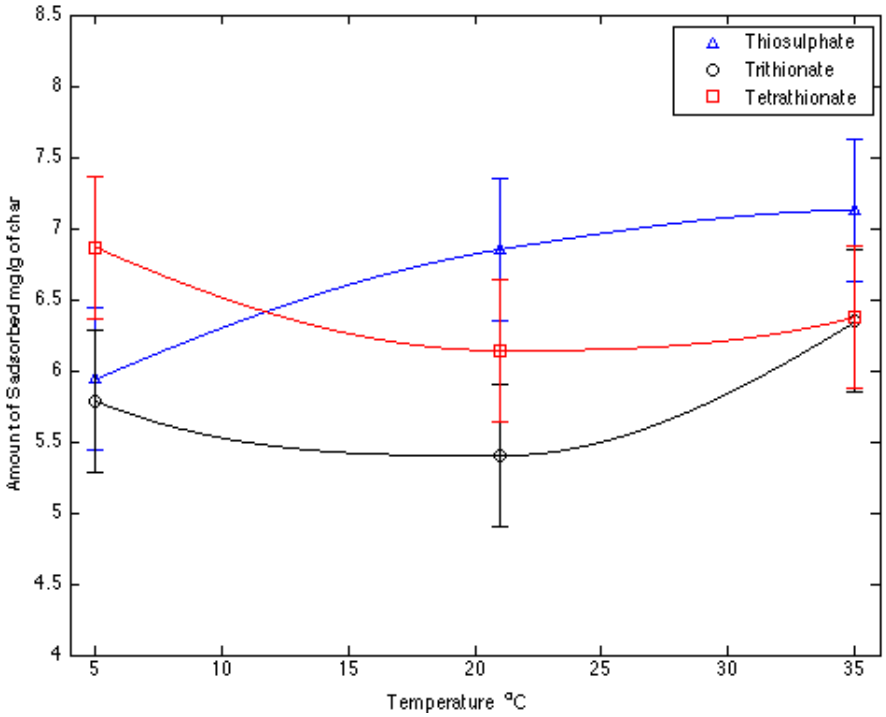

Figure 5-6: Temperature (^{o}C) vs. amount of sulphur adsorbed (mg/g of char)

5.4.6 Adsorption Isotherms

The experimental data were fitted to linear equations of Langmuir isotherm (equation 5-6) and Freundlich isotherm (equation 5-7) by plotting C_e/q_e against C_e (Figure 5-9) and ln q_e against ln C_e (Figure 5-10) for thiosulphate, trithionate and tetrathionate solutions separately. The isotherms constants calculated from the linear regression equations and regression coefficients (R^2) generated for Langmuir and Freundlich isotherms are also given in Table 5-6 and Table 5-7 respectively.

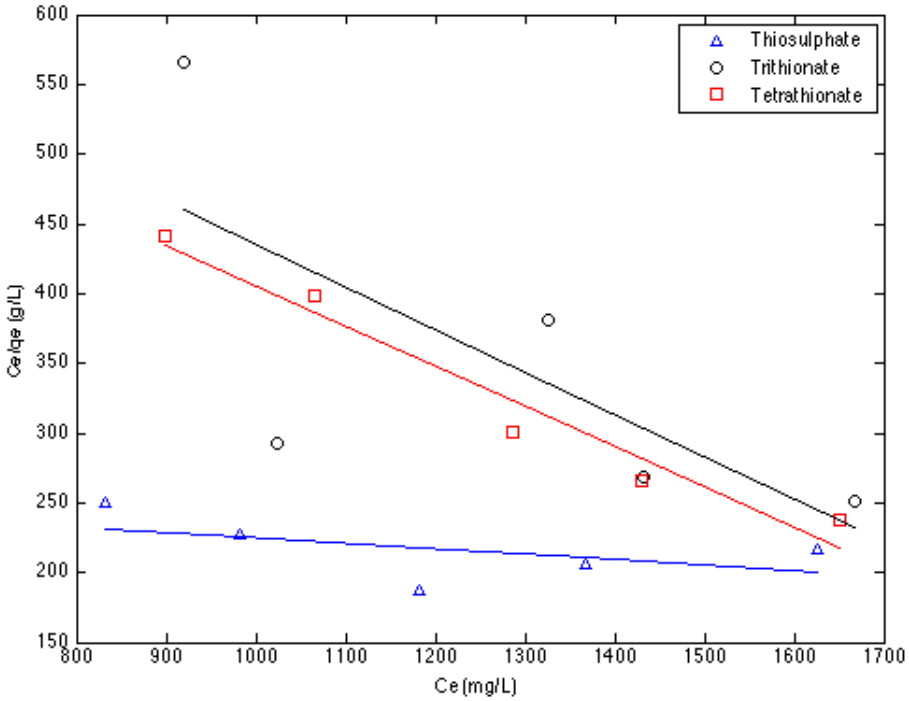

Figure 5-7: Langmuir isotherms for S adsorption onto biomass char at 21 ^{o}C and pH 2

The regression coefficients (R^2) are very poor for the Langmuir isotherm. The regression values for S adsorption from thiosulphate and trithionate solutions are 0.2744 and 0.5060 respectively. Although, the regression coefficient for sulphur adsorption from tetrathionate solutions is high (0.9577), the negative values obtained for Langmuir constants (q_m and K_L) confirm that the Langmuir model does not give a good fit to the sorption data and it is not a suitable model when compared to the Freundlich isotherm. Further, calculated R_L (separation factor) values are greater than 1, which means the adsorption process is not favorable.

Table 5-6: Langmuir isotherm constants at 21 ^{o}C and pH 2

S species	q_m (mg/g)	K_L (L/mg)	R^2	R_L values
Thiosulphate	-25.374	-1.49×10^{-4}	0.2744	1.11 - 1.42
Trithionate	-3.300	-4.11×10^{-4}	0.5060	1.40 - 5.59
Tetrathionate	-3.464	-4.16×10^{-4}	0.9577	1.26 - 5.93

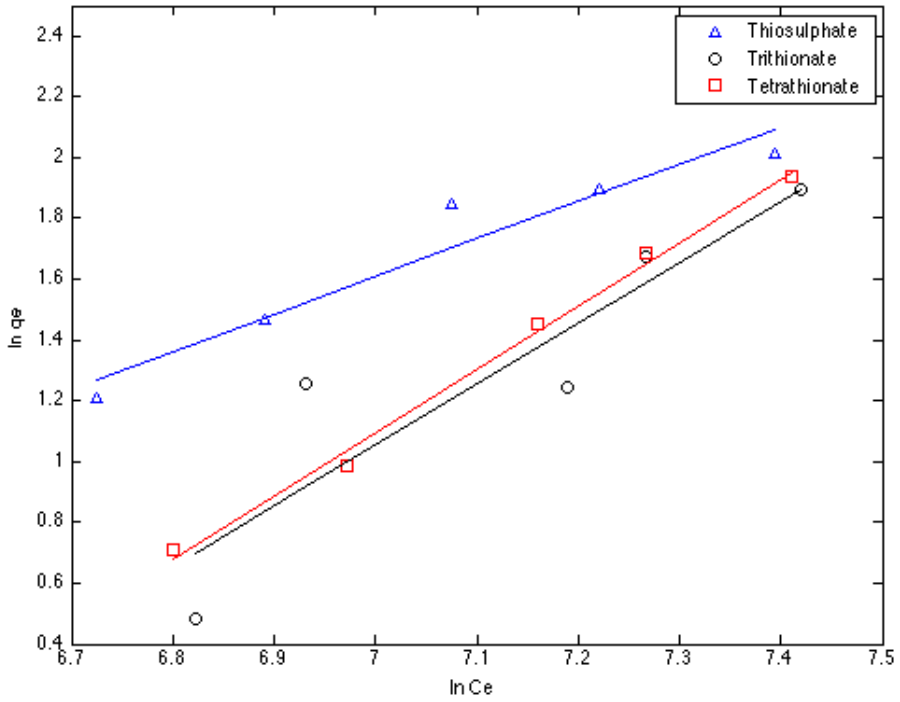

Figure 5-8: Freundlich isotherms for S adsorption onto biomass char at 21 ^{o}C and pH 2

The Freundlich isotherm is a better fit for experimental isotherm data than the Langmuir isotherm. The regression coefficients (R^2) obtained for sulphur adsorption onto biomass char from all three solutions are greater than 0.80; 0.9298 for thiosulphate, 0.8257 for trithionate, 0.9949 for tetrathionate (Table 5-7). Generally, for the adsorption process to

be favorable, value of n should fall within 1 and 10 (or 1/n value should fall in between 0 and 1) (Nettem and Almusallam, 2013; Sharma and Sanghi, 2013). 1/n values obtained in this study fall between 1.2 - 2.1 which means that the interaction between the adsorbent (biomass ash) and the adsorbate (sulphur species) is not very strong. When the 1/n values are very small (<1), it indicates that there is a strong interaction between the adsorbent and the adsorbate (Sharma and Sanghi, 2013). In conclusion, Freundlich isotherm is a better representative of the experimental data. However, it may not be the best model to follow in understanding and predicting the behavior of sorption of sulphur onto biomass ash from thiosulphate, trithionate and tetrathionate solutions as the calculated 1/n values are greater than one.

Table 5-7: Freundlich isotherm constants at 21 ^{o}C and pH 2

S species	1/ n	K_f	R^2
Thiosulphate	1.234	8.86×10^{-4}	0.9298
Trithionate	2.002	2.35×10^{-6}	0.8257
Tetrathionate	2.088	1.34×10^{-6}	0.9949

5.4.7 Thermodynamic Parameters

Thermodynamic parameters (ΔG : Gibbs free energy change of adsorption, ΔH: enthalpy change, ΔS: entropy change) are typically assessed in all processes to determine the thermodynamic nature of the process (e.g. tendency to occur at given conditions). K_D (distribution coefficient) vs. the inverse absolute temperature (1/T) graphs can generally

be used to determine ΔH and ΔS values for sulphur adsorption from thiosulphate, trithionate and tetrathionate solutions. In this case, however, a noticeable trend in sulphur adsorption with increase in temperature was not identified for sulphur adsorption from all three solutions. To illustrate this point, K_D vs. (1/T) graph (Figure 5-9) obtained for trithionate is shown below (R-squared = 0.4575). Conducting the experiments at a wider temperature range (5, 40, 75 ^oC instead of 5, 21, 35 ^oC) might address this concern.

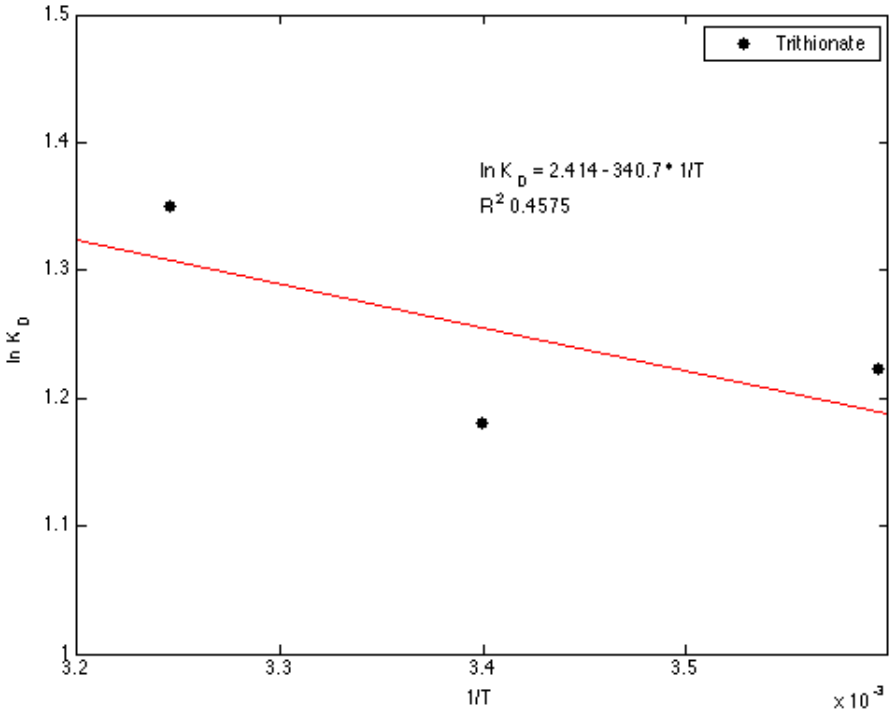

Figure 5-9: ln K_D vs. I/ T(K^{-1}) plot for trithionate

5.5 Conclusion and Recommendations

CBM-W biomass char sample obtained from Corner Brook Pulp and Paper Mill was selected as the best adsorbent from the three biomass ash/char samples used in this study,

giving the following characteristics: high specific surface area; low density; high carbon content; presence of minerals favorable to be used as adsorbents and neutralizing agents such as char, silica and calcium carbonate. Initial results confirmed that CBM-W biomass char sample is a more suitable adsorbent for removal of sulphur from aqueous solutions of thiosulphate, trithionate and tetrathionate than the CLM1 and CBM-D1 biomass ash samples.

The adsorption experiments were carried out using synthesized solutions of thiosulphate, trithionate, tetrathionate at varying pH, biomass ash dose and temperature. Variation in pH and temperature didn't have a significant effect on sulphur adsorption from all three thiosalt solutions where the sulphur removal percentage was 10 - 13.6 % within the pH range of 2 - 9 and sulphur removal percentage was 13.5 - 17.8 % within the temperature range of 5 - 35 ^{o}C. To represent the acidic conditions present in the mining effluent water, the pH was maintained at 2 for further experiments. An increase in biomass char dose from 20 g/L to 80 g/L significantly increased the percentage adsorption of sulphur from all three solutions: 10.1 - 27.1 % for thiosulphate; 6.6 - 25.7 % for trithionate; 7 - 35.6 % for tetrathionate. The highest adsorption capacities were recorded at the maximum dose used (80 g/L) which are 10.82, 10.29, 14.24 mg/g of biomass char for thiosulphate, trithionate and tetrathionate respectively. Moderate neutralization capacities were recorded where final pH values of all the solutions fall in the range 6.6 - 9.4.

In understanding and predicting the nature of adsorption of sulphur species onto biomass ash, the Freundlich isotherm equation was found to be a better representative than the Langmuir isotherm equation. Freundlich isotherm gave a better fit for experimental data where the regression coefficients were determined to be 0.9298 for thiosulphate, 0.8257 for trithionate and 0.9949 for tetrathionate. Negative values of mono-layer sorption capacities (q_m) and separation factor values (R_L>1) obtained from Langmuir isotherm equation indicated that the assumptions of Langmuir equation were not satisfied by the adsorption process at the experimental conditions under consideration (Temperature 21^oC, pH 2, initial S concentration 2000 mg/L, biomass ash/char dose 50 g/L). Therefore, Langmuir isotherm is not suitable to model the adsorption of sulphur species on to biomass ash. Even though, 1/n values obtained from the Freundlich isotherm equation were not less than 1, it could still be concluded that there is considerable interaction between the adsorbent (biomass ash) and the adsorbate (sulphur species).

Recommendations for future work include;

- Characterization of spent adsorbents from these experiments to understand which specific properties may have involved in sulphur removal and to understand the adsorption mechanism.
- In this work the sulphur percentage in the spent adsorbent was analyzed and the adsorption capacity and percentage removal of sulphur was calculated from that value as methods such as ICP-MS, capillary electrophoresis and iodine titration was found to be challenging. However, as biomass ash samples are not

homogenous, analysis of the solution rather than the spent adsorbent may be more accurate. Therefore, a more accurate analytical method to determine the amount of sulphur in the solution would aid in analysis.

- Selection of a narrow size range of the CBM-W sample as well as higher dose may provide significant variation in results with varying parameters.
- FTIR analysis of the CBM-W sample did not show presence of any functional groups. If these samples can be chemically modified to have positively charged functional groups, the sulphur oxy-anions may be able to remove by ion exchange.
- Conduct column experiments to obtain more information in designing an adsorption process.
- Perform experiments using simulated effluent streams with various other compounds to determine any interference these compounds may have in adsorption
- Conduct kinetic experiments to determine rates for reactor type selection and design of the overall selenium treatment process.
- Assess the leaching characteristics of the spent ash to determine further disposal options for these ash (e.g. use as an additive for construction purposes, landfill disposal etc.)

Bibliography - Chapter 5

Adeoti, I. A.: Characterization and Alternative Use Study of Fly Ash, 160 pp., Memorial University of Newfoundland., 2011.

Berra, M., Casa, G. De, Orso, M. D., Galeotti, L., Mangialardi, T., Paolini, A. E. and Piga, L.: Reuse of Woody Biomass Fly Ash in Cement-Based Materials : Leaching Tests, in Recycling of Biomass Ashes, edited by H. Insam and B. A. Knapp, pp. 133–146, Springer Berlin Heidelberg., 2011.

Chanda, M., O'Driscoll, K. F. and Rempel, G. L.: Ion-Exchange Sorption of Thiosulfate and Tetrathionate on Protonated Poly(4-Vinyl Pyridine), React. Polym., 2, 269–278, 1984.

Dinardo, O. and Sally, J.: Treatment of Thiosalts in Milling Effluents: A Review of Treatment Processes., 1998.

El-Shafey, E. I.: Removal of Se(IV) from aqueous solution using sulphuric acid-treated peanut shell., J. Environ. Manage., 84(4), 620–7, doi:10.1016/j.jenvman.2007.03.021, 2007.

Environment Canada: Environmental Code of Practice for Metal Mines., 2009.

IUPAC: PAC, 1979, 51, 2243. General aspects of trace analytical methods - IV. Recommendations for nomenclature, standard procedures and reporting of experimental data for surface analysis techniques, edited by H. Burrows, R. Weir, and J. Stohner., 2009.

Karagozoglu, B., Tasdemir, M., Demirbas, E. and Kobya, M.: The adsorption of basic dye (Astrazon Blue FGRL) from aqueous solutions onto sepiolite, fly ash and apricot shell activated carbon: kinetic and equilibrium studies., J. Hazard. Mater., 147(1-2), 297–306, doi:10.1016/j.jhazmat.2007.01.003, 2007.

Li, L., Yu, C., Bai, J., Wang, Q. and Luo, Z.: Heavy metal characterization of circulating fluidized bed derived biomass ash., J. Hazard. Mater., 233-234, 41–7, doi:10.1016/j.jhazmat.2012.06.053, 2012.

Liu, Z., Zhang, F.-S. and Wu, J.: Characterization and application of chars produced from pinewood pyrolysis and hydrothermal treatment, Fuel, 89(2), 510–514, doi:10.1016/j.fuel.2009.08.042, 2010.

McCafferty, E.: Introduction to Corrosion Science, Springer New York., 2010.

Miranda-Trevino, J. C., Pappoe, M., Hawboldt, K. and Bottaro, C.: The importance of thiosalts speciation: review of analytical methods, kinetics and treatment, Crit. Rev. Environ. Sci. Technol., doi:10.1080/10643389.2012.672047, 2012.

Monier, M., Ayad, D. M. and Abdel-Latif, D. a: Adsorption of Cu(II), Cd(II) and Ni(II) ions by cross-linked magnetic chitosan-2-aminopyridine glyoxal Schiff's base., Colloids Surf. B. Biointerfaces, 94, 250–8, doi:10.1016/j.colsurfb.2012.01.051, 2012.

Negeri, T., Paktune, A. D., Boisclair, M. and Kingston, D. M.: Characterization of Thiosalts Generation During Milling of Sulphide Ores., 1999.

Nethaji, S. and Sivasamy, a: Adsorptive removal of an acid dye by lignocellulosic waste biomass activated carbon: equilibrium and kinetic studies., Chemosphere, 82(10), 1367–72, doi:10.1016/j.chemosphere.2010.11.080, 2011.

Nettem, K. and Almusallam, A. S.: Equilibrium, Kinetic and Thermodynamic Studies on the Biosorption of Selenium (IV) Ions onto Ganoderma Lucidum Biomass, Sep. Sci. Technol., (June), doi:10.1080/01496395.2013.791318, 2013.

Pan, H. and Eberhardt, T.: Characterization of Fly Ash from the Gasification of Wood and Assessment for Its Application as a Soil Amendment., 2011.

Shang, G., Shen, G., Wang, T. and Chen, Q.: Effectiveness and mechanisms of hydrogen sulfide adsorption by camphor-derived biochar, J. Air Waste Manage. Assoc., 62(8), 873–879, doi:10.1080/10962247.2012.686441, 2012.

Sharma, S. K. and Sanghi, R.: Wastewater Reuse and Management, Springer., 2013.

Vassilev, S. V., Baxter, D., Andersen, L. K. and Vassileva, C. G.: An overview of the composition and application of biomass ash. Part 2. Potential utilisation, technologcal and ecological advantages and challenges, Fuel, 105, 19–39, doi:10.1016/j.fuel.2012.10.001, 2013.

Vongporm, Y.: Thiosalt Behaviour in Aqueous Media, 171 pp., Memorial University of Newfoundland., 2008.

Wasserlauf, M. and Dutrizac, J. E.: The Chemistry, Generation and Treatment of Thiosalts in Milling Effluents - A Non-Critical Summary of CANMET Investigations 1976-1982, CANMET Report 82-4E., 1982.

Chapter 6 : Adsorption of Selenite and Selenate Using Biomas Ash/Char

Bhagya M.K. Range, Kelly A. Hawboldt

Faculty of Engineering and Applied Science, Memorial University of Newfoundland, St John's, NL, Canada. A1B3X5

Abstract

Selenium is an essential nutrient for plants, animals and humans, but can be toxic at higher concentrations. Adsorption of selenium by naturally available adsorbents can be a cost effective process in treatment of selenium. Biomass ash is generated as a combustion by-product in the pulp and paper industry. In the present study, suitability of using biomass ash as an adsorbent to remove selenite and selenate from aqueous solutions is analyzed. Biomass ash used in this study is collected from Zellstoff Celgar Limited Partnership (ZCLP), BC, Canada and characterized to understand physical, chemical, thermal and structural properties in a previous paper (Chapter 4). Batch experiments were conducted by mixing different doses of ash (CLM2) sample (20, 50, 80 g/L) with Se(IV) and Se(VI) solutions (50 mg/L Se concentration) at different pH (pH 2, 4, 7, 9) and temperature (5, 21, 35 ^{o}C) until equilibrium is achieved (24 hrs). Maximum percentage removal for Se(IV) and Se(VI) was 10.3% and 15.2% at 35^{o}C. When the pH was decreased from pH 9 to 2 adsorption percentage increased by 5%. Varying the biomass ash dose did not have a significant effect on Se removal percentage. However, high adsorption capacities were recorded at lower adsorbent doses (20 g/L). Adsorption

capacities obtained for Se(IV) (0.195 mg/g) and Se(VI) (0.211 mg/g) are similar to capacities recorded in (Hasan et al., 2010) and higher than the capacities recorded in (Gulipalli et al., 2011). High neutralization capacities were recorded with both Se(IV) and Se(VI) solutions where final solution pH of all samples fall within pH 10.5 - 11.4 despite the value of initial pH.

6.1 Introduction

Biomass ash is generated in the pulp and paper industry from the combustion of hog fuel. Hog fuel can be a combination of bark and sawdust, forestry residues with petroleum. At the Zellstoff Celgar (ZCLP) plant, hog fuel is made up of wood particles (sawdust/pin chips), bark, sludge from their bio-treatment facility (organic matter, fibre, and lime), and other impurities. Ash is the single largest contributor of material going to the ZCLP landfill, at 6500 m^3/year. Fuel, manpower, and permitting for the landfill are all significant costs to the mill. In addition, the heat of the ash may contribute to landfill fires, a safety concern. Developing an alternative market for the ash would decrease the load on the landfill, reduce safety and environmental concerns, and decrease overall costs. As indicated above, the costs associated with disposing of and handling ash for ZCLP are significant. However, this is not a company specific problem. It is estimated up to 480 million tonnes of biomass ash could be generated worldwide annually. This is similar to that of coal ash at 780 million tonnes/year (Vassilev et al., 2013a). As biofuel is a carbon neutral form of energy, there will be increases in large-scale combustion of biomass and co-combustion with contaminated biomass/solid fossil fuels and subsequent increases in

biomass ash and risks related to disposal and handling. When compared to the coal ash, biomass ash is more heterogeneous and composition is a function of the parent biomass and mineralogy/crystallography is a function of combustion (Vassilev et al., 2013a). Within woody biomass ash, composition varies depending on species and nature of feedstock. The literature and our work demonstrate that ash properties are site specific and to determine the best use of the ash, characterization is a necessary and challenging step. In this project, we characterized the hog fuel ash and based on this characterization we investigated the hog fuel ash as an adsorbent for treatment of selenium oxy-anions in mining waste streams.

Selenium is an essential nutrient for plants, animals and humans, but can be toxic at higher concentrations. Selenium can exist in inorganic or organic forms (Sheha and El-Shazly, 2010). Inorganic forms of selenium are selenate, selenite, insoluble elemental selenium, selenides (Li et al., 2013). Selenium exists in several oxidation states (-2, 0, +2, +4, +6). The most common selenium species in aqueous systems are selenite (SeO_3^{2-}) and selenate (SeO_4^{2-}) (Li et al., 2013). Selenium is generally found in mining effluent waters in concentrations ranging from 3 µg/L to even above 12,000 µg/L (Envirogen Technologies, 2011). According to the guidelines set for selenium by the Ministry of Environment of British Columbia, Canada, the mean concentration of total selenium should not exceed 2 µg/L to protect freshwater and marine aquatic life (Environment protection Division Ministry of Environment Government of British Columbia, 2001). As per WHO Guidelines for Drinking Water Quality, maximum allowable concentration of

selenium in drinking water is 10 µg/L (World Health Organization, 2003), while the US EPA sets a maximum contaminant level (MCL) of selenium in drinking water at 50 µg/L (US EPA, 1992).

Adsorption of selenium species by naturally available adsorbents like ash/char can be a cost effective process in treatment of selenium in aqueous media. There are a number of studies published on using various adsorbents to determine selenium adsorption capacity, to understand the sorption mechanism, and most importantly, to assess the overall ability of using these adsorbents to remove selenium oxy-anions from industrial effluents. A summary of various adsorbents used in the removal of Se(IV) and Se(VI) ions and monolayer sorption capacities (q_m) of Se(IV) and Se(VI) sorption onto various adsorbents calculated by Langmuir isotherm at specific experimental conditions (pH, Temperature) are provide in Chapter 3 (Review on Selenium Removal). The utilization of the ash as an adsorbent would benefit Canada economically and environmentally in reducing the demand for landfill space and reducing the toxicity of mining effluents. This is a sustainable approach to waste handling, in that one waste stream is utilized for the treatment of another.

In this paper, we investigate the possibility of using biomass ash/char from pulp and paper mill boilers to treat two selenium species, selenite (SeO_3^{2-}) and selenate (SeO_4^{2-}).

6.2 Selenium Pourbaix (Eh-pH) Diagrams

Pourbaix or Eh-pH diagrams developed by the Belgian Chemist, Marcel Pourbaix, illustrate the thermodynamic stability of an element as a function of electrode potential and pH in an aqueous electrochemical system. These diagrams illustrate the oxidizing and reducing abilities of the major stable compounds of an element. However, these diagrams do not provide information on chemical kinetics. Eh-pH diagrams are widely used in corrosion, geochemical, environmental applications (McCafferty, 2010).

In a Pourbaix diagram, there are 3 possible straight lines: Horizontal lines which are for reactions involving electrode potential; Vertical lines which are for reactions involving only pH; Graduated lines which are for reactions including both electrode potential and pH. The regions or fields in between various lines represents where specific species or chemical compounds are thermodynamically stable (McCafferty, 2010). Understanding the form in which an element is present at a certain pH/ electrode potential is very useful in designing treatment processes for removal of these elements from effluent water systems.

The following Eh-pH-diagram (Figure 6-1) generated by HSC Chemistry 7.1 software, shows the thermodynamic stability areas of different selenium species that may be present in aqueous solutions at 21 ^{o}C. Selenium species considered in this Eh-pH analysis are elemental selenium(Se), $H_2Se(a)$, $HSe^-(a)$, $Se^{2-}(a)$, $HSeO_3^-(a)$, $HSeO_4^-(a)$, $H_2SeO_4(a)$,

H_2SeO_3(a), SeO_4^{2-}(a), SeO_3^{2-}(a). The region in between the dotted lines in the diagrams are the stability area for water (H_2O). Selenium concentration is 50 mg/L.

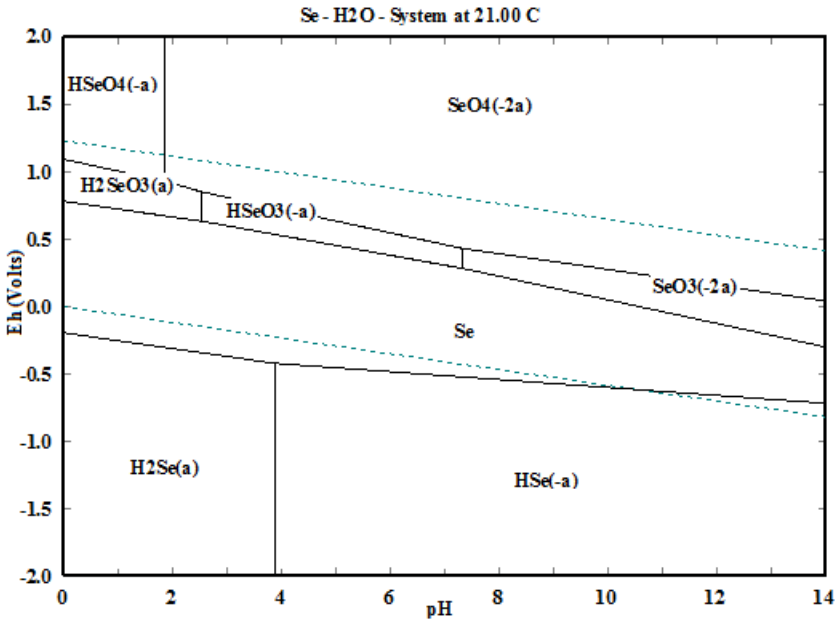

Figure 6-1: Pourbaix diagram for the Se-O-H system at temperature 21 ^{o}C, molality 6.332 x10^{-4} mol/kg H_2O, pressure 1 atm

6.3 Materials and Experimental Methodology

6.3.1 Characterization of Biomass Ash

The biomass ash sample used for this study was collected from ZCLP, which is located in Castlegar, BC Canada. The Zelstoff Celgar Mill ash sample (CLM) used in this study is bottom ash, which is ash residue left in boiler as opposed to fly ash which is a result of particulate matter from the flue gas. The sample was dried at 105 ^{o}C for 24 hours and

sieved to obtain only two size fractions (CLM1: d < 500 µm and CLM2: 500 µm < d < 1.18 mm) and CLM2 sample is used for the batch adsorption experiments.

The CLM2 biomass ash sample was characterized by standard methods: inductively coupled plasma and optical emission spectrometry (ICP-MS, ICP-OES), CNS (carbon, nitrogen, sulphur) analysis, mineral liberation analysis (MLA), X-ray diffraction (XRD), Fourier transform infrared spectroscopy (ATR- FT-IR), scanning electron microscopy (SEM) analysis, specific surface area, pore volume, bulk density, pH, total alkalinity, thermo-gravimetric analysis (TGA).

The characterization results are briefly described in the Results section and for the detailed characterization methodology and discussion on results please refer Chapter 4.

6.3.2 Batch Adsorption Experiments

Sodium selenite (Na_2SeO_3) 99% and sodium selenate (Na_2SeO_4) ≥95% (Sigma-Aldrich Canada Co) were used as the sources of Se(IV) and Se(VI) respectively. Se concentrations were determined by ICP-MS technique at TERRA (The Earth Resources Research and Analysis) Facility at Memorial University using ELAN-DRC-II (ICP-MS) Instrument.

Batch experiments were conducted by mixing (at 120 rpm) different doses of CLM2 sample (20, 50, 80 g/L) with Se(IV) and Se(VI) solutions (50 mg/L Se concentration) at

different pH (pH 2, 4, 7, 9) and temperature (5, 21, 35 ^{o}C) until equilibrium is achieved (24 hrs). Solution pH values were adjusted by using dilute HNO_3 acid before mixing the ash. Samples were filtered through No.42 Whatman filter paper and a 13 mm Nylon 0.2 µm syringe filter and submitted for ICP-MS analysis. Duplicate samples were run and the maximum calculated standard deviation for the results were +/- 2.1%.

Adsorption percentage and adsorption capacity were calculated using the following equations.

$$\text{Adsorption capacity}\left(\frac{mg}{g}\right) = \frac{(C_i - C_e)\ x\ V}{m} \qquad (6\text{-}1)$$

$$\text{Adsorption \%} = \frac{(C_i - C_e)\ x\ 100}{C_i} \qquad (6\text{-}2)$$

C_i = Initial concentration of adsorbate (mg/L)

C_e = Equilibrium adsorbate concentration (mg/L)

V = Volume of the solution (L)

m = Mass of the adsorbent(g)

Thermodynamic parameters (ΔG, ΔH, ΔS) were calculated using equations (5-3), (5-4) and (5-5). The Distribution Coefficient at different temperatures were calculated using the following relation;

$$K_D = \frac{q_e}{C_e} \quad (6\text{-}3)$$

K_D = Distribution coefficient (mL/g)

q_e = Amount of selenium adsorbed by the adsorbent at equilibrium (mg/g)

C_e = Equilibrium concentration of selenium in the solution (C_e in mg/mL only in this equation)

The free energy change (ΔG) at different temperatures were calculated from the following relation:

$$\Delta G = -RT \ln K_D \quad (6\text{-}4)$$

R = Universal gas constant (8.314 $Jmol^{-1}K^{-1}$)

T = Absolute temperature (K)

The Van't Hoff equation was applied to calculate the enthalpy change (ΔH) and entropy change (ΔS). ΔS ($Jmol^{-1}K^{-1}$) and ΔH ($Jmol^{-1}$) can be calculated from the intercept and slope of the linear plot of ln K_D versus 1/T .

$$\ln K_D = \frac{\Delta S}{R} - \frac{\Delta H}{R} \times \frac{1}{T} \quad (6\text{-}5)$$

6.4 Results and Discussion

6.4.1 Biomass Ash Characteristics (CLM2 Sample)

Major elements present in the analyzed samples are Ca, Si, Al, Na, K, Fe, Mn, Mg, P. Very high Ca (75,168 ppm) and Si (60, 535 ppm) elemental compositions are recorded in the samples. Compounds rich in Ca, Na (50,083 ppm), K (29,045 ppm), Mg (8,017 ppm) are excellent materials that can be used to neutralize and increase pH of acidic effluent water streams such as AMD (Vassilev et al., 2013b). Si and Al (14,903 ppm) content is an important factor for zeolite synthesis (Adeoti, 2011; Vadapalli et al., 2012).

Carbon, nitrogen and sulphur percentages were 40.79 %, 0.09% and 0.99% respectively and sulphur percentage in the CLM2 ash sample is higher than published data for different ash in some literature (Li et al., 2010).

The main minerals/phases identified by Mineral Liberation Analyzer were alkali-feldspar, SiO_2, Ca-rich slag, Char, Ca-rich char, Ca-carbonate. Other phases present included iron oxide, slag enriched in Ca, Si, Fe, P,Mg, Al, Fe, Mn, K.

The XRD pattern showed that these samples are partially crystalline (Berra et al., 2010) and indicated the presence of calcite, graphite and these results are in agreement with the results (elements/minerals/phases) obtained from elemental analysis (ICP-MS, ICP-OES, CNS Elemental Analysis) and MLA.

FTIR analysis identifies the functional groups (key to adsorption applications) in the ash samples. Based on the prominent stretch bands identified at 1400,1100, 800 cm^{-1} possible functional groups that can be present are C-O (carbonate at 1450-1410 and 875, 713), S-O (sulphate at 1140-1080) and Si-O (quartz at 1080) (Smidt et al., 2011).

Scanning electron micrographs of CLM2 sample is given in Figure 6-2. The images also show the presence of a large number of fine particles on the carbon surface in the CLM2 sample which may have been caused as a result of condensation of trace elements (amorphous slag caused during combustion and cooling) or due to the deposition of different species of alkali and other elements (Li et al., 2012). This can be further confirmed by the results from the MLA which confirms the presence of calcium rich char, alkali-feldspar, silica, slag rich in Si, Al, Mg, S, Ca, Ti in these samples.

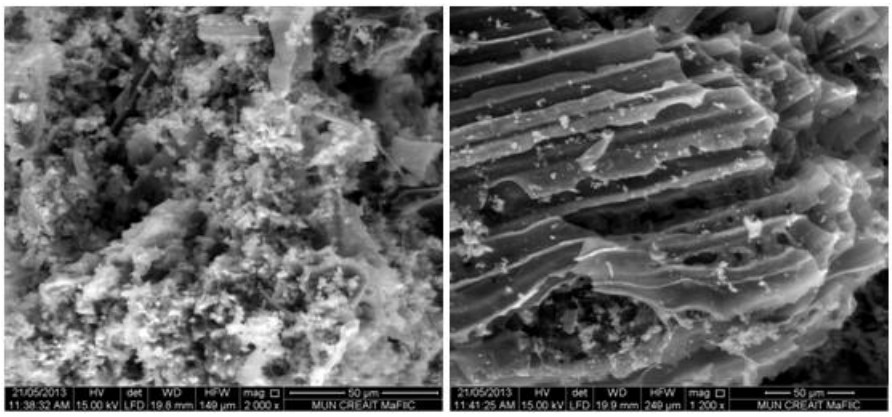

Figure 6-2: CLM2 (500 µm < d < 1.18 mm) SEM images

The nitrogen gas adsorption measurement at liquid nitrogen temperature (77 K) is used to determine the BET surface area and pore size distribution of CLM2 sample and the sample was pre-treated for 4 hours at 200 ^{o}C before the measurement. BET surface area was 241.480 m^2 /g, total pore volume was 0.1667 cm^3/ g and the mean pore diameter was 2.3694 nm.

Bulk density of a porous solid is the ratio of the bulk mass to the bulk volume. The low bulk density value of 0.263 g/cm^3 of CLM2 sample is a result of presence of char particles in the samples. Typically, biomass ash is alkaline in nature (Adeoti, 2011; Liu et al., 2010; Pan and Eberhardt, 2011; Shang et al., 2012) and CLM2 samples were also found to be highly basic with a pH value of 11.1 at 25^{o}C.

Total alkalinity is a measure of resistance of water to change in pH. It can also be called as buffering capacity of water. Materials such as carbonate, bicarbonate, hydroxides can contribute towards increased alkalinity in water. Total Alkalinity is defined as the amount of acid required to lower the pH of the sample to a pH value of 4.5 (endpoint) at which all carbonate and bicarbonate ions are converted to carbonic acid (H_2CO_3). The total alkalinity of CLM2 sample is high at 2720 mg/L $CaCO_3$ indicating that the ash has a great potential to reduce acidity in mining effluent water.

Thermal properties of the samples were analyzed by heating the sample to 1000 ^{o}C under inert (N_2) atmosphere. Weight percentage and the derivative weight percentage with

increase in temperature was analyzed. Thermo gravimetric Analysis (TGA) determines the presence of unburned carbon (weight loss in the range of 300 - 500 ^{o}C) and inorganic carbon (weight loss in the range of 630 - 750 ^{o}C) in the ash samples (Berra et al., 2011). Residue weight percentage for CLM2 was 33.51%. During 650 ^{o}C - 850 ^{o}C, the rate of weight loss increased significantly for CLM2 which may be due to decomposition of calcite in this temperature range (Rajamma et al., 2009).

6.4.2 Effect of pH

The detailed results from the pH study are shown in Table 6-1. Initial Se concentration is 50 mg/L and the adsorbent does is 50 g/L. The tests were initially performed at room temperature (21 ^{o}C). As per Figure 5-3, when pH is decreased from 9 to 2, the amount of selenium adsorbed increases in both Se(IV) and Se(VI) solutions. Amount of Selenite, Se(IV) adsorbed increased from 0.010 to 0.060 mg of Se/g of CLM2 ash. Amount of Selenate, Se(VI) adsorbed increased from 0.015 to 0.061 mg of Se/g of CLM2 ash (Table 6-1).

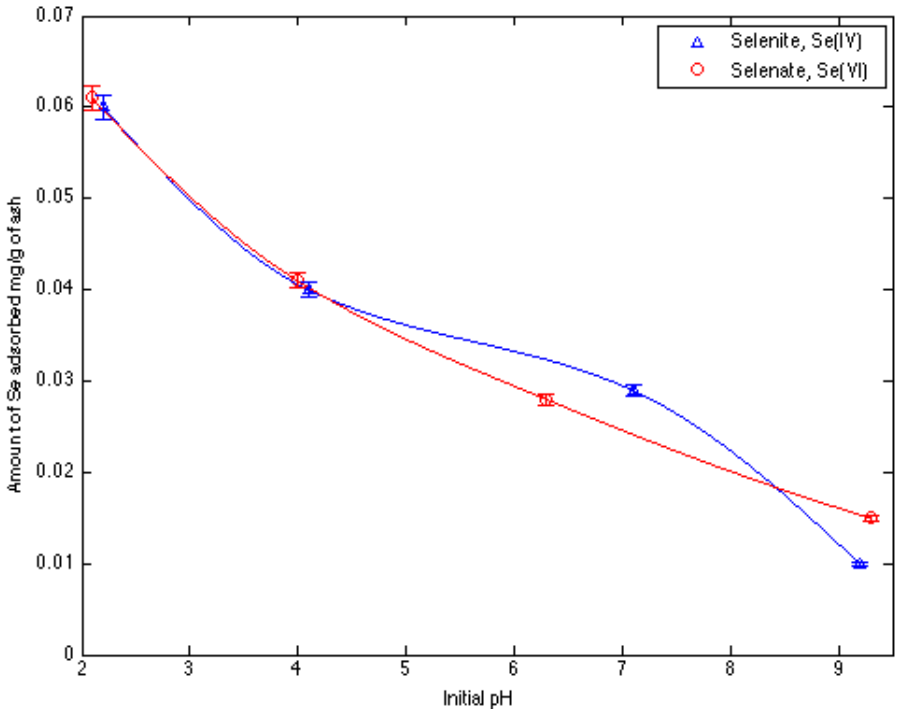

Figure 6-3: Amount of selenium adsorbed (mg/g of ash) at different initial pH values

Table 6-1: Effect of pH on selenium adsorption

	Initial pH	Final pH	Se conc (mg/L)	Se removed (mg/L)	Adsorption percentage (%)	Adsorption capacity (mg/g)
Selenite, Se(IV)						
Se4 - pH2	2.2	10.7	46.566	2.998	6.0	0.060
Se4 - pH4	4.1	11.2	47.543	2.021	4.1	0.040
Se4 - pH7	7.1	11.3	48.101	1.462	3.0	0.029
Se4 - pH9	9.2	11.3	49.072	0.491	1.0	0.010

Selenate, Se(VI)						
Se6 - pH2	2.1	10.7	46.846	3.074	6.2	0.061
Se6 - pH4	4.0	11.3	47.876	2.045	4.1	0.041
Se6 - pH7	6.3	11.3	48.507	1.414	2.8	0.028
Se6 - pH9	9.3	11.3	49.194	0.726	1.5	0.015

Note: Analyzed initial concentrations; 49.564 mg/L Se(IV); 49.920 mg/L Se(VI), Standard deviation of +/- 2.1% of adsorption capacity is illustrated in the graphs.

The increase in Se adsorption at low pH may be due the charge at the adsorbent surface which becomes positively charged at low pH due to H^+ ions. The H^+ ions are actively involved in the adsorption of negatively charged selenite and selenate ions onto the adsorbent (biomass ash) surface (Kongsri et al., 2013). Also, as per the Pourbaix diagram (Figure 6-1) acidic conditions can reduce the Se(IV) and Se(VI) into elemental selenium, Se(0) which would in turn be adsorbed onto the biomass ash surface as outlined by (El-Shafey, 2007a). However, it should be noted that, the percent increase in adsorption at low pH is only 5 %.

As shown in Figure 6-4, despite different initial pH values of the solutions (2, 4, 7, and 9), the final pH values of both solutions after mixing with CLM2 ash sample fall within pH 10.7 - 11.3. This can be attributed to the high total alkalinity of the sample which is 2720 mg/L $CaCO_3$.

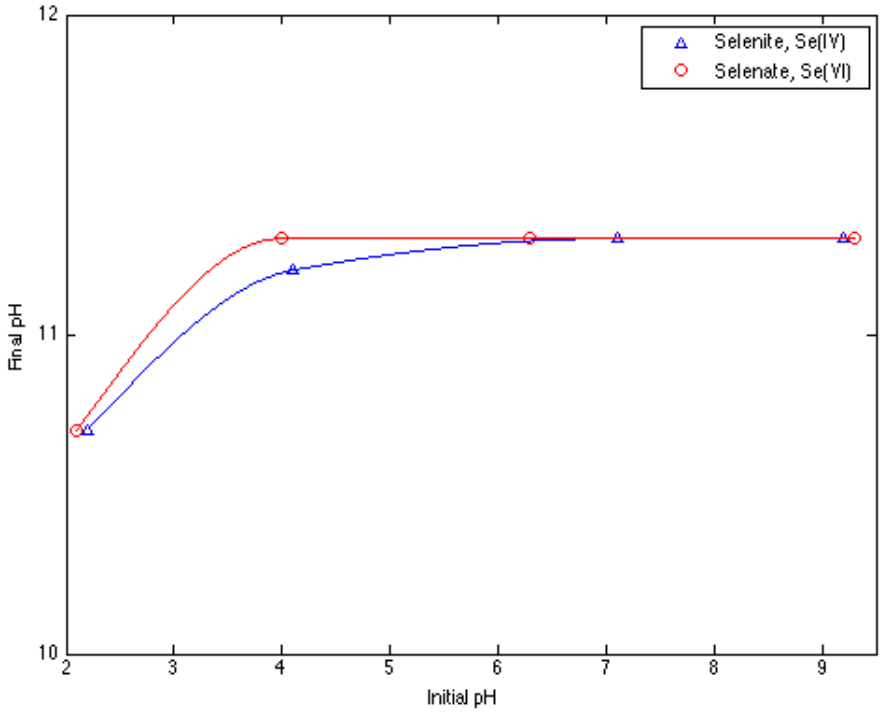

Figure 6-4: Initial pH vs. Final pH

The maximum percent adsorption of Se(IV) and Se(VI) on to CLM2 ash sample was 6% at room temperature (21^{o}C). Hence, solution pH was controlled at pH 2 for further experiments which also represents the acidic conditions present in mining effluent water streams.

6.4.3 Effect of Adsorbent Dose

Batch mixing tests were carried at different CLM2 ash doses of 20, 50, 80 g/L. The amount of Se adsorbed (mg/g) at different ash doses are shown in Figure 6-5 and Table 6-2. Selenite, Se(IV) adsorption capacity increased from 0.043 mg/g to 0.195 mg/g when the dose was decreased from 80 g/L to 20 g/L. Also, selenate, Se(VI) adsorption capacity increased from 0.055 mg/g to 0.211 mg/g when the dose was decreased from 80 g/L to 20

g/L. Although this seems counter intuitive (increasing adsorption capacity with decreasing dosage) it should be noted that the percentage of selenium adsorbed onto biomass ash remained the same at all three ash doses. The mixtures, as the ash dosage increased became more viscous, and likely resulted in poor mixing of sample and ash hence, the lower adsorption capacity. Other possible reasons for the increase in adsorption capacity with decrease in dose may be due to the fact that high amount of elements are leaching into the solution from the sample with increasing adsorbent dose which in-turn compete for the adsorption sites present in the ash samples along with Se(IV) and Se(VI) ions. Further, high adsorbent doses with high alkalinity tend to add more hydroxyl ions into the solution which increase the pH of the solution and these may also act as competing ions causing low amount of Se(IV) and Se(VI) adsorbed per g of ash. At all biomass doses, amount of Se(VI) adsorbed was slightly higher than the amount of Se(IV) adsorbed.

Table 6-2: Effect of adsorbent dose on selenium adsorption

	Initial pH	Final pH	Se conc (mg/L)	Se removed mg/L	Adsorption percentage (%)	Adsorption capacity (mg/g)
Selenite, Se(IV)						
Se4 - 20D	2.2	10.5	45.319	3.909	7.9	0.195
Se4 - 50D	2.2	11.2	45.879	3.349	6.8	0.067
Se4 - 80D	2.2	11.4	45.752	3.476	7.1	0.043

Selenate, Se(VI)						
Se6 - 20D	2.2	10.8	45.690	4.220	8.5	0.211
Se6 - 50D	2.2	11.1	45.384	4.526	9.1	0.091
Se6 - 80D	2.2	11.4	45.499	4.410	8.8	0.055

Note: Analyzed initial concentrations: 49.228 mg/L Se(IV); 49.910 mg/L Se(VI), Standard deviation of +/- 2.1% of adsorption capacity is illustrated in the graphs.

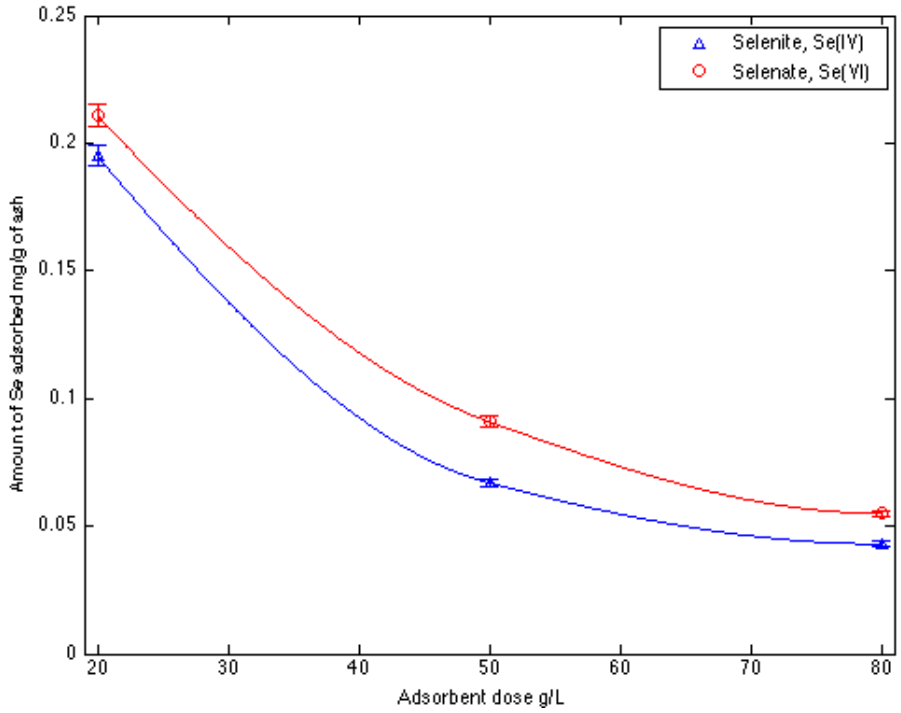

Figure 6-5: Biomass ash dose (g/L) vs. amount of selenium adsorbed (mg/g of ash)

6.4.4 Effect of Temperature

In the next set of experiments, temperature was varied (5, 21, 35 ^{o}C) maintaining the biomass ash dose at 50 g/L and solution pH at 2. Initial tests were run at room

temperature and here, the tests were run at a lower temperature (at 5 ^{o}C to represent the cold climate present in Canada) as well as at a higher temperature (at 35 ^{o}C to understand if high temperatures favor the adsorption). pH 2 was selected as the highest Se removed percentage was recorded at that value. 50 g/L dose was maintained for these tests as there is little effect on adsorption percent with varying dose. Se adsorption percentage and capacity increased with increase in temperature (Figure 6-6). At 5 ^{o}C, amount of Se(IV) adsorbed was 3.7% and 0.037 mg/g of CLM2 ash and Se(VI) adsorbed was 5.9% and 0.059 mg/g of CLM2 ash. However, at 35 ^{o}C, amount of Se (IV) adsorbed increased to 10.3% and 0.101 mg/g of CLM2 ash and Se(VI) adsorbed was 15.2% and 0.152 mg/g of CLM2 ash. Also, at all temperatures, amount of Se(VI) adsorbed was slightly higher than the amount of Se(IV) adsorbed (Table 6-3).

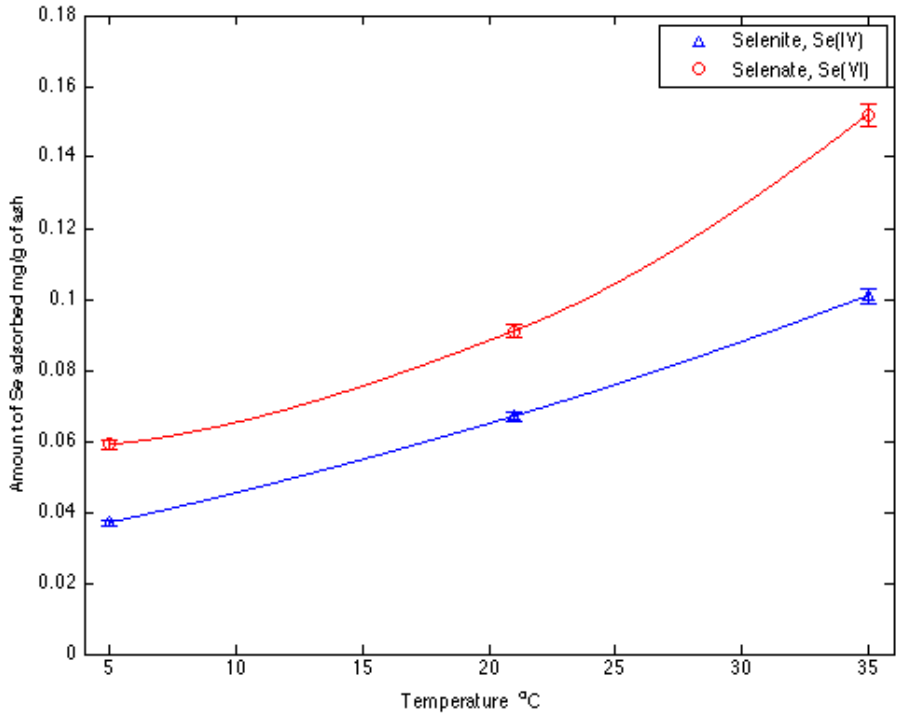

Figure 6-6: Temperature (^{o}C) vs. amount of selenium adsorbed (mg/g of ash)

The reasons for the high Se adsorption at high temperature may be due to expansion or swelling of adsorption sites in CLM2 sample at high temperatures allowing contact with more Se(IV) and Se(VI) ions. Similar results have been recorded in selenium adsorption studies done using sulphuric acid treated peanut shell and modified rice husk (El-Shafey, 2007a, 2007b).

Table 6-3: Effect of temperature on selenium adsorption

	Initial pH	Final pH	Se conc (mg/L)	Se removed (mg/L)	Adsorption percentage (%)	Adsorption capacity (mg/g)
Selenite, Se(IV)						
Se4 - 5C	2.2	11.1	47.393	1.836	3.7	0.037
Se4 - 21C	2.2	11.2	45.879	3.349	6.8	0.067
Se4 - 35C	2.2	11.3	44.181	5.047	10.3	0.101
Selenate, Se(VI)						
Se6 - 5C	2.2	11.0	46.962	2.947	5.9	0.059
Se6 - 21C	2.2	11.1	45.384	4.526	9.1	0.091
Se6 - 35C	2.2	11.3	42.321	7.589	15.2	0.152

Note: Analyzed initial concentrations: 49.228 mg/L Se(IV); 49.910 mg/L Se(VI), Standard deviation of +/- 2.1% of adsorption capacity is illustrated in the graphs.

Overall, the low selenium adsorption efficiency and adsorption capcaity by CLM2 samples may be due to the following reasons: adsorbent surface can be negatively charged which may repel the selenite and selenate anions; high adsorbent doses with high alkalinity adding more hydroxyl ions into the solution which may act as competing ions causing low amount of Se(IV) and Se(VI) adsorbed per g of ash.

6.4.5 Thermodynamic Parameters

Thermodynamic parameters (ΔG : Gibbs free energy change of adsorption, ΔH: enthalpy change, ΔS: entropy change) are typically assessed in all processes to determine the thermodynamic nature of the process (e.g. tendency to occur at given conditions). K_D (distribution coefficient) vs. the inverse absolute temperature graphs for Se(IV) and Se(VI) are shown in Figure 6-7 and 6-8. ΔH and ΔS values were calculated from the intercept and gradient of these graphs and results are given in Table 6-4.

Table 6-4: Thermodynamic parameters

Temperature (K)	ΔG (kJ/mol)	ΔS (kJ/mol.K)	ΔH (kJ/mol)
Selenite			
278.15	0.5905	0.09054	25.774
294.15	-0.9257		25.707
308.15	-2.1167		25.783

Selenate			
278.15	-0.5255	0.09046	24.635
294.15	-1.6884		24.919
308.15	-3.2719		24.602

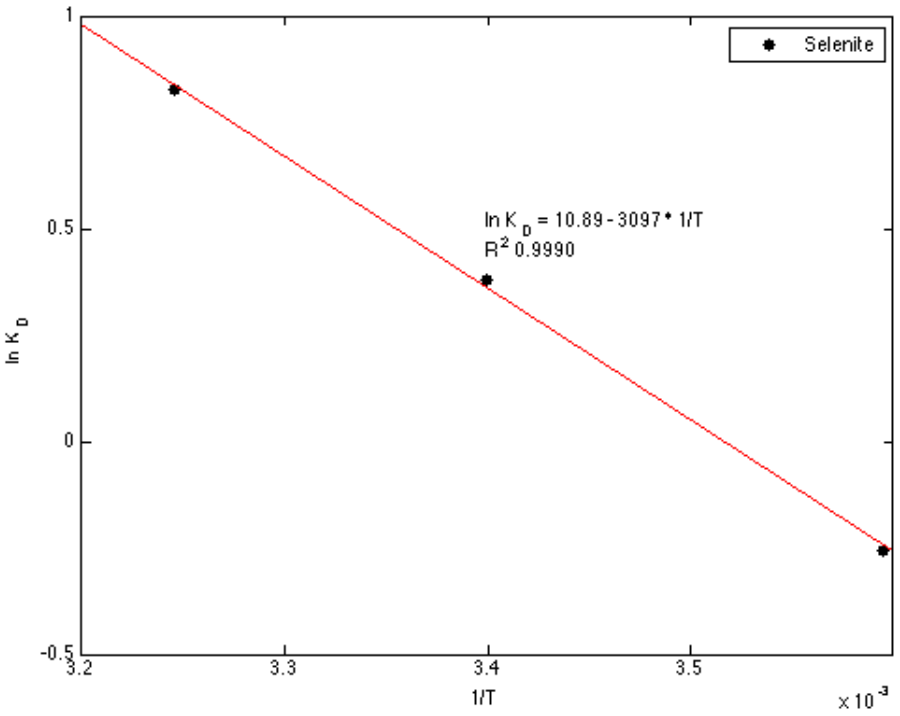

Figure 6-7: ln K_D vs. I/T(K^{-1}) plot for selenite, Se(IV)

Positive ΔG values indicate the process is not thermodynamically favoured and negative ΔG values indicate the process is favoured. Here, the ΔG values become more negative with temperature increase, indicating that at high temperatures the adsorption process is more favourable (Jordan et al., 2013a). Positive ΔH values indicate the endothermic

nature of adsorption. Positive ΔS values indicate the increased degree of randomness at the adsorbent/solution interface (Nettem and Almusallam, 2013).

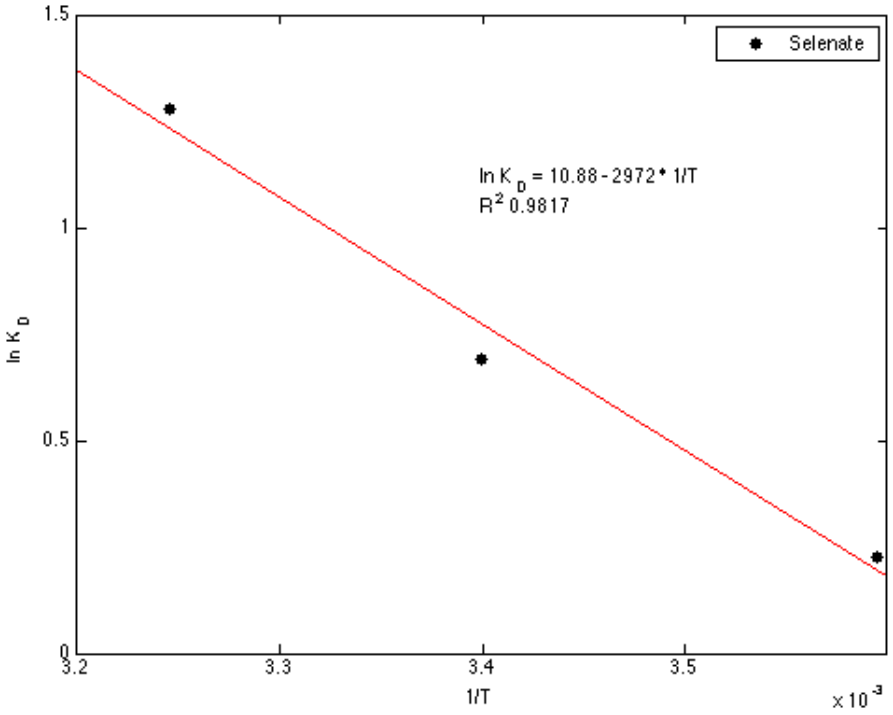

Figure 6-8: ln K_D vs. I/ T(K^{-1}) plot for selenate, Se(VI)

6.5 Conclusion and Recommendations

The biomass ash used in this study was collected from ZCLP giving the following: high specific surface area; low density; high carbon content; presence of S-O, C-O and Si-O surface functional groups; high total alkalinity with neutralization capacity; presence of minerals favorable to be used as adsorbents such as calcite, alkali-feldspar, quartz. These results confirmed the suitability of using these biomass ash as an adsorbent for treatment of contaminants in mining effluent water streams.

The adsorption experiments were carried out using synthesized solutions of selenite, Se(IV) and selenate, Se(VI) at varying pH, biomass ash dose and temperature. Maximum percentage removal for Se(IV) and Se(VI) was 10.3% and 15.2% at 35^{o}C. When the pH was decreased from pH 9 to 2 adsorption percentage increased by 5%. Varying the biomass ash dose did not have a significant effect on Se removal percentage. However, high adsorption capacities were recorded at low adsorbent dose (20 g/L). Adsorption capacities obtained for Se(IV) (0.195 mg/g) and Se(VI) (0.211 mg/g) are similar to capacities recorded in Hasan et al., 2010 and higher than the capacities recorded in Gulipalli et al., 2011. High neutralization capacities were recorded with both Se(IV) and Se(VI) solutions where final solution pH of all samples fall within pH 10.5 - 11.4 despite the initial pH value.

Although, selenium adsorption capacities onto biomass ash are relatively low compared with the monolayer sorption capacities of various adsorbents recorded in Table 3-2, it may be possible to increase the adsorption capacities of biomass ash by chemical modification.

Recommendations for future work include;

- Characterization of spent adsorbents from these experiments to understand which specific properties may have involved in selenium removal. By comparing ash characteristics before and after mixing with Se, it will be possible to understand

what properties should be enhanced to increase Se adsorption capacity/removal percentage.

- Identify suitable chemical modification methods to increase the selenium sorption capacity. These chemicals should be selected such that, modified ash will have increased anion exchange capacity or increased positively charged functional groups or increased ability to convert selenite and selenate ions to elemental selenium.
- Perform experiments using simulated effluent streams with various other compounds to determine any interference these compounds may have in adsorption.
- Conduct kinetic experiments to determine rates for reactor type selection and design of the overall selenium treatment process.
- Assess the leaching characteristics of the spent ash to determine further disposal options for these ash (e.g. use as an additive for construction purposes, landfill disposal etc.).

Bibliography - Chapter 6

Adeoti, I. A.: Characterization and Alternative Use Study of Fly Ash, 160 pp., Memorial University of Newfoundland., 2011.

Berra, M., Casa, G. De, Orso, M. D., Galeotti, L., Mangialardi, T., Paolini, A. E. and Piga, L.: Reuse of Woody Biomass Fly Ash in Cement-Based Materials : Leaching Tests, in Recycling of Biomass Ashes, edited by H. Insam and B. A. Knapp, pp. 133–146, Springer Berlin Heidelberg., 2011.

Berra, M., Dell'orso, M., Mangialardi, T., Paolini, A. E. and Piga, L.: Chemical and Environmental Characterization of Fly Ash from Woody Biomass Combustion, in Internation Symposium on Energy from Biomass and Waste, CISA, Environmental Sanitary Engineering Centre, Venice., Italy., 2010.

El-Shafey, E. I.: Removal of Se(IV) from aqueous solution using sulphuric acid-treated peanut shell., J. Environ. Manage., 84(4), 620–7, doi:10.1016/j.jenvman.2007.03.021, 2007a.

El-Shafey, E. I.: Sorption of Cd(II) and Se(IV) from aqueous solution using modified rice husk., J. Hazard. Mater., 147(1-2), 546–55, doi:10.1016/j.jhazmat.2007.01.051, 2007b.

Envirogen Technologies: Treatment of Selenium-Containing Coal Mining Wastewater with Fluidized Bed Reactor Technology. [online] Available from: http://www.envirogen.com/files/files/ETI_Selenium_GrayPaper_V_FINAL.pdf, 2011.

Environment protection Division Ministry of Environment Government of British Columbia: Ambient Water Quality Guidelines for Selenium, [online] Available from: http://www.env.gov.bc.ca/wat/wq/BCguidelines/selenium/selenium.html, 2001.

Gulipalli, C. H. S., Prasad, B. and Wasewar, K. L.: Batch Study, Equilibrium and Kinetics of Adsorption of Selenium using Rice Husk Ash (RHA), J. Eng. Sci. Technol., 6(5), 586–605 [online] Available from: http://jestec.taylors.edu.my/Vol 6 Issue 5 October 11/Vol_6_5_586_605_WASEWAR.pdf, 2011.

Hasan, S. H., Ranjan, D. and Talat, M.: Agro-industrial waste "wheat bran" for the biosorptive remediation of selenium through continuous up-flow fixed-bed column., J. Hazard. Mater., 181(1-3), 1134–42, doi:10.1016/j.jhazmat.2010.05.133, 2010.

Jordan, N., Müller, K., Franzen, C. and Brendler, V.: Temperature impact on the sorption of selenium(VI) onto anatase., J. Colloid Interface Sci., 390(1), 170–5, doi:10.1016/j.jcis.2012.09.021, 2013.

Kongsri, S., Janpradit, K., Buapa, K., Techawongstien, S. and Chanthai, S.: Nanocrystalline hydroxyapatite from fish scale waste: Preparation, characterization and application for selenium adsorption in aqueous solution, Chem. Eng. J., 215-216, 522–532, doi:10.1016/j.cej.2012.11.054, 2013.

Li, L., Yu, C., Bai, J., Wang, Q. and Luo, Z.: Heavy metal characterization of circulating fluidized bed derived biomass ash., J. Hazard. Mater., 233-234, 41–7, doi:10.1016/j.jhazmat.2012.06.053, 2012.

Li, X., Guo, X., Wang, S., Wang, K., Luo, Z. and Wang, Q.: Characterization and Analysis of Char Produced by Biomass Fast Pyrolysis, 2010 Asia-Pacific Power Energy Eng. Conf., 1–4, doi:10.1109/APPEEC.2010.5448524, 2010.

Li, Z., Li, H., Yang, X., Zhang, H., Liu, C. and Cao, B.: Characterization of Se(IV) removal from aqueous solution by Aspergillus sp. J2, Chem. Eng. J., 220(3), 67–71, doi:10.1016/j.cej.2012.11.136, 2013.

Liu, Z., Zhang, F.-S. and Wu, J.: Characterization and application of chars produced from pinewood pyrolysis and hydrothermal treatment, Fuel, 89(2), 510–514, doi:10.1016/j.fuel.2009.08.042, 2010.

McCafferty, E.: Introduction to Corrosion Science, Springer New York., 2010.

Nettem, K. and Almusallam, A. S.: Equilibrium, Kinetic and Thermodynamic Studies on the Biosorption of Selenium (IV) Ions onto Ganoderma Lucidum Biomass, Sep. Sci. Technol., (June), doi:10.1080/01496395.2013.791318, 2013.

Pan, H. and Eberhardt, T.: Characterization of Fly Ash from the Gasification of Wood and Assessment for Its Application as a Soil Amendment., 2011.

Rajamma, R., Ball, R. J., Tarelho, L. a C., Allen, G. C., Labrincha, J. a and Ferreira, V. M.: Characterisation and use of biomass fly ash in cement-based materials., J. Hazard. Mater., 172(2-3), 1049–60, doi:10.1016/j.jhazmat.2009.07.109, 2009.

Shang, G., Shen, G., Wang, T. and Chen, Q.: Effectiveness and mechanisms of hydrogen sulfide adsorption by camphor-derived biochar, J. Air Waste Manage. Assoc., 62(8), 873–879, doi:10.1080/10962247.2012.686441, 2012.

Sheha, R. R. and El-Shazly, E. a.: Kinetics and equilibrium modeling of Se(IV) removal from aqueous solutions using metal oxides, Chem. Eng. J., 160(1), 63–71, doi:10.1016/j.cej.2010.03.004, 2010.

Smidt, E., Böhm, K. and Schwanninger, M.: Fourier Transforms - New Analytical Approaches and FTIR Strategies, edited by G. Nikolic, InTech., 2011.

US EPA: Basic Information about Selenium in Drinking Water, [online] Available from: http://water.epa.gov/drink/contaminants/basicinformation/selenium.cfm#four, 1992.

Vadapalli, V. R. K., Gitari, M. W., Petrik, L. F., Etchebers, O. and Ellendt, A.: Integrated acid mine drainage management using fly ash, J. Environ. Sci. Health. A. Tox. Hazard. Subst. Environ. Eng., 47(1), 60–9, doi:10.1080/10934529.2012.629582, 2012.

Vassilev, S. V., Baxter, D., Andersen, L. K. and Vassileva, C. G.: An overview of the composition and application of biomass ash. Part 1. Phase–mineral and chemical composition and classification, Fuel, 105, 40–76, doi:10.1016/j.fuel.2012.09.041, 2013a.

Vassilev, S. V., Baxter, D., Andersen, L. K. and Vassileva, C. G.: An overview of the composition and application of biomass ash. Part 2. Potential utilisation, technologcal and ecological advantages and challenges, Fuel, 105, 19–39, doi:10.1016/j.fuel.2012.10.001, 2013b.

World Health Organization: Background document for preparation of WHO Guidelines for drinking-water quality, (WHO/SDE/WSH/03.04/13), 2003.

Chapter 7 : Summary

This study investigated the possibility of using biomass ash/ char, a byproduct of combustion of forestry residue and/or fossil fuels in pulp and paper mill boilers, as an adsorbents to treat sulphur and selenium oxy-anions present in mining effluent water.

Chapter 1 provides the 'Introduction and Overview'. The main objectives of the study, structure of the thesis as well as the importance and value of the current research were discussed in this chapter.

Chapter 2 provided a comprehensive review on removal of sulphur-oxy anions (thiosalts and sulphates) from mining effluent water. The generation and importance of Acid Mine Drainage (AMD), different sulphur species present in AMD, mainly, sulphate and thiosalts (thiosulphate, trithionate, tetrathionate), behavior of thiosalts at different pH (2, 4, 7, 9) and temperature (4, 15, 30 ^{o}C) and various thiosalt treatment methods such as natural degradation, chemical oxidation, biological oxidation were discuseed. Furthermore, use of various carbonaceous adsorbents, ion exchange resins, fly ash and fly ash zeolites used for sulphate and thiosalt removal by adsorption and ion exchange were discussed in detail.

Chapter 3 provided a comprehensive review on removal of selenium oxy-anions (selenite and selenate) from aqueous media by adsorption. This chapter summarizes recent work on adsorbent types used in selenium oxy-anions (selenite and selenate) treatment such as

activated carbon, biomass, biomass ash, iron oxides, aluminium based adsorbents, silica, apatite, rutile etc. The effect of pH (1.5 - 11.5), temperature (18 - 50 ^{o}C), initial concentration of selenium in the solution (0.8 - 100 mg/L), adsorbent dosage (0.5 - 20 g/L) on the sorption capacity was reviewed. Monolayer sorption capacities for selenium ranging from 0.081 mg/g to 126.99 mg/g of adsorbent have been reported. Further details on isotherm models, kinetic models and thermodynamic parameters such as Gibbs free energy change, enthalpy change, entropy change as well as techniques used in adsorbent characterization (XRD, SEM, FT-IR, BET surface area, point of zero charge pH, and analytical determination of selenium were also discussed.

Chapter 4 provided the methodology used for characterization of eight biomass ash/char samples collected from three pulp and paper mill boilers (Kruger Brompton Mill, Corner Brook Pulp and Paper Limited, Zellstoff Celgar Limited Partnership) and extensive discussion on results. Eight ash/char samples were characterized chemically, physically, thermally, and structurally by inductively coupled plasma mass spectrometry and optical emission spectrometry (ICP-MS, ICP-OES), CNS (carbon, nitrogen, sulphur) elemental analysis, mineral liberation analysis (MLA), X-ray diffraction (XRD), Fourier transform infrared spectroscopy (ATR-FTIR), scanning electron microscopy (SEM), specific surface area, pore volume, bulk density, pH, total alkalinity, thermo-gravimetric analysis (TGA) and results were discussed in detail.

Chapter 5 provided the results from the batch experiment studies on removal of sulphur from thiosulphate, trithionate and tetrathionate solutions using biomass ash/char (CBM-W sample) characterized in Chapter 4. Batch mixing experiments were conducted with 3 different types of biomass ash/char (CBM-D1, CBM-W, CLM1) by varying initial solution pH (2, 4, 7, 9), adsorbent dose (20, 50, 80 g/L of CBM-W sample) and temperature (5, 21, 35 ^{o}C) until equilibrium was achieved (24 hrs). Highest adsorption capacities were recorded at the highest adsorption dose used (80 g/L) which were 10.822, 10.291, 14.235 mg/g of biomass ash for thiosulphate, trithionate and tetrathionate respectively. Variation in pH and temperature didn't have a significant effect on sulphur adsorption from all three solutions. Moderate neutralization capacities were recorded where final pH values of all solutions fall in the range 6.6 - 9.4. Freundlich isotherm equation was found to be a better fit than the Langmuir isotherm equation.

Chapter 6 provided the results from the batch experiment studies on removal of selenium from selenite and selenate solutions using biomass ash/char (CLM2) characterized in Chapter 4. Batch experiments were conducted by mixing different doses of ash (CLM2) sample (20, 50, 80 g/L) with Se(IV) and Se(VI) solutions (50 mg/L Se concentration) at different pH (2, 4, 7, 9) and temperature (5, 21, 35 ^{o}C) until equilibrium is achieved (24 hrs). Maximum percentage removal for Se(IV) and Se(VI) was 10.3% and 15.2% at 35^{o}C. When the pH was decreased from pH 9 to 2 adsorption percentage increased by 5%. Varying the biomass ash dose did not have a significant effect on Se removal percentage. However, high adsorption capacities were recorded at lower adsorbent doses (20 g/L).

Adsorption capacities obtained for Se(IV) (0.195 mg/g) and Se(VI) (0.211 mg/g) are similar to capacities recorded in Hasan et al., 2010 and higher than the capacities recorded in Gulipalli et al., 2011. High neutralization capacities were recorded with both Se(IV) and Se(VI) solutions where final solution pH of all samples fall within pH 10.5 - 11.4 despite the value of initial pH.

Recommendations for future work are as follows;

- Characterization of spent adsorbents from to understand which specific properties may have involved in sulphur and selenium removal and to understand the adsorption mechanism.
- Using a more accurate analytical method to determine the amount of sulphur in the solution would aid in analysis.
- Selection of a narrow size range of the CBM-W sample as well as higher dose to obtain significant variation in results with varying parameters.
- Identify suitable chemical modification methods to increase the selenium sorption capacity. These chemicals should be selected such that, modified ash will have increased anion exchange capacity or increased positively charged functional groups or increased ability to convert selenite and selenate ions to elemental selenium.
- Conduct column experiments to obtain more information in designing an adsorption process.

- Perform experiments using simulated effluent streams with various other compounds to determine any interference these compounds may have in adsorption
- Conduct kinetic experiments to determine rates for reactor type selection and design of the overall selenium treatment process.
- Assess the leaching characteristics of the spent ash to determine further disposal options for these ash (e.g. use as an additive for construction purposes, landfill disposal etc.)

Appendix

Appendix A: ATR-FTIR spectrums

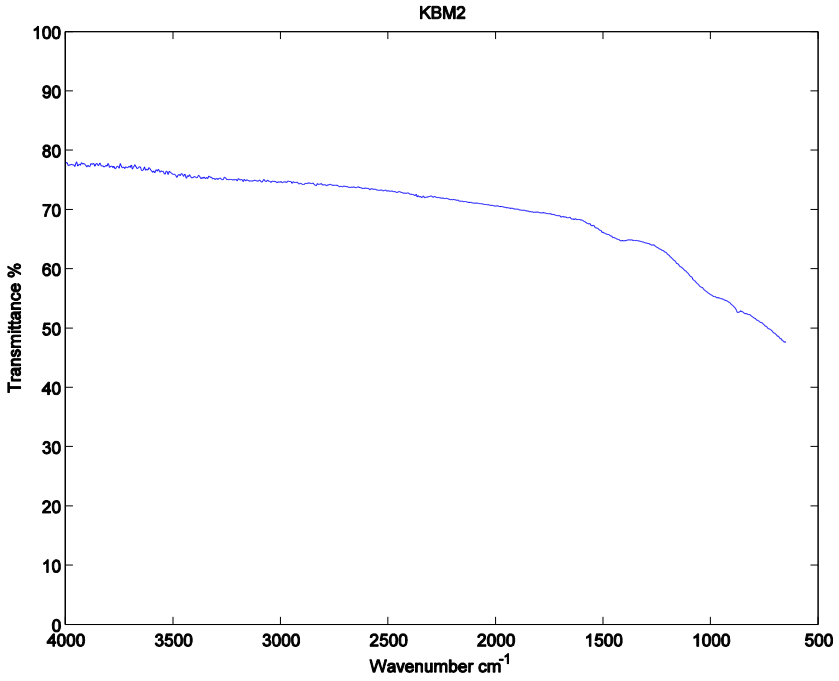

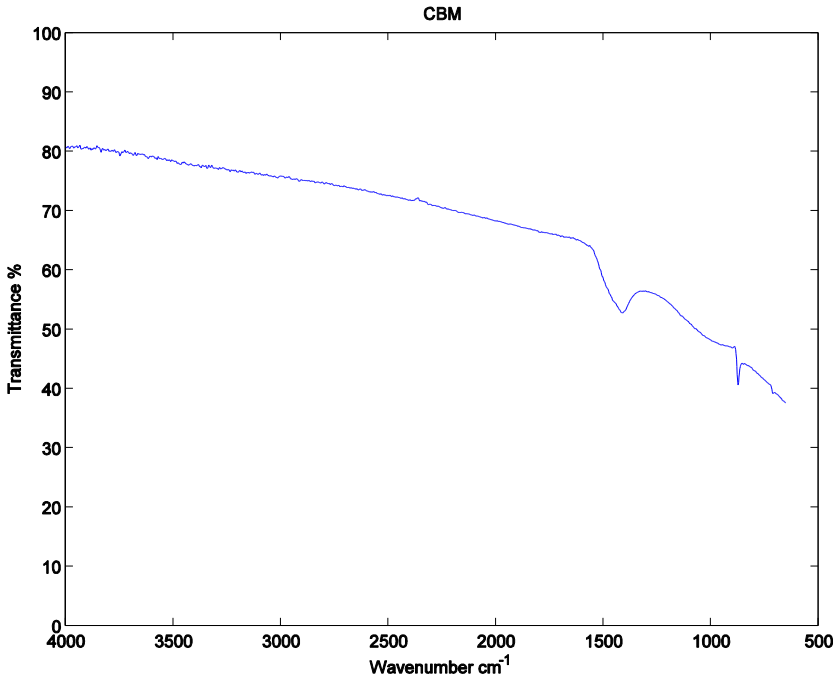

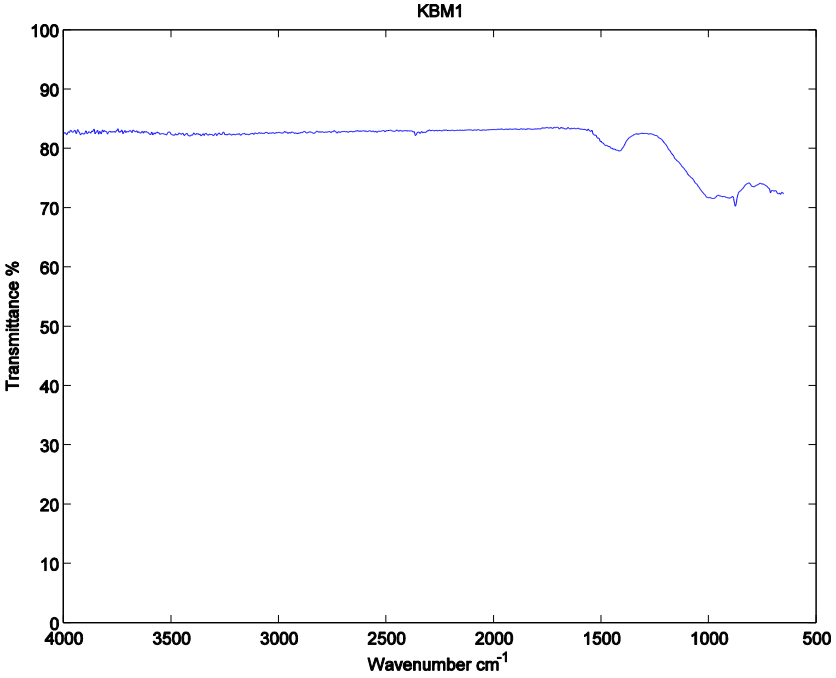
KBM1
Transmittance %
Wavenumber cm-1
100
90
80
70
60
50
40
30
20
10
0
4000
3500
3000
2500
2000
1500
1000
500

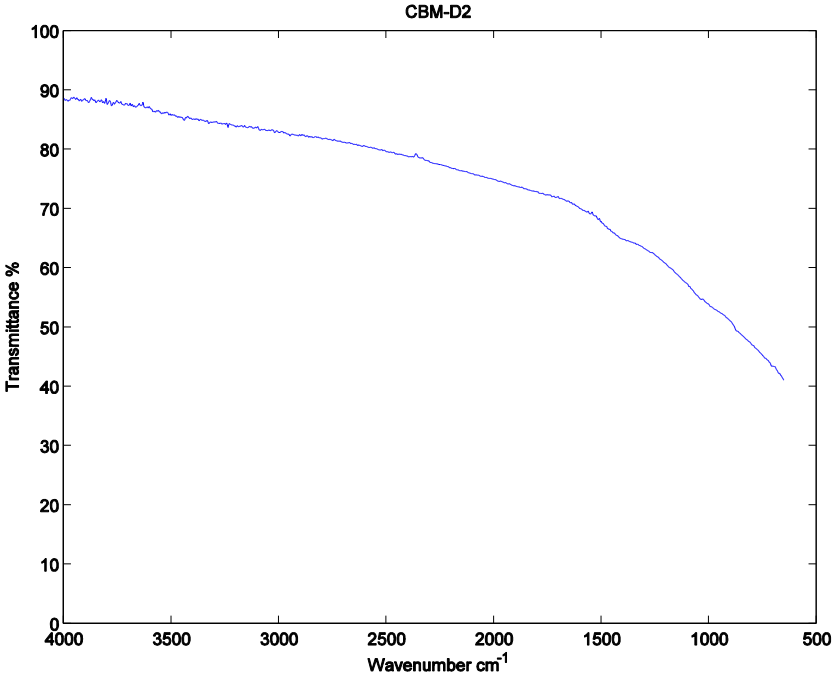
CBM-D2
Transmittance %
Wavenumber cm-1
100
90
80
70
60
50
40
30
20
10
0
4000
3500
3000
2500
2000
1500
1000
500

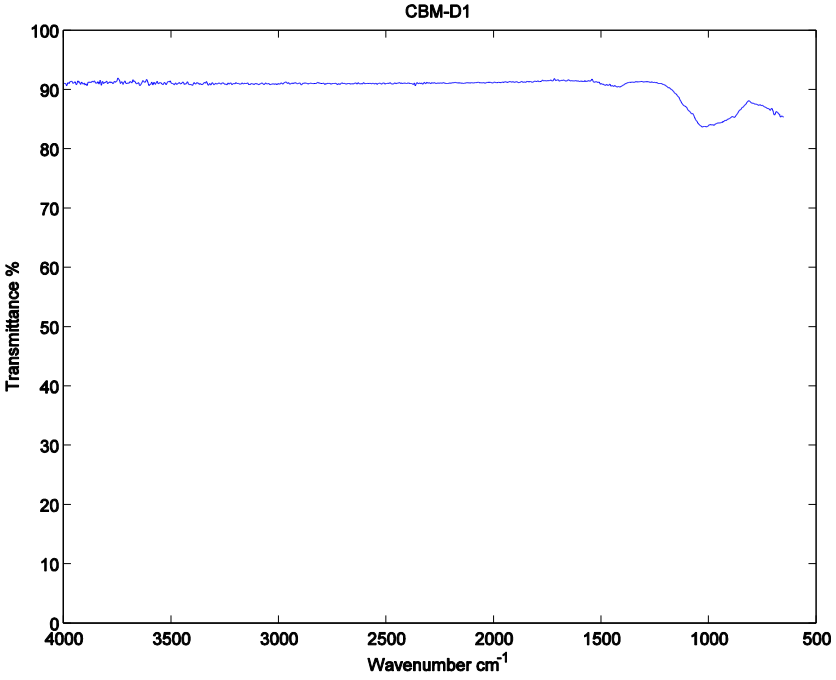
CBM-D1
Transmittance %
Wavenumber cm-1
100
90
80
70
60
50
40
30
20
10
0
4000
3500
3000
2500
2000
1500
1000
500

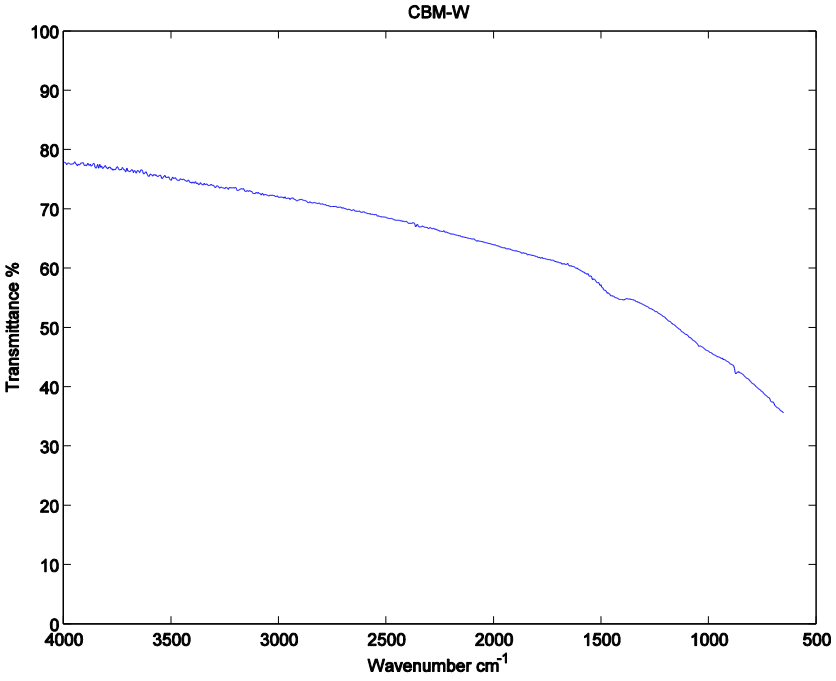
CBM-W
Transmittance %
Wavenumber cm-1
100
90
80
70
60
50
40
30
20
10
0
4000
3500
3000
2500
2000
1500
1000
500

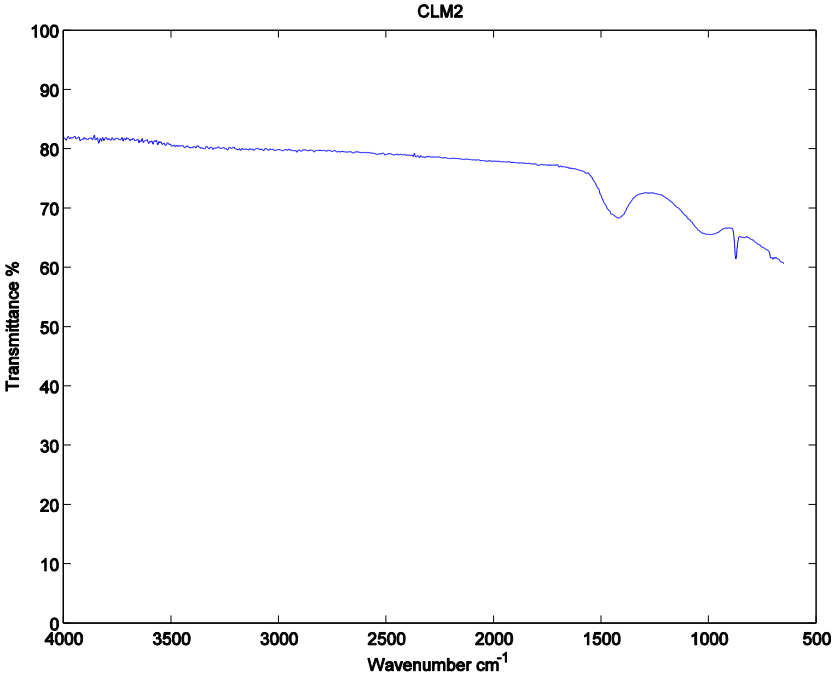
CLM2
Transmittance %
Wavenumber cm-1
100
90
80
70
60
50
40
30
20
10
0
4000
3500
3000
2500
2000
1500
1000
500

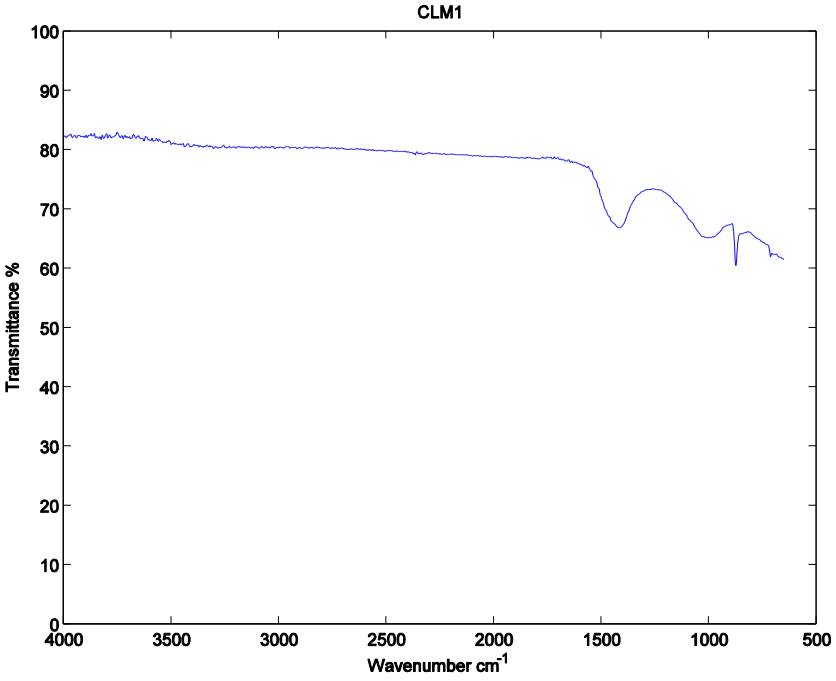
CLM1
Transmittance %
Wavenumber cm-1
100
90
80
70
60
50
40
30
20
10
0
4000
3500
3000
2500
2000
1500
1000
500

Appendix B: Weight% and derivative weight(%/^{o}C) vs temperature graphs (TGA)

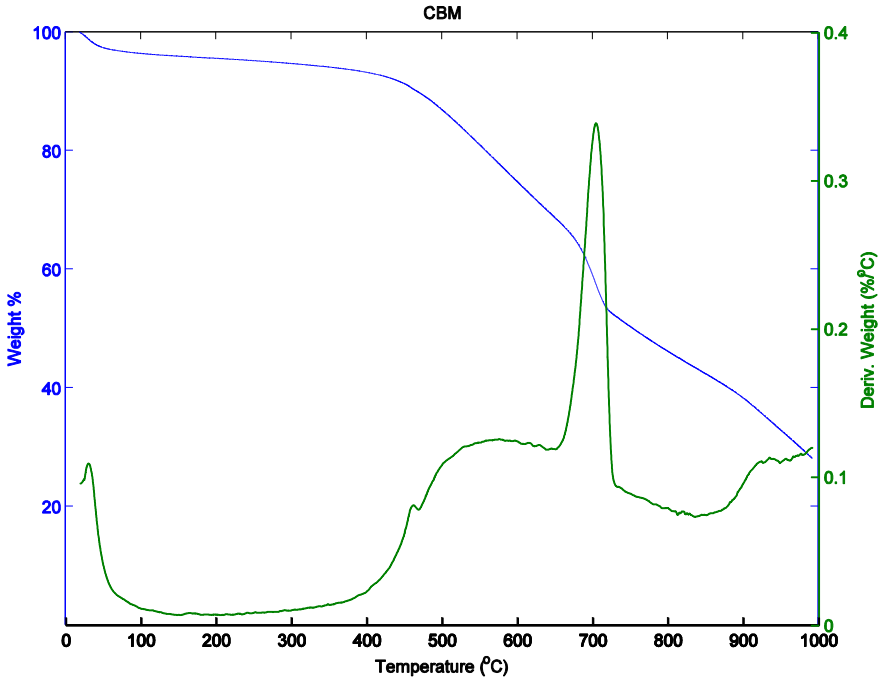

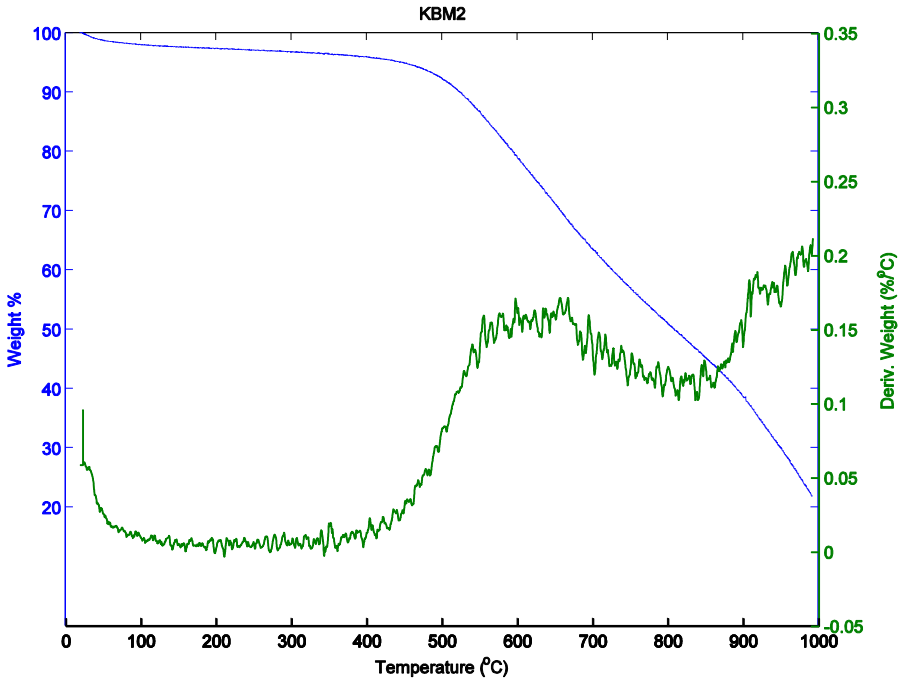

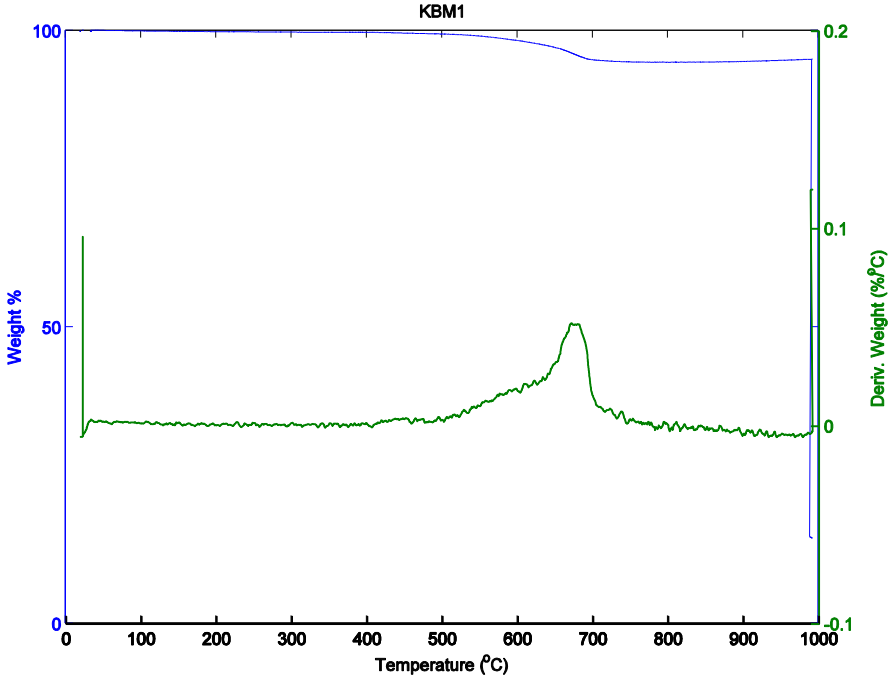
KBM1
100
50
0
Weight %
0.2
0.1
0
-0.1
Deriv. Weight (%/°C)
0
100
200
300
400
500
600
700
800
900
1000
Temperature (°C)

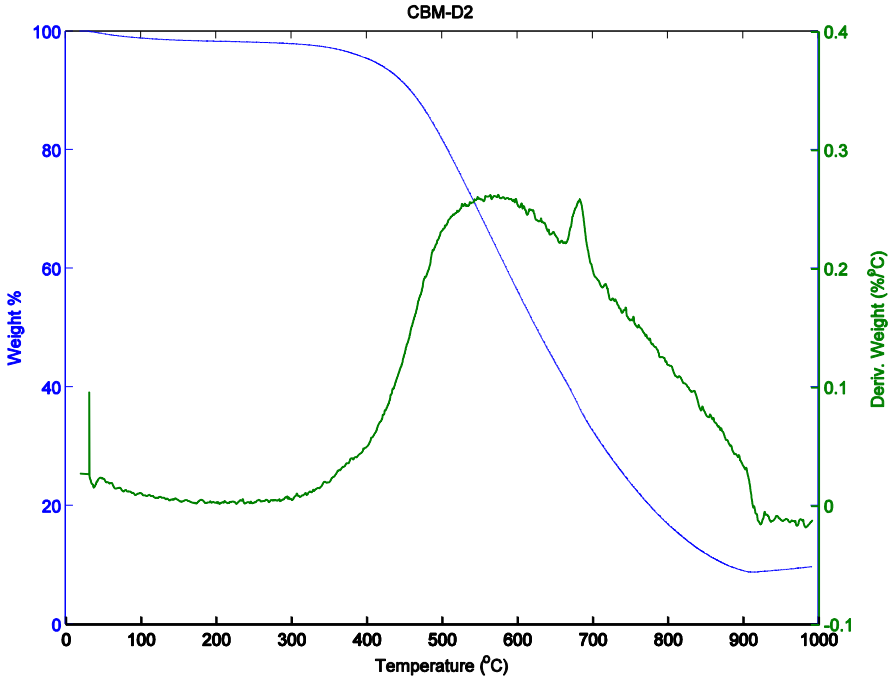
CBM-D2
100
80
60
40
20
0
Weight %
0.4
0.3
0.2
0.1
0
-0.1
Deriv. Weight (%/°C)
0
100
200
300
400
500
600
700
800
900
1000
Temperature (°C)

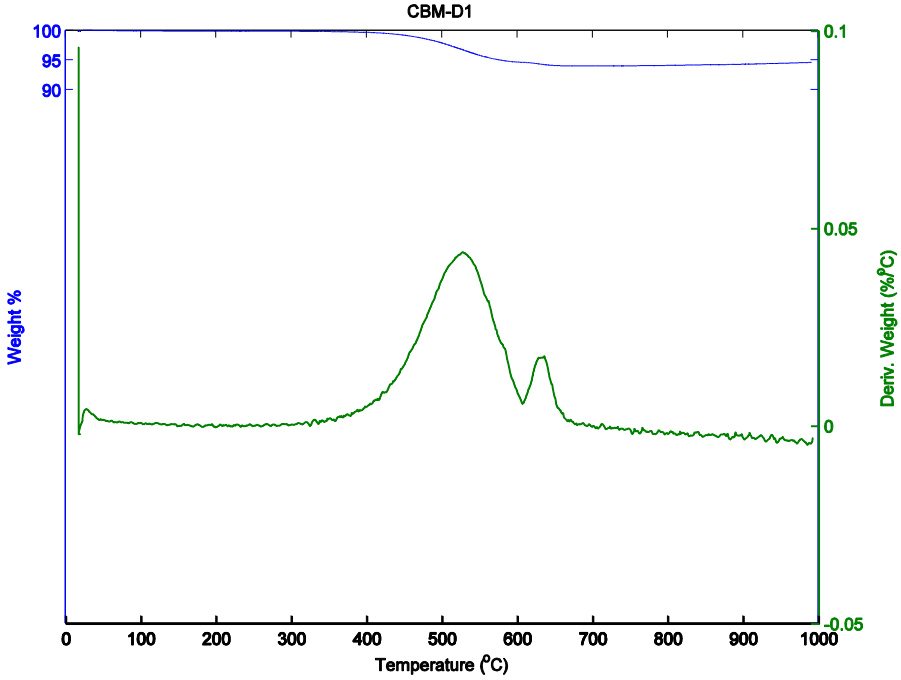
CBM-D1
100
95
90
0.1
0.05
0
-0.05
Weight %
Deriv. Weight (%/°C)
0
100
200
300
400
500
600
700
800
900
1000
Temperature (°C)

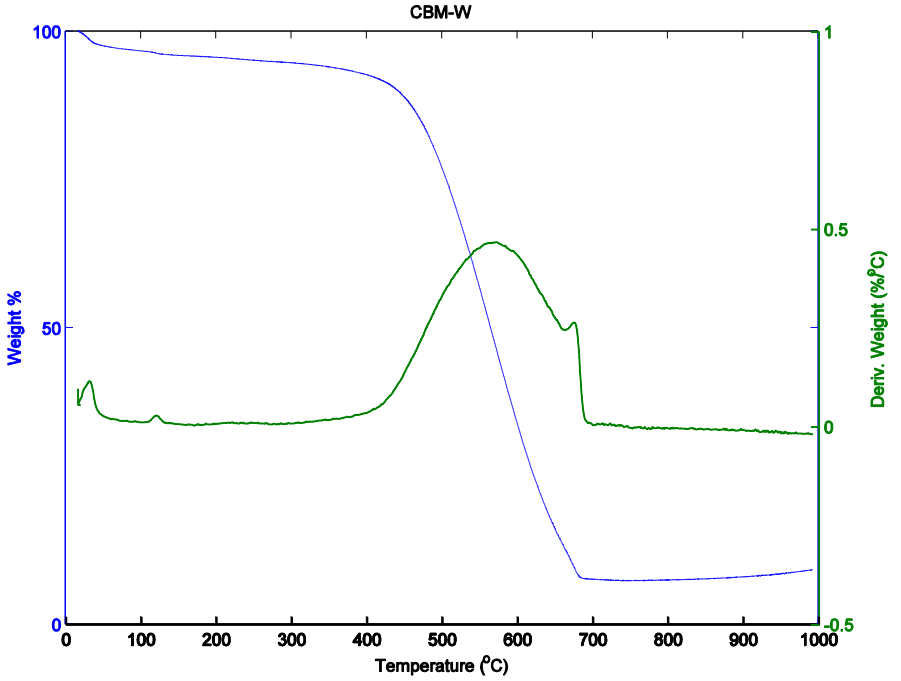
CBM-W
100
50
0
1
0.5
0
-0.5
Weight %
Deriv. Weight (%/°C)
0
100
200
300
400
500
600
700
800
900
1000
Temperature (°C)

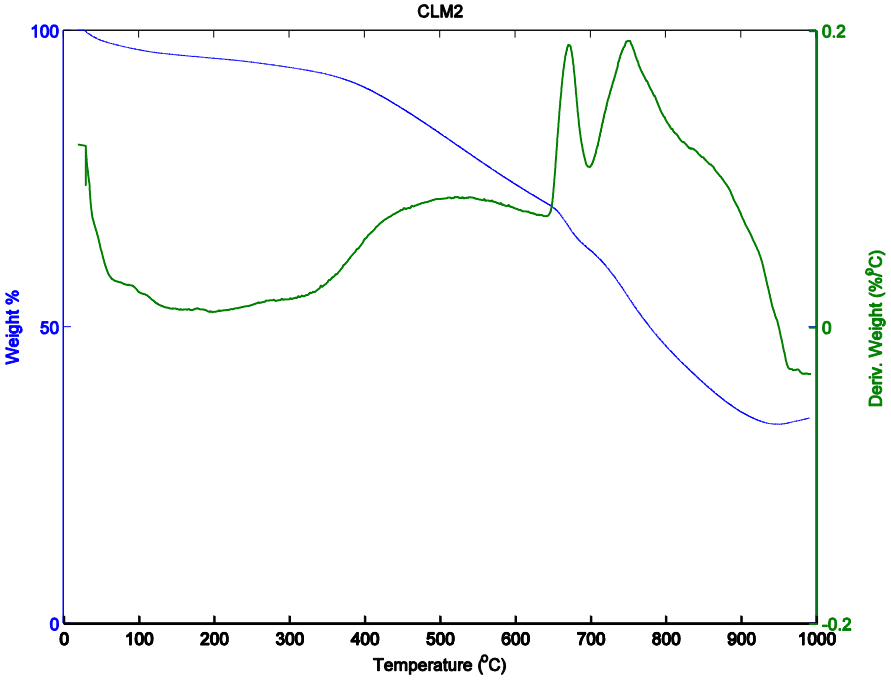
CLM2
100
50
0
Weight %
0.2
0
-0.2
Deriv. Weight (%/°C)
0
100
200
300
400
500
600
700
800
900
1000
Temperature (°C)

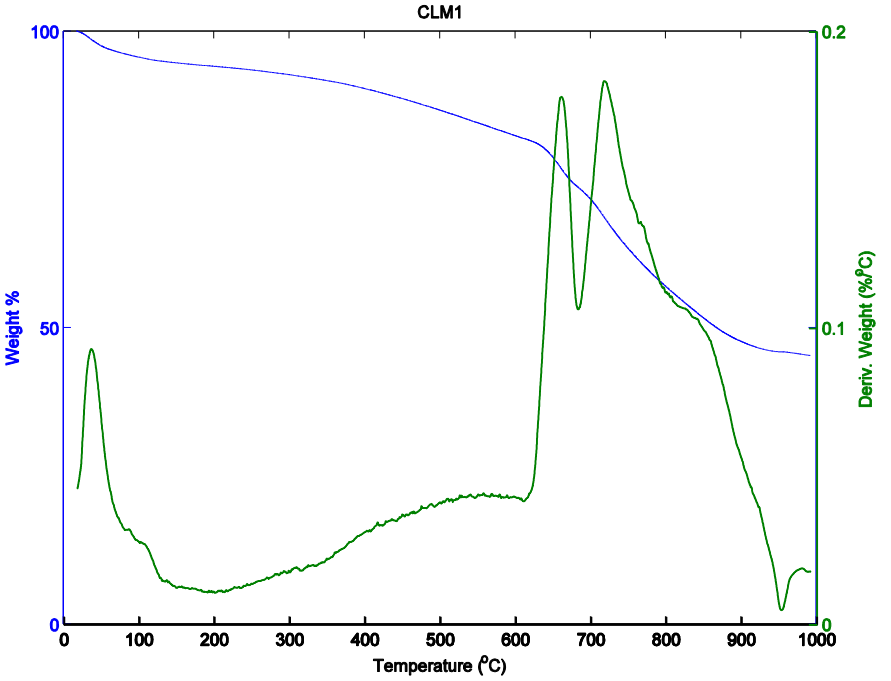
CLM1
100
50
0
Weight %
0.2
0.1
0
Deriv. Weight (%/°C)
0
100
200
300
400
500
600
700
800
900
1000
Temperature (°C)

Appendix C: XRD spectra

1. CBM

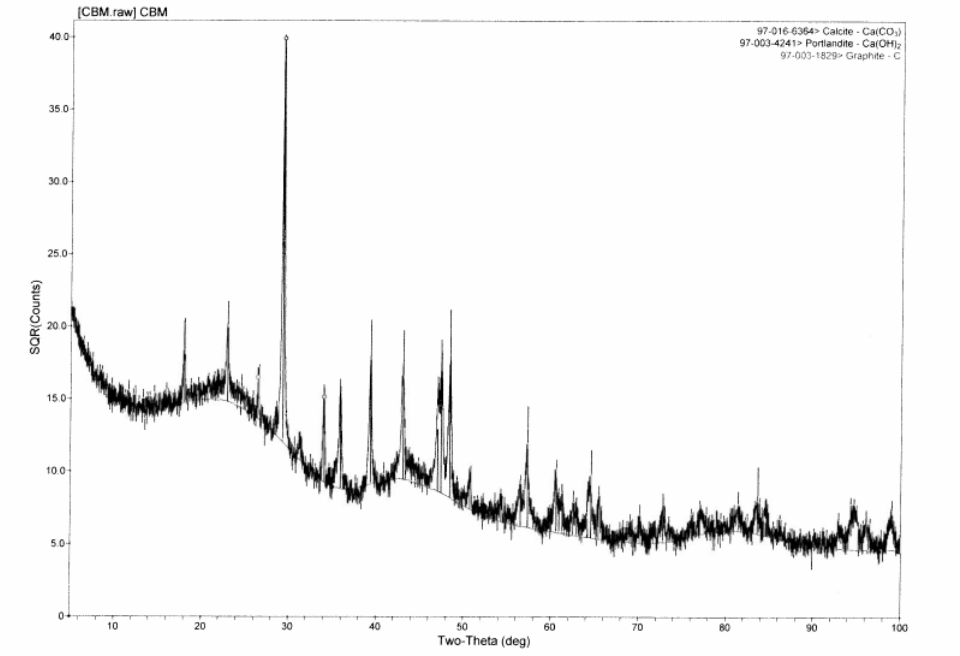

2. KBM2

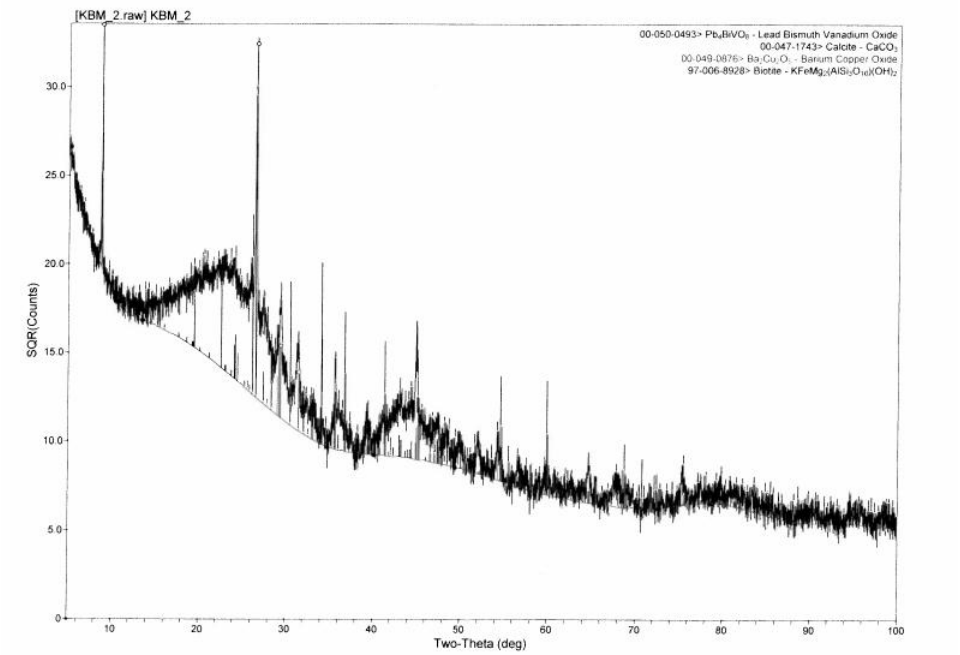

3. KBM1

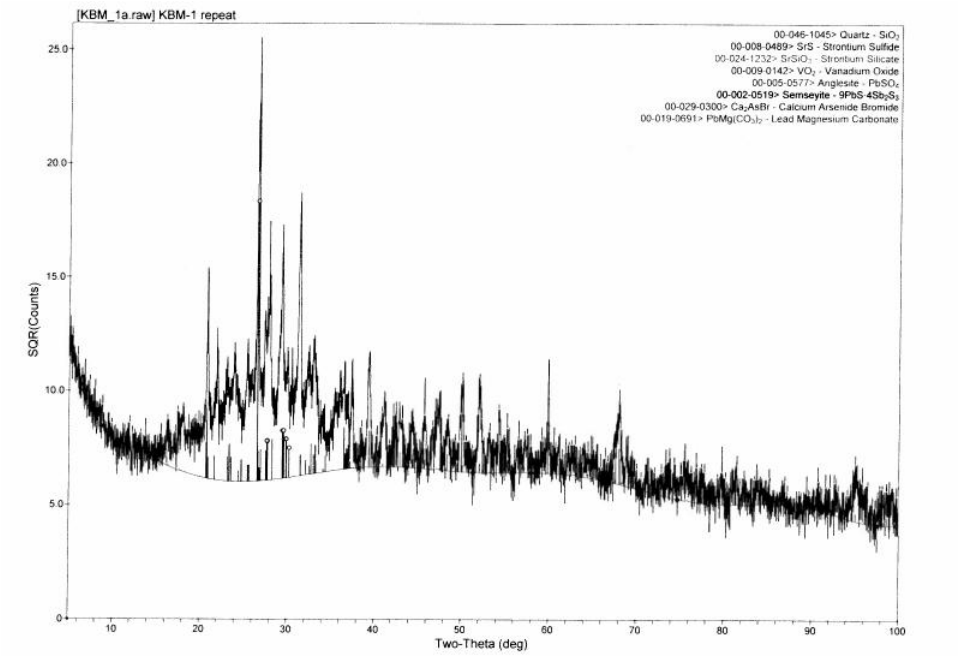

4. CBM-D2

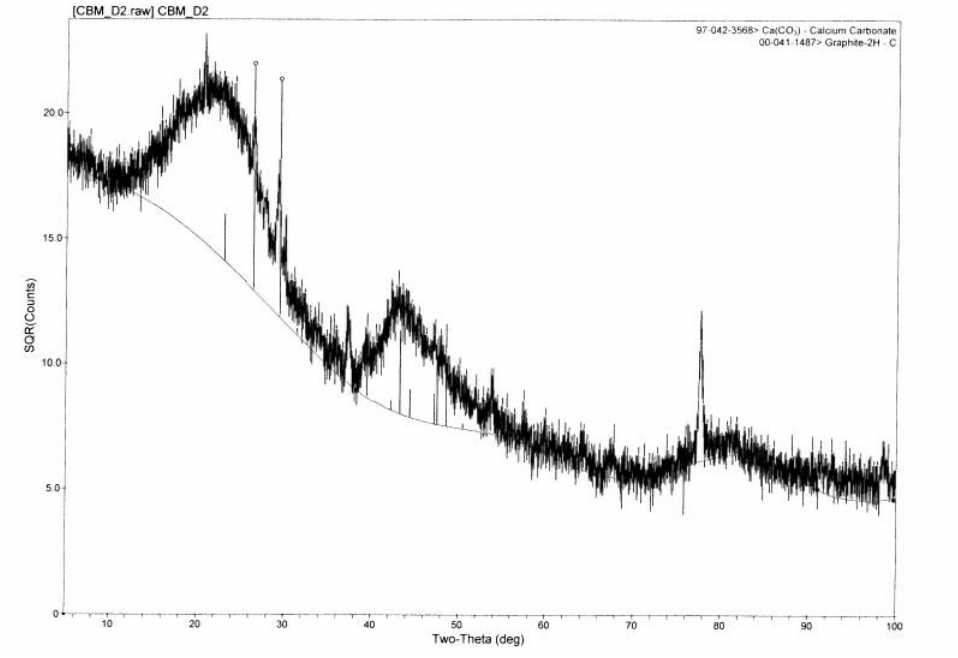

5. CBM-D1

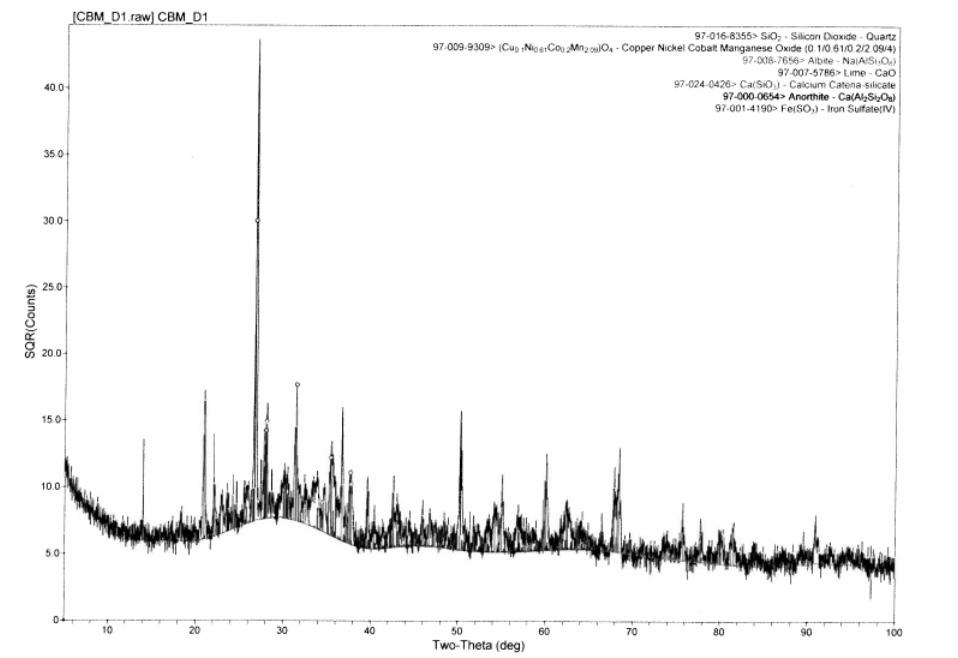

6.CBM-W

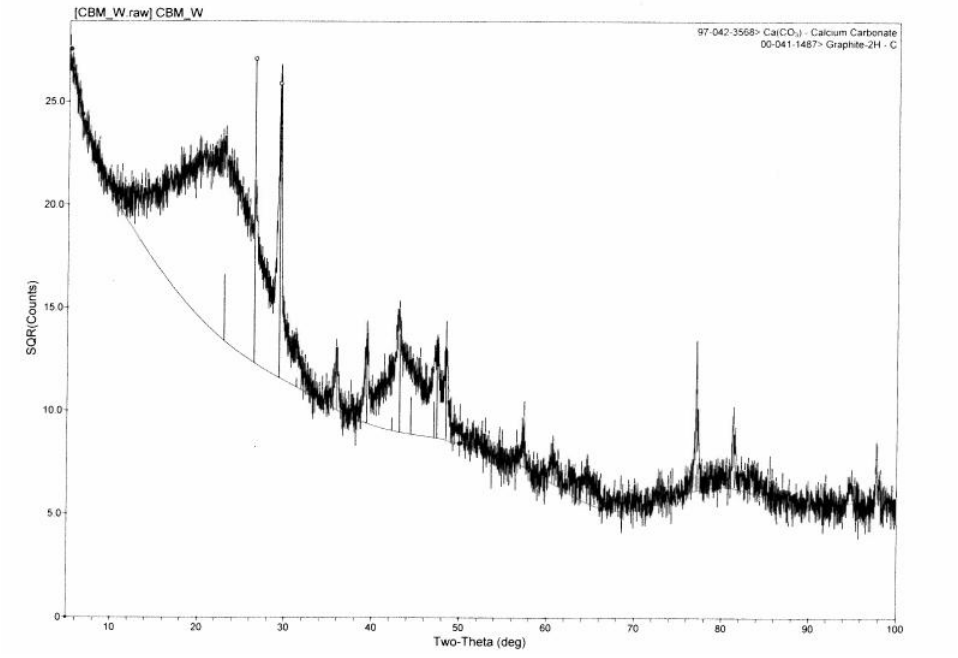

7. CLM2

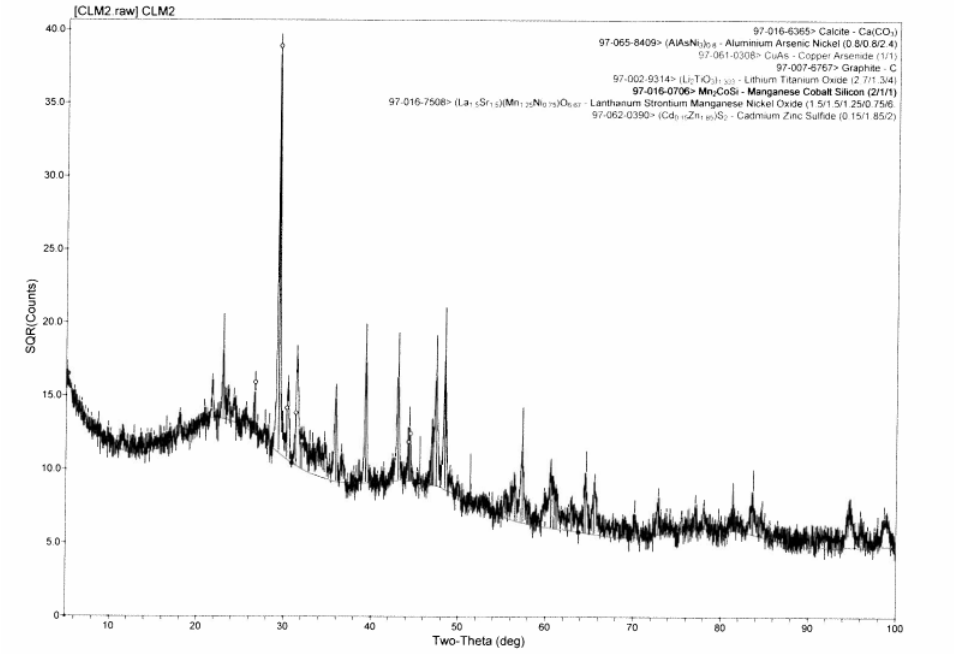
[CLM2.raw] CLM2
97-016-6365> Calcite - Ca(CO3)
97-065-8409> (AlAsNi)0.4 - Aluminium Arsenic Nickel (0.8/0.8/2.4)
97-061-0308> CuAs - Copper Arsenide (1/1)
97-007-5767> Graphite - C
97-002-9314> (Li2Ti3O7)1.333 - Lithium Titanium Oxide (2.7/1.3/4)
97-016-0706> Mn2CoSi - Manganese Cobalt Silicon (2/1/1)
97-016-7508> (La1.5Sr1.5)(Mn1.25Ni0.75)O6.67 - Lanthanum Strontium Manganese Nickel Oxide (1.5/1.5/1.25/0.75/6.
97-062-0390> (Cd0.15Zn1.85)S2 - Cadmium Zinc Sulfide (0.15/1.85/2)
SQR(Counts)
Two-Theta (deg)

8.CLM1

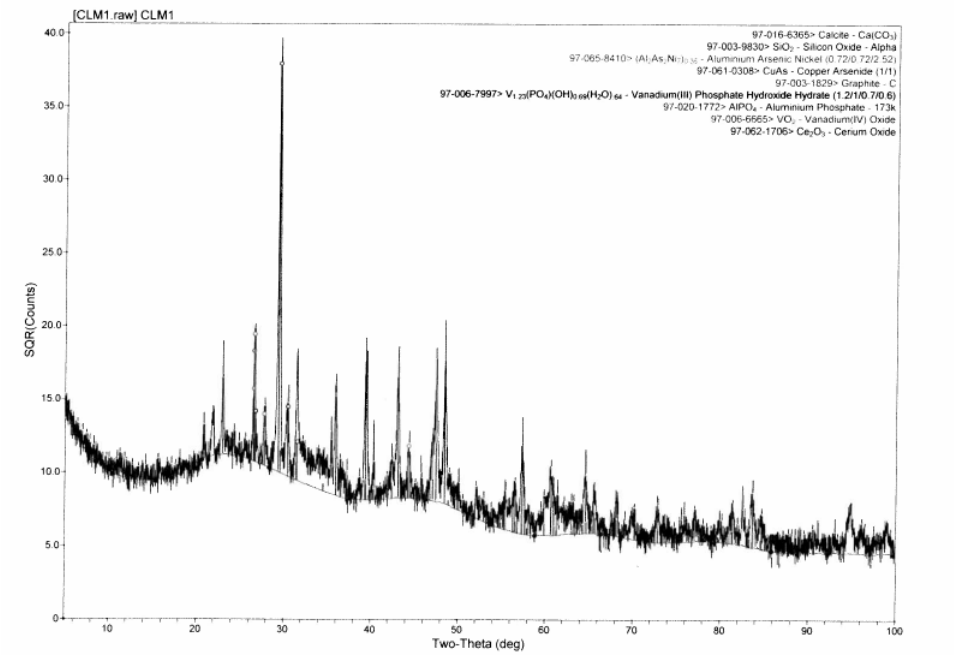
[CLM1.raw] CLM1
97-016-6365> Calcite - Ca(CO3)
97-003-9830> SiO2 - Silicon Oxide - Alpha
97-065-8410> (Al2As3Ni13)0.12 - Aluminium Arsenic Nickel (0.72/0.72/2.52)
97-061-0308> CuAs - Copper Arsenide (1/1)
97-003-1829> Graphite - C
97-006-7997> V1.23(PO4)(OH)0.69(H2O)0.64 - Vanadium(III) Phosphate Hydroxide Hydrate (1.2/1/0.7/0.6)
97-020-1772> AlPO4 - Aluminium Phosphate - 173k
97-006-6565> VO2 - Vanadium(IV) Oxide
97-062-1706> Ce2O3 - Cerium Oxide
SQR(Counts)
Two-Theta (deg)